Plastic anisotropy of additively manufactured maraging steel : influence of the build orientation and heat treatment

UNIVERSITY *of* LIMERICK

OLLSCOIL LUIMNIGH

Plastic Anisotropy of Additively Manufactured Maraging Steel: Influence of the Build Orientation and Heat Treatment

Barry Mooney

Thesis submitted for the Degree of Master of Engineering by Research

Primary Supervisor: Dr Kyriakos I. Kourousis | Senior Lecturer
External co-Supervisor: Dr Ramesh Raghavendra

Submitted to the University *of* Limerick, Ireland, October 2018.

Plastic Anisotropy of Additively Manufactured Maraging Steel: Influence of the Build Orientation and Heat Treatment

Barry Mooney

Abstract

This study investigates the combined effect of three Additive Manufacturing (AM) build orientations (0°, 45°, and 90°) and an extensive array of heat-treatment plans on the plastic anisotropy of EOS maraging steel 300 (coded by EOS as '*MS1*') fabricated on the EOSINT M280 Direct Metal Laser Sintering (DMLS) system. A comparison between the material microstructural characteristics, mechanical performance, plastic strain behaviour and anisotropy levels of identical parts fabricated on two of these independently operated DMLS systems was also conducted. Considerable plastic anisotropy has been confirmed in the as-built condition, which can be reduced by aging heat-treatment, as verified in this study. However, it has identified that a degree of transverse strain anisotropy is likely to remain due to the AM alloy's fabrication history, a finding that has not been previously reported in the literature. Significant microstructural discrepancies, affecting mechanical performance, plasticity and anisotropy levels, have also been observed in the as-built samples obtained from the two DMLS systems. A difference in the angle of the laser scan strategy, in conjunction with unfavourable powder feedstock characteristics, are understood to have had a profound influence on the plasticity and anisotropy divergences observed. A comprehensive visual representation of the material's overall mechanical properties against the various heat-treatment plans is offered through time-temperature contour maps. Moreover, the heat-treatment plan (6h at $490°C$) recommended by the DMLS system manufacturer has been found not to be the optimal in terms of achieving high strength, hardness, ductility and low anisotropy for the MS1 material. With the use of the comprehensive experimental data collected and analysed in this study, and presented in the constructed contour maps, the alloy's heat-treatment parameters (time, temperature) can be tailored to meet the desired strength/ductility/anisotropy design requirements, either for research or part production purposes.

Declaration

This thesis is the result of a twelve-month research project which has been jointly funded by the Irish Research Council (IRC), through the Government of Ireland Postgraduate Scholarship Research Programme, and the Faculty of Science and Engineering of the University of Limerick. It presents the technical status of the maraging steel 300 alloy which has been fabricated using EOS powder-bed laser additive manufacturing technology (AM), and brings together a large body of knowledge with regard to the metallurgical characteristics and static mechanical properties (including anisotropic behaviour) for a broad array of strengthening heat-treatment plans.

Trends in the industrial adoption of AM technologies have given fresh impetus to alloys such as maraging steel 300 due to the advantages offered (structural optimization, design complexity, manufacturing flexibility, cost, and speed). Current research is expected to result in further improvements and applicability of this AM fabricated alloy for general industrial applications. Accordingly, the work presented in this thesis has led to the submission of two research articles for publication in peer-reviewed scholarly journals. These articles can be found in Appendices A and B of this manuscript.

I declare that this work is my own, and that all contributions from other persons have been identified and appropriately acknowledged.

Signed: 

Barry Mooney

Date: 04 / 12 / 2018

DD/MM/YYYY

Acknowledgements

Special thanks are due to Dr. Kyriakos I. Kourousis who, throughout this project, provided sound academic guidance and contributed greatly to the quality and standard of this research. The assistance and cooperation offered by other faculty members of the University of Limerick's School of Engineering is gratefully acknowledged. The author also wishes to express his gratitude to Dr. Ramesh Raghavendra and his colleagues in the Waterford Institute of Technology (WIT) South Eastern Applied Materials (SEAM) centre for their investment of time and expertise during the fabrication and characterization of test specimens. The scholarship support provided by the Irish Research Council is also very much appreciated.

Barry Mooney

Contents

List of Figures

List of Tables

1. Introduction

Structure-critical metallic components produced by powder-bed laser additive manufacturing (AM) are expected to display a high degree of isotropy. The dependence of mechanical properties on orientation, known as *anisotropy*, is a consequence of the metal's fabrication history which places limitations on the design of the part.

Maraging steels possess the mechanical properties which give them engineering significance in applications where high strength, toughness and ductility (at high hardness), and dimensional stability are required [1–3]. *Maraging* refers to ***mar***tensitic microstructure, commonly found in steels, which can be strengthened/hardened through an ***aging*** heat-treatment [4, 5]. Based on the binary Fe-Ni primary phase system, the highly alloyed steel is strengthened by finely dispersed precipitates, which block movement of dislocations/defects within the crystal lattice. The dispersion of secondary phase alloying elements (Mo, Co, and Ti), mobilized through a straightforward and relatively expeditious aging heat-treatment, leads to an exceptional combination of strength and toughness [2, 6–8]. Maraging steel's low-carbon soft martensitic matrix is mostly free from interstitial alloying elements, which rank it as an excellent candidate for synthesis by AM and welding [1, 8–10]. The 18Ni (300) grade, or slight modifications thereof, has been used widely in AM, and is retailed commercially in powder form under several aliases. The quality assured *MS1* is one such powder supplied by EOS [11], a major AM technology manufacturer. This powder has been suitably refined for EOS's powder-bed AM systems and processing techniques, which have retained the historical proprietary name *Direct Metal Laser Sintering* (DMLS). Another, commonly used, term for this process is Selective Laser Melting (SLM), since the technique employs a high-powered laser-beam

energy source to fully melt powder particles into a high density, and chemically homogeneous composition. Driven by computer aided design (CAD) data, the laser's scanning strategies can be used to achieve layer-wise growth of imaginative, and relatively unconstrained geometries [8, 9, 11–13].

It is the alloy's outstanding properties and heat-treatment expediency in conjunction with the AM process's shaping efficiency that give DMLS produced maraging steel 300 such appeal. These factors allow for a much-accelerated fabrication route than conventionally manufactured parts, and thus offsets the high acquisition cost of the alloy, as well as the process costs. DMLS built maraging steel 300, however, has a major drawback amongst its conventionally manufactured counterpart. The mechanical properties are known to be anisotropic due to an inherent sensitivity with regards to how a part is orientated within the AM build volume [12, 14, 15]. This anisotropy is manifested through the fabrication process where large thermal gradients during melt-pool solidification, combined with the layer-wise deposition of the powder, planar movement of the heat-source, and uniaxial movement of the build-plate, make it difficult to homogenize the microstructure and mechanical properties of the as-built metal. A mesostructure of fine solidification cells, unique to the powder processing method and consequent to the powder granule melt dynamics, is coupled with continuous re-melting/heating of material beneath the melt-pool during build-up causing a distinct three-dimensional (3D) microstructural pattern to form. This results in mechanical properties which vary with direction and causes the material to exhibit anisotropic mechanical properties. Furthermore, the state of anisotropy can be exacerbated by ancillary process defects, such as residual stresses, and porosity, and a number of researchers have investigated the effect of AM processing parameters to improve the build quality of maraging steel 300 [16–18].

As indicated by EOS in the MS1 material data sheet (MDS) [12], the material becomes isotropic following application of a specified aging heat-treatment (6h at $490°C$), however, the MDS is not sufficient to characterize the material performance for engineering designs and products, since it covers only the primary build orienta-

tions (0°, 90°), and comes from a single source (EOS). The effectiveness of both the AM fabrication and heat-treatment procedure can only be measured by the extent to which the as-built and heat-treated component behaves under mechanical loading, yet very limited published research [19, 20] exists concerning the build orientation influence on mechanical behaviour of AM produced maraging steel 300. Croccolo et al. [20], who investigated the dependence of build orientation relative to the build plane (0°, 45°, and 90°) on the high-cycle fatigue life of EOS M280 produced MS1 specimens in the aged (6h at 490°C) condition only, found no substantial difference on the fatigue properties. Recently, Monkova et al. [19] examined the tensile properties of EOS MS1 fabricated at 0°, 45°, and 90°, and contrary to the EOS published MDS [12] they observed no significant orientation dependence in the tensile stress-strain behaviour for as-built, solution heat-treated (1h at 820°C), and aged (6h at 490°C) material. Other available test-data is mainly limited to static testing (tensile, and/or hardness) of maraging steel specimens fabricated in only one [3, 8, 9, 16, 21–26], or two [14, 18, 27–29] of the primary AM build orientations. The most comprehensive of these studies in terms of the reported mechanical properties is [9], which monitors the effect of an array of aging heat-treatments on the static properties of the AM fabricated alloy. While the study presents a broad range of hardness results, limited tensile properties are reported (i.e. for the as-built and five other peak-aged heat-treatment conditions). Furthermore, only the horizontal (0°) build-orientation is considered. Authors Yin et al. [30] and Bai et al. [31] and Mutua et al. [18] also present hardness and tensile data for horizontal specimens tested under a narrow array of aging treatments. In these studies, however, non-characteristic fluctuations/ variations in the AM alloy's elasticity and plasticity behaviour can be observed. While explanations for these abnormalities are not asserted, they may indeed be introduced during the fabrication process and/or during the material characterization process (e.g. due to the tensile test rates employed). Nevertheless, these irregularities mandate a more comprehensive and detailed experimental analysis of AM maraging steel 300's monotonic behaviour. So far, the

effect of aging heat-treatment on stress and strain anisotropy for this particular material has not been previously addressed, and there have been no reported findings on strain anisotropy for parts fabricated at various build orientations (i.e. 0°, 45°, and 90°). Moreover, the availability of tensile properties for AM fabricated maraging steel 300 for the primary build orientations (0°, and 90°) is limited. Since it is necessary to consider the material's multiaxial mechanical properties during the process of mechanical component design, the lack of orientation dependence data presents challenges for engineers when it comes to utilising the highly advantageous AM technology for their engineering designs and products.

As AM technology matures it is progressively becoming a viable option for the serial production of structure critical engineering components due to technological developments and improved process awareness [32, 33]. Key to this successful advancement is a clear understanding of the factors which influence the metallurgical soundness of the produced parts. As well as accumulating knowledge around orientation dependence, another important aspect for the serial production of AM parts is the ability to achieve consistent and repeatable mechanical properties outputs for identical parts produced on alternative machines, however, very limited published research exists on the repeatability of mechanical behaviour in AM-produced metals [24, 34–36]. Indeed, there is variation in the EOS-reported as-built MS1 mechanical properties for identical test-coupons fabricated on EOS DMLS equipment [12, 14], but also among maraging steel 300 properties reported in the open literature for contrasting test-coupon geometries which have been fabricated on EOS and other metal AM systems [3, 9, 18, 19, 21, 23, 24, 26, 27, 29, 37]. The spread of the as-built tensile properties reported across these studies (i.e. elasticity modulus (E): 150-194 GPa [12, 27]; yield strength ($R_{p0.2}$): 768-1214 MPa [23, 29]; tensile strength (R_m): 1010-1325 MPa [27, 29]; and elongation to fracture (A_t): 6.1-14.3 % [9, 26]) is a measure of the variability observed. This highlights the need for a deeper understanding of the factors that affect the reproducibility of AM parts, since engineers seeking to use this advantageous technology for structure-critical designs require a

greater control of the achievable mechanical properties.

In order to address the aforementioned research literature gaps, in this work, a comprehensive experimental analysis of maraging steel 300 mechanical properties and plastic anisotropy behaviour is reported.

Plastic anisotropy describes an uneven response of the alloy's plastic properties (or flow-strain relationships) with respect to the AM build orientations and has been quantified in this investigation by the *R-value* parameter. R-value is the ratio of true width-to-thickness plastic strains, and this parameter allows an examination of the alloy's tendency to deform non-uniformly by consequence of the test-coupon's build-orientation. In this work, both the effect of three AM build-orientations (0°, 45°, and 90°), as well as a large array of heat-treatment plans (combinations of time, and temperature) are considered to allow for a wide-scale investigation of anisotropic variation, not previously conducted in the past for this AM material. A complete visual representation of the material's overall mechanical properties, for all three AM build orientations, against the various heat-treatment plans is offered through time-temperature contour maps. The full mapping of AM fabricated maraging steel 300 mechanical properties for all three build orientations, in conjunction with their respective R-values has not previously been reported in the literature, and can serve as a very practical tool for AM engineers and researchers wishing to tailor the output of the EOS MS1. This novel experimental work is particularly focused on providing a means of AM maraging steel 300 heat-treatment selection to meet individual strength/ ductility/ anisotropy engineering design requirements, and intends to act as a guide project for other AM manufactured metals exhibiting anisotropy. Furthermore, the material characteristics, microstructures, tensile properties, and anisotropy variation of identical maraging steel test-coupons which have been fabricated on two EOS EOSINT M280 AM machines belonging to and operated by different users, are examined. For this purpose, the relationship between the AM process phenomena and the resulting mechanical properties, including plastic anisotropy, have been investigated.

2. Background

2.1 Maraging Steel

The 18% Ni 300 grade maraging steel was one of four strength grades (200, 250, 300, 350) developed by International Nickel (Inco) during the late 1950's [2, 4]. Each grade was optimised in terms of strength and toughness. The *300* designation represents the alloy's yield strength in ksi units, whereas the *maraging* classification indicates a strong martensitic structure which can be improved significantly by a precipitation hardening heat-treatment (aging) [5, 38]. Maraging steel 300 became a highly important military-grade alloy between 1960 and 1980, having large application scope in the aerospace/marine, defence and industrial sectors (e.g. in fabricating large welded artillery shells/vessels, precision load-bearing structures, and tooling mold and die) [2, 10, 39–41]. The alloy's appeal centred on a remarkable structural strength and fracture toughness combination, complimented by processing advantages such as an insensitivity to welding, and an ease of heat-treatment [2]. High strength is achieved in these alloys by second phase precipitation of intermetallic compounds rather than by carbide precipitation [28, 42]. Carbon is in fact an impurity which somewhat retracts from the steel's advantageous characteristics (strength-toughness combination, harden-ability, formability) [4]. Once these intermetallic compounds are present as a fine dispersion uniformly distributed throughout the softer Fe-Ni matrix, a condition of optimum strength can be obtained.

Due to the fact that maraging steel 300 was already recognised as a very important hardenable alloy in the mold and tooling industry, it was quickly identified that it might be especially well-qualified for use with contemporary metal AM process in-

novations when this technology emerged in the mid 90's [43–45]. During metal AM's early days, the advanced manufacturing technique was championed as a complete pre-production/ short-run thermoplastic injection mould and tool-making solution based on EOS's direct metal laser sintering technology [45, 46]. The technology permitted the creation of small, complex mould-cavity and tool geometries that incorporated conformal cooling channels which were difficult or impossible to fabricate otherwise - particularly, the complexity of the part placed no practical significance on the AM fabrication time and cost [45–48]. These unique processing advantages offered by AM have therefore given maraging steel 300 modern engineering significance for the fabrication of general mechanical components where high-resolution, high-precision, ultra-high-strength, toughness and ductility, and dimensional stability are required [1–3]. An example from a recent case-study published by Renishaw [49] demonstrates how engineers have capitalised on AM's design freedom, and maraging steel 300's outstanding properties, to fabricate a structure-critical component for a 'down-the-hole drill hammer' which reduced cost and improved reliability for the heavy mining industry.

2.2 Direct Metal Laser Sintering (DMLS)

The major interest in the field of metal AM in recent times is its emergence from prototype to serial production [32, 50]. To this aim, powder-bed metal AM systems are better suited to serial production as they provide more consistent and repeatable outputs and are capable of producing metallic components with the durability, quality, and precision adequate to meet demands of industrial engineering applications. These machines have therefore made the greatest technological strides and are currently dominating metallic AM processing [36]. EOS develop such systems which are designated with their proprietary *Direct Metal Laser Sintering* (DMLS) process name. Consonant with EOS's DMLS process, other leading AM system sup-

pliers use proprietary process names[1], but when dealing with metallic powders that are fully melted to achieve full-density high-strength components, the science is in essence equivalent. Controlled by existing Computer Aided Design (CAD)/ Computer Aided Manufacturing (CAM) know-how, these systems drive a high-wattage laser energy source to selectively melt successive thin layers of metallic powder particles, which in turn produces high density functional components, often without the need for additional finishing. The basic process schematic is shown in Figure 2.1.

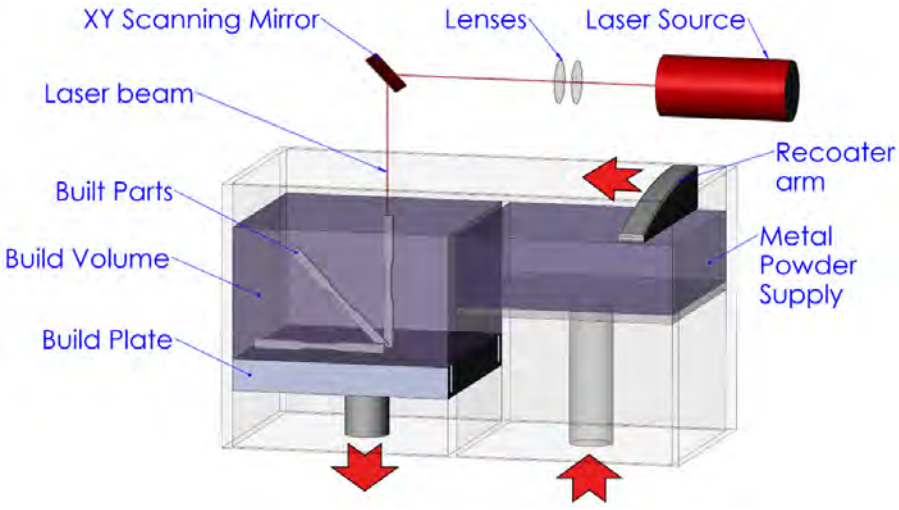

Figure 2.1: Schematic of the basic process configuration for powder-bed laser additive manufacturing systems.

Since the mid 90's, there have been major advancements in controlling the technology's underlying physics, and as a result, DMLS is less complicated to implement in practice, and has become much more prevalent in recent years [11, 45]. The aerospace industry has been the principal driving force behind AM's fast development and increasing application trend [51]. AM has expanded their capabilities in terms of structural optimization, design complexity, manufacturing flexibility, cost, and speed, with the transition from prototype production to serial manufacture is now well under way [32, 52–54]. On account of the significant technological developments, the range of AM processable materials has been expanding simultaneously, where so far, the compositions have closely followed that of standard alloys. The

[1] *Direct Metal Laser Sintering (DMLS)* belongs to EOS; *LaserCUSING* to Concept Laser, and *Selective Laser Melting (SLM)* to SLM Solutions.

logic being, for structural applications, it is desirable that AM parts do not deviate characteristically from those produced traditionally [54, 55].

As the technology continues to mature, more is expected of the functional parts produced, with special attention towards achieving metallurgical soundness by tackling the factors which influence mechanical performance [50]. As highlighted in Chapter 1, among the issues identified are the dependence of mechanical properties on the build orientation (anisotropy), and the repeatability of mechanical properties outputs for products produced on different machines. The AM build-process itself is inherently anisotropic. Uniaxial movement of the build plate, layer-wise powder deposition, planar movement of the heat-source (scanning strategy), and the subsequent heat-transfer through pre-deposited layers, all promote orientation dependant properties. In addition, AM's build conditions (environmental conditions, processing parameters, and quality of raw materials) are known to influence part performance and can amplify/ exaggerate the condition of anisotropy and affect repeatability. Part density is compromised by imperfections such as regions of un-melted powder, and the presence of voids/porosity and inclusions [27, 31, 56]. Porosity reduces the fabricated component's effective cross-sectional area and can act as stress raisers and potential loci for fracture initiation [27, 36]. Lower fatigue strengths have been reported for AM components due to these defects [57]. Furthermore, the correct use of support structures during the AM build process is essential for controlling deformation of parts from thermal residual stresses which are the unavoidable consequence of the mandatory high melt-pool temperatures and rapid cooling rates. Residual stresses can lead to dimensional instability either during the build, or during secondary machining operations (e.g. when the parts are removed from the AM build plate). The residual stress distribution through the material also plays a significant role in the component's directional mechanical properties. The severity of these process induced imperfections has somewhat abated in recent years, with the continued harmonization of processing conditions, and the improved quality of raw materials [32, 58]. Nonetheless, the art has not been completely mastered,

meaning the defects that persist are more than enough to impact the mechanical performance and intensify anisotropy in AM fabricated metals. The multitude of fabrication variables (e.g. laser power, scan speed, layer thickness etc.) which require optimization in order to ensure sound metallurgical bonding whilst curtailing process defects, signify the level of control complexity that industrial practitioners must grapple with. Some AM system providers ameliorate the cause by providing factory default, undisclosed, and pre-optimized sets of parameters for specific material and machine combinations. These support reliable mechanical properties and bolsters a repeatable industry level of quality making it possible to directly fabricate near fully dense components which exhibit the mechanical functionality necessary for heavy-duty tasks [59].

2.3 DMLS induced anisotropy

As previously mentioned, when powerful laser scanning strategies are employed to successively melt thin layers of fine powder particles, it provokes a distinct 3D macrostructural pattern formation. At a deeper metallurgical level, the dynamics of heat-transfer within the melt-pool and surrounding material provokes specific microstructures. For example, maraging steel 300 produced by AM exhibits fine cellular martensitic grain morphologies compared to the conventionally produced alloy which exhibits parallel packets of lath martensite. Depending on the particular alloy's chemistry as well as the laser scan algorithm employed, this heat-transfer can cause directionality of crystal growth (*fibre texture*) and non-random crystalline orientation effects (*crystallographic texture*) [58, 60–63]. Cyclic high-temperatures and rapid melt-pool cooling rates, along with the magnitude and direction of heat-flow, continually change grain-boundary location within and between build layers as a result of dynamic recrystallization [5] which are key parameters for the AM microstructure evolution, crystalline orientation, and fibrous alignment. Both fibrous and crystallographic textures have been correlated to mechanical property anisotropy in a range of AM materials (e.g. IN738LC alloy, Hastelloy X) [60, 62].

Columnar grains have been reported in several studies, with their axis orientated parallel to the direction of build and concurrent with the direction of maximum heat-flow [51, 58, 64]. Through dynamic recrystallization, the preferential growth of columnar grains for a given build layer, can be broken up by rotating the laser scan direction (e.g. 90°) for subsequent layers as demonstrated by AlMangour et al. [65]. This approach led to decreased texture and reduced mechanical property anisotropy in TiB_2/316 L stainless steel nanocomposites. Similarly, Bhardwaj et al. [66] recently demonstrated how the laser scan direction has a strong influence on the crystallographic texture and mechanical properties in DMLS MS1, showing that the texture depends on the adopted scan strategy.

As stated earlier, the state of anisotropy in the as-built metal is further exacerbated by ancillary process defects, such as residual stresses, and porosity. The anisotropic macrostructures and microstructures that develop, while undesired, may be difficult to eradicate from powder-bed AM processing methods. The solution towards achieving mechanical isotropy using current AM methods may therefore rely upon the optimization of a blend of inputs, for example: (i) a material specific approach to process parameter optimization, (ii) the use of appropriate scanning strategies/algorithms and (iii) suitable post-processing thermal treatments. So far, much of the research focus has been placed on parameter optimization to achieve high density parts, and there has been very limited published research concerning the effect of alternative scan-strategies on the microstructural integrity and anisotropy of maraging steel 300 [66]. Furthermore, and until now, no studies have examined various strengthening heat-treatment plans to assess the influence of the time and temperature combinations on plastic anisotropy and mechanical properties (e.g. strength, ductility) of maraging steel 300.

2.4 Heat-treatment of maraging steel

Conventionally produced (CP) maraging steel 300 has traditionally achieved its strength by means off a two-stage heat-treatment: 1. Solution-annealing, and 2. Isother-

mal aging [5, 38]. The goal of the solution-anneal, whereby the alloy is heated and held in the fully austenitic phase (Typical: 1h @ $815°C$), is to disperse the concentration of hardening elements, which have accumulated at grain boundaries, by fully dissolving them into a supersaturated solid solution [10]. As the alloy cools back down to room temperature, the austenite transforms into extremely ductile, body centre cubic (bcc) martensite [5]. This diffusionless transformation is easily achieved at low temperatures ($\approx 135°C$) and cooling rates by virtue of the alloy's high Ni content (18%) as indicated by the phase diagrams presented in Figure 2.2 [4, 5]. Furthermore, Figure 2.2a shows how the alloy must be re-heated to much higher temperatures ($\approx 600°C$) to transform back into austenite. This hysteresis contributes to precipitation hardening (aging) in maraging steels [4, 10]. The out-

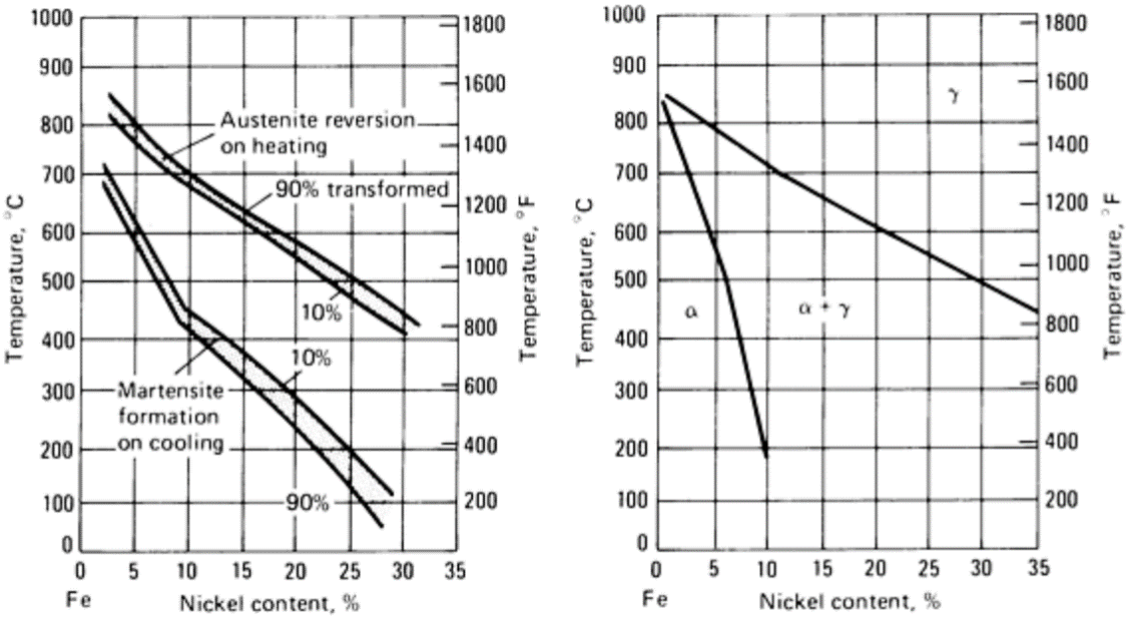

(a) (b)

Figure 2.2: Phase transformation diagrams upon cooling and the martensite-to-austenite reversion upon heating (a) Fe-Ni (metastable) transformation diagram showing austenite-to-martensite regions, and (b) Equilibrium diagram which illustrates that for 18% nickel, the equilibrium phases at low temperatures are a strong but ductile mixture austenite α, and ferrite γ. From ASM International [5].

come of the solution annealing process paves the way for the ensuing precipitation hardening response, which causes the second phase alloying elements to precipitate locally. Maraging steel producers supply the alloy in its solution annealed condition, which can be readily fabricated by conventional methods. In fabrication,

components exhibiting work-hardening can benefit from a repeated solution anneal, which re-homogenizes the microstructure, suppresses anisotropy (i.e. caused by cold-working), and alleviates residual fabrication stresses. The material will once again display homogeneous mechanical properties, although naturally, this supplementary heat-treatment step incurs additional fabrication cost [5, 10].

In contrast to conventionally produced alloy, and by reason of the rapid melt-pool cooling rates, the DMLS process provides a solid solution with full potential for precipitation strengthening [9]. Cooling rates circa 10^3 to 10^8 $K.s^{-1}$ provide a metastable martensite structure which is supersaturated with respect to the solute [5, 28, 42, 67]. This affords the heat-treater/ AM practitioners with an opportunity to by-pass solution annealing and commence precipitation-hardening directly post-fabrication, which allows for a much-accelerated fabrication route than that of the CP-alloy.

2.4.1 Precipitation hardening (aging)

As previously noted, strength is achieved when the dispersion of hardening particles precipitate locally to impede the motion of dislocations. These obstacles heighten the stress required for dislocation motion, hence enhancing the alloy's strength and hardness. Furthermore, when good toughness is sought, maraging steel alloys are aged past their peak-hardness condition (*overaged*), where a decomposition of metastable martensite to austenite (or austenite reversion) takes place [68]. To that end, these two topics, 1. precipitate formation, and 2. martensite-to-austenite reversion, which are known to have high importance to the properties of maraging steel, will be discussed [4]. The following description does not attempt to review all aspects of the substantive physical changes that occur in reality, however, it is believed to be an adequate explanation in order to clarify the work undertaken by this investigation.

Precipitate formation

The structure at room temperature consists of ductile martensite, with finely dispersed and uniformly distributed brittle phase particles in solution [4]. A *coherency*[2] exists amid solvent and solute atoms in the lattice, and dislocations can shear through the material with relative ease while in this condition. Precipitation hardening is induced when the structure is heated above the martensite start temperature (M_s), causing thermally activated second phase elements to emerge from solution by diffusion - as represented by the nanoparticles shown in Stage 1 of Figure 2.3. The chemical arrangement of the existing precipitate phase depends on the alloy composition, and the period within the precipitation hardening process [42, 68]. The precipitates that form initially in 18% Ni maraging steels comprise of mainly Ni_3Ti and Ni_3Mo, which get replaced later with Fe_2Mo or Fe_7Mo_6 during a second stage of the process[3] [4, 28, 42]. Over a period of time, these precipitates first become stable or nucleate (corresponding to the Gibbs critical energy), then evolve by diffusive mechanisms to develop into small and underdeveloped (underaged) precipitate particles. The stress required to shear these particles increases with precipitate radius, and when such material is stressed, passing dislocations bow around the precipitates (Stage 2 of Figure 2.3). The strengthening to this point is dominated by lattice coherency and chemical bonding. When the nanometric particles have developed to an optimum size and distribution (Stage 3 of Figure 2.3), the bowing of passing lines of dislocations reaches its greatest extent. This degree of bowing causes a culmination of strain fields at the precipitate interface. It is this condition that provides the optimum effect in the alloy towards obstructing and retarding the movement of dislocations [4]. Further growth of precipitates, termed *overaging*, gives rise to the *Orowan Mechanism* of strengthening, which coincides with the degradation of coherency [4]. To this point the bowing dislocation line has reached a critical radius

[2]Atomic matching or shared lattice parameter across the interface of solvent and solute phases.

[3]The literature is at variance as to the composition of second stage precipitates in the 18Ni steel, mainly due to the difficulties in analysing the composition of nanometric particles. Studies employing transmission electron microscopy (TEM) identify Fe_2Mo, however studies employing higher resolution atom probe tomography (ATM) report Fe_7Mo_6 precipitates

of curvature. When further stressed, the line passes between the obstacles, enclosing the particle in a 'loop' of dislocations (Stage 4 of Figure 2.3). Also known as *dislocation pinning*, each subsequent gliding dislocation adds a loop around the obstacle, heightening the degree of back-stress in the lattice. The build-up of loops corresponds to strain-hardening behaviour, whereby materials with a wider dispersion of particles will display increased strain-hardening. The continued straining eventually reaches the point when looping stresses are high enough to shear either the particles or the surrounding matrix. First established by Orowan, this relationship forms a basis for describing the interaction between precipitates and dislocations during overaging in precipitation hardenable alloy systems [4, 63].

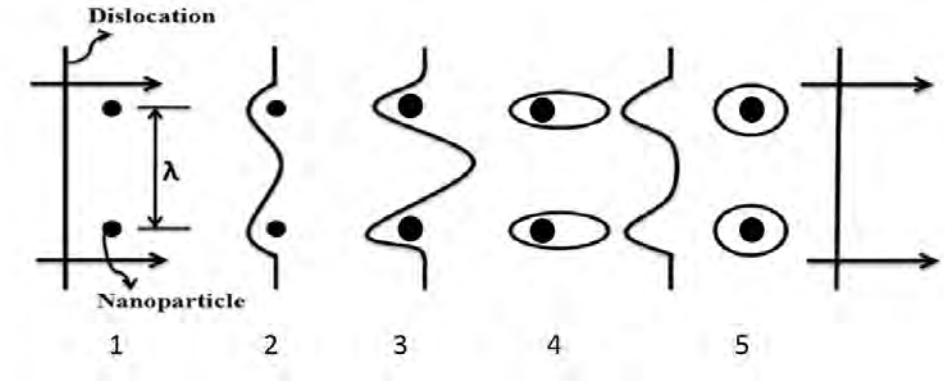

Figure 2.3: Schematic representation of the five stages of interaction between dislocations and precipitate particles based on the Orowan mechanism of dispersion hardening. Adopted from Dieter [63].

The aging time (t) and temperature (T) parameters exert significant authority on the size development of precipitates [38]. The situation is further complicated by the change in nature of coherency as solute atoms diffuse towards precipitate particles in the lattice. Two mechanisms of precipitate evolution are acting as illustrated in Figure 2.4: 1. *Growth* which relates to a period of underaging, and 2. *Coarsening* which refers to the period of overaging. It is the interaction between dislocations and precipitates which determines the materials strength, thus, both mechanisms enhance strengthening by increasing precipitate size through the diffusion of solutes in the matrix. However, the achievable strength is very much reliant on heat-treatment parameters, since they control the population and size of the precipitates that form.

Since diffusion is thermally activated, the treatment temperature dictates the kinetics of phase separation, i.e. the rate at which precipitation reaches its equilibrium fraction. At the early stage of precipitation hardening (or during *Growth* as shown in Figure 2.4a), depletion of solutes by diffusion from the surrounding supersaturated matrix causes the saturation of nucleation sites. This describes the normal (or homogeneous) phase change reaction in a solid solution. It is the temperature during this early aging phase changes which ultimately determines the population and size of precipitates which form by the *growth* mechanism. This stage leads to the peak hardness for a given set of heat-treatment parameters since dislocations require greater forces to bow around and cut through the densely packed matrix of small-to-moderately sized precipitate particles.

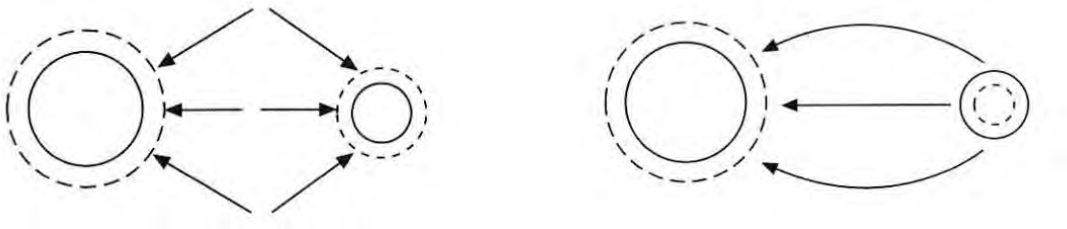

(a) Growth (b) Coarsening

Figure 2.4: Schematic comparison of the different diffusive mechanisms for precipitate evolution in maraging steel. The origin of diffusive atoms dictates how the particles evolve. (a) Atoms from the surrounding saturated matrix diffuse to cause particle *growth*, while (b) particle *coarsening* is facilitated by atoms which diffuse from both the surrounding matrix and from smaller dissolving particles. From Sha et al. [4].

As precipitation continues after peak hardness has been reached, and during continued heat-treatment, the size of certain precipitates increases through *Coarsening*. Diffusion by growth has now ended on account of the rapid depletion of solute concentration in the surrounding matrix. This overaging stage sees the particle population (precipitate density) deplete, which comes at the expense of smaller precipitates, as illustrated in Figure 2.4b. The size development of surviving precipitates during coarsening is slower than development during earlier stages, and the precipitates that form are larger and more widely spaced [4]. Moreover, as precipitates enlarge further, phase coherency breaks-down. The combined loss of coherency

and increasing sparsity of particles during overaging reduces the effectiveness of dislocation hindrance. Researchers have also attributed coarsening and coherency loss to matrix embrittlement, whereby the coarsened precipitates act as sites for crack nucleation [68]. It is of interest for the following section that prolonged holding at temperatures below austenite start (A_s) (see Figure 2.2a) will eventually lead to a decomposition of the metastable martensite by diffusion-controlled reactions to a stable blend of austenite and ferrite [68, 69]. The austenite so formed is known as *reverted* austenite, and when the propensity for reversion is higher (i.e. at high treatment temperatures), its formation can even precede precipitation in maraging steel [69]. Lower temperatures, somewhat regulate early precipitation diffusion kinetics by allowing particles to *grow* to a greater extent before *coarsening* dominates. For this reason, the greater population of particles at lower treatment temperatures gives an enhanced strengthening effect, but the time taken to achieve peak strength/hardness increases alongside. As before, when precipitates increase past a critical size at the expense of their smaller neighbouring counterparts, these larger and more dispersed obstacles loose coherency in the matrix, resulting ultimately in a loss of strength.

Austenite retention and reversion

The presence of austenite in AM maraging steel 300 can either be from 1. uncompleted transformation into martensite due to rapid melt-pool cooling-rates (i.e. retained austenite), or 2. from severe heat-treatment parameters (high temperatures and/or prolonged holding times) which cause martensite to austinite reversion (i.e. reverted austenite)[70].

Retained austenite presents itself in maraging steel 300 when the material cools rapidly from austenite finish (A_f) to ambient-temperature. This essentially freezes in place solute-rich austenite leaving it untransformed, whereas solute-depleted austenite transforms into martensite [71]. Since austenite is a soft phase, its has an adverse effect on the material's strength. Alloying elements have higher solubility in this

softer phase, which subtracts from the effectiveness of precipitation during subsequent heat-treatment [71]. The decrease in strength, however, can be accompanied by a marketable improvement in ductility and toughness, providing of course that these enhancements have not been counteracted by overaging-related matrix embrittlement after aging.

Reverted austenite occurs during extended isothermal aging at temperatures which support the dissolution of Ni_3Mo precipitates. Ni_3Mo is a metastable phase, and when it breaks-down, it enriches the localized matrix with Ni. This in turn promotes austenite nucleation [4, 5]. At temperatures below A_f, the bcc martensite is attempting to achieve its equilibrium structures of austenite and ferrite. The metastable Ni_3Mo is one of the phases which lead to the initial beneficial precipitation hardening reaction during early aging. To begin, this phase fits coherently within the bcc martensite matrix, however, once the equilibrium amount of this precipitate has been attained, the accompanying coherency strains and lattice parameter misfit make it unstable. At this point Ni_3Mo dissolves and is replaced with Fe_7Mo_6. As this new phase nucleates and grows it depletes the matrix of iron, further enhancing the Ni concentration, thus augmenting austenite reversion [5]. The balance of alloying micro-constituents such as Co and Mo and Ti have a handle on the rate at which the reversion takes place, however, prolonged heat-treatment will generate significant amounts of reverted austenite [71]. Martensite-to-austenite reversion increases when the temperature rises past $450°C$ (see Figure 2.2a), where the material will quickly soften thorough the combined effects of precipitate *coarsening*, and austenite reversion [4]. For this reason EOS assert that the maximum operational temperature of MS1 is $400°C$ [12].

In summary, the temperature parameter has the most significant effect on precipitate size and dispersion in maraging steels, and thus their mechanical performance after the precipitation heat-treatment. The 440-$540°C$ (low-high) temperature range is considered to be suitable for the aging of 18% Ni grades. Over time at high temperatures ($540°C$), nucleation sites quickly saturate by diffusion from the surrounding

lattice. The *growth* stage is quickly completed, and coherency strain-hardening decreases with increasing particle size, bringing about a condition of maximum strength and peak hardness due to the critical radius of dislocation bowing [4]. This condition is met with the early onset of coarsening, loss of coherency, and ultimately a lattice with fewer blocking obstacles. The high-temperature treatment's maximum attainable hardness peaks early, failing to reach the alloy's optimal design strength. After reaching a peak-hardness, precipitation continues, however the alloy experiences relatively rapid loss in strength due to an accelerated coarsening and reversion to austinite. At low temperatures ($440°C$), the precipitate nucleation and growth phase is controlled/extended allowing a populous dispersion of small precipitates. With these smaller particles', coherency strain hardening increases with increasing particle size, thus the alloy reaches greater peak strength [4]. However, considerable time is required for precipitates to reach a size where dislocation bowing is maximized. The effects of coarsening and austenite reversion are also somewhat suppressed by the lower temperature.

3. Problem Statement and Research Questions

Metal additive manufacturing is still at its infancy when compared with conventional manufacturing methods. AM's industrial practicality and potential adoption for the serial production of components used in demanding engineering applications relies on a foundational level of process control and an ability to regulate metallurgical outputs. Without this mandatory process knowledge, AM technology is at risk of becoming endangered.

The lack of available data presents challenges for engineers and small and medium-sized enterprises (SMEs) - who do not have abundance of financial resources to fund Research and Development (R&D) activities - when it comes to utilising the highly advantageous AM manufacturing technology. In practice each small/medium design and manufacturing project influenced by issues such as material anisotropy and microstructural defects etc., incurs additional costs from the significant R&D efforts needed to resolve these issues. Furthermore, unique attention for the produced parts in terms of extensive post-processing (i.e. surface finishing, heat-treatment and non-destructive inspections) is necessary.

The ideal situation is a stand alone AM technology which can produce parts exhibiting predictable, repeatable and reliable mechanical properties with implicit material characteristics. Comprehensive metallurgical evaluations and assessments of machine specific behaviours are absolutely necessary in pursuit of this goal. In the case of AM fabricated maraging steel 300, however, the reality is that the AM system/feedstock suppliers provide very limited data on the output of the process in terns of the material's performance. Moreover, the metallurgical observations in the

literature are highly varied and the body of published research is currently inadequate to characterize material performance for engineering designs and products. The following research gaps have been identified and are addressed by the current work:

- There are no reported findings on the plastic anisotropy of as-built DMLS fabricated maraging steel 300 (and other AM metals) at various build orientations;
- A direct comparison of the microstructural characteristics and mechanical properties of maraging steel 300 produced on two AM systems of the same type, but different machine number, has not been previously conducted;
- The effect of post AM heat-treatments on the plastic anisotropy of maraging steel 300 (and other AM metals) has not been previously investigated;
- No study has attempted to assist AM end-users towards appropriate heat-treatment selection for mechanical component design by mapping maraging steel 300's mechanical performance and plastic anisotropy levels against a wide array of heat-treatments.

The purpose of this study is to contribute knowledge and value to the field by addressing the following research questions:

1. How does the building angle influence mechanical properties of the as-built and heat-treated AM maraging steel parts?
2. Does the EOS recommended aging treatment of 6h at 490° provide optimal strength in the MS1 material?
3. Which heat-treatment plans can reduce/eliminate the plastic anisotropy of DMLS maraging steel 300 without compromising significantly on the alloy's achievable strength?

4. What level of repeatability and reproducibility can be expected for parts produced on independently operated machines of the same type in terms of build quality (surface finish, density), microstructure, mechanical properties (strength, ductility etc.) and plastic anisotropy?

4. Literature Review

Four main topics are covered in this review: 1. Powder feedstock quality; 2. DMLS material microstructure; 3. Process parameters, laser scan strategies, and build defects; and 4. Mechanical properties. These four areas - which place the spotlight exclusively on the extant literature concerning AM fabricated maraging steel 300 - provide a comprehensive overview of the current status of the alloy and articulate the concerns most closely related to the research questions.

4.1 Powder feedstock quality

An area of primary research is focused on AM system parameter optimisation with the prevailing goal of eliminating microstructural defects such as porosity, un-fused particles, and micro-cracking. While the user can impose certain authority over the AM system's control parameters and performance towards this goal, the feedstock quality (chemical composition, size and morphology) is more intractable, and plays an important role in the final quality and properties of the fabricated part.

The chemical composition specification ranges covering the main commercially available maraging steel 300 powders (including MS1 from EOS, CL50WS from Concept Laser and M300 from Renishaw) [12, 15, 72–77], which are typically controlled by AM machine manufacturers, are presented in Table 4.1. Individual suppliers work within these specification limits for their specific powder blend. The defined chemical specification of a given powder variant is critical towards the achievable properties of the finished part, however, these specifications are often difficult to achieve in production because the powders tend to vary within specification (e.g. through regulation of gas and vacuum parameters during atomization). Therefore, a degree of

supplier and batch variability is inevitable [78, 79]. Slight alterations to the powder's chemistry can have major implications on the produced parts as discussed in a case study by feedstock supplier LPW Technology [78]. The discovery of cracking in bulk AM processed maraging steel 300 was traced back to the presence of residual chemical elements - in particular Silicon, Manganese and Boron - which were not deliberately added to the alloy but were present in raw material despite the powder falling within specification for the main comprising elements. This highlights the alloy's sensitivity to upstream contamination and signifies the importance of sourcing quality assured product from reputable suppliers who can meet narrow chemical specification requirements and mitigate against residual element contamination.

Table 4.1: Typical chemical composition ranges (%wt) of 18% Ni maraging steel 300 powders used in metal AM [12, 15, 72–77].

Ni	**Mo**	**Co**	**Ti**	**Cr**	**Si**	**Mn**	**C**	**Fe**
17-19	4.5-6	8.5-11	0.6-1.2	0-0.5	≤ 1.0	≤ 1.0	≤ 0.03	Bal.

As with the powder's chemistry, subtle alterations to its morphology (size and shape) can exert significant control over the AM build quality, particularly, the as-built surface roughness and relative density of the parts. The powder granule shape and size distribution determine the achievable layer-wise packing density, flowability and inter-particle sintering kinetics during fabrication [80], yet very few AM maraging steel 300 researchers [21, 24, 37, 81, 82] have performed particle analysis on the starting material, thus making it difficult to correlate observed microstructural defects and mechanical properties variations with the feedstock characteristics. In these studies, unimodal distributions of spherically shaped granules having size range $10\mu m$-$70\mu m$, and central tendency of $\approx$ 35-40μm, have been generally acknowledged. When a batch of powder is cycled through multiple AM builds, the feedstock experiences a steady gain in Nitrogen and Oxygen concentrations [83], as well as a shift towards larger and agglomerated powder granules which tend to get pushed cross-platform into the system's collection chamber during recoating. Contrastingly, smaller spherical granules, which permit high packing efficiencies, are

more readily consumed by the process. These symptoms of powder recycling will impede flow behaviour due to inter-particle friction during the recoating process, lead to reduced packing efficiencies, and effect the feedstock's interaction with the laser-beam. Together these factors will ultimately lower the AM part's build quality (i.e. surface roughness and relative density) [80, 84]. Irregular shaped microstructural defects/pores are indicative of powder packing deficiencies, whereas the formation of spherical pores pertain to melt-pool gas entrapment. So far, only one early study by Hoeges et al. [85] has presented findings on the the influence of maraging steel 300 feedstock on the produced metal. The study deals with a comparison between gas and water atomized maraging steel 300 powders, and their influence on the properties of AM fabricated test-coupons. Despite only slight differences in the powder morphologies, it was necessary to modify the AM processing parameters for each of these powder variants in order to achieve similar relative densities in the produced parts, thus confirming previous comments regarding the influence of powder morphology on part relative density. To-date, however, no study has examined the role of particle morphology on the achievable surface roughness, relative density and mechanical properties of maraging steel 300 by holding constant the AM processing parameters. Perhaps the on-going development of new in-situ techniques for AM process monitoring/diagnostics will allow enhanced process reliability by compensating for feedstock variations in real-time fabrication, and ultimately facilitate the production of components exhibiting enhanced material performance.

4.2 DMLS material microstructure

4.2.1 As-built material microstructure

The typical low-magnification maraging steel 300 microstructure has a complect appearance, with bundled interconnections of fan-shaped solidification cells between molten lines [9, 25]. An example of the sectioned microstructure is shown in Figure 4.1a. The particular development/detail (i.e. melt-pool width and depth) is subject

to the AM processing parameters employed (e.g. the layer thickness, scan strategy, scan spacing, speed and laser power). Nonetheless, several maraging steel 300 studies [9, 25, 29, 86] employing alternative AM systems and process parameter settings report very similar microstructures. In these studies the melt-pools were observed to range in width (75-100μm) and depth (40-50μm) which is reflective of the applied laser spot-size, energy and layer-thickness. Variations in the reported AM systems' laser input energy (i.e. ranging between 105-400W), laser scanning strategies (e.g. the scan rotation angle between successive layers), and the use of pulsed versus continuous line scanning, were also observed across these studies. These general observations serve to demonstrate how the AM processing procedure is not a standardized practice, and the methods by which it is administered, along with the metallurgical results achieved, are subject to variation between producers.

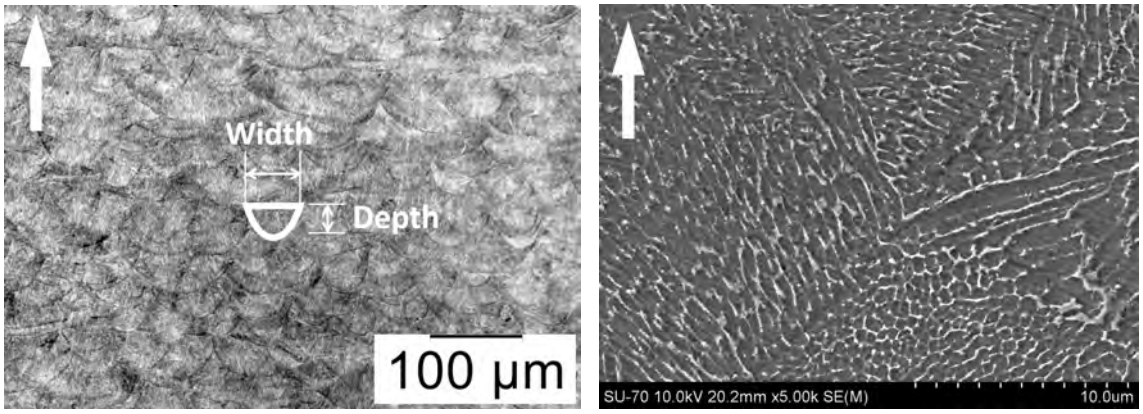

(a) (b)

Figure 4.1: (a) Low magnification optical and (b) high magnification Scanning Electron Microscope (SEM) images of laterally sectioned structure fabricated with the EOS EOSINT M280 DMLS system using the manufacturer's recommended set of parameters (MS1 Performance 2.0) and maraging steel 300 powder (MS1). The arrows indicate the AM build-direction.

A higher magnification image revealing the formation of a mesostructure of very fine solidification cells is shown in Figure 4.1b. These cellular martensite bundles comprise a compact arrangement of fine, coarse, and dendrite cell formations having sub-micron intercellular spacing, and grow epitaxially across laser-tracks and build-layers [25, 28, 29, 31, 42, 86]. Assisted by rapid melt-pool cooling rates (circa 10^3 to 10^8 $K.s^{-1}$), the evolution mechanisms of these cells relate to the melt-region

thermal flux direction which changes for successive layers whereby the cells orientate themselves concurrent with the direction of heat-flow/removal. A theoretical explanation of their formation is presented in a recent study by Tan et al. [37]. This characteristic cellular structure, unique to the powder processing method, is believed to be a major contributor to the strength difference between as-built-AM versus the solution-annealed conventionally prodiced alloy, which in-contrast does not display retained austenite in its microstructure, and exhibits random parent grains, each containing coarse and disordered packets of parallel lath-martensite [3, 8, 18, 86, 87].

As shown in Figure 4.1b, retained austenite is easily distinguishable in the high magnification microstructure where it presents as the bright phase which aggregates at cell boundaries. It arises in the as-built alloy from an uncompleted transformation into martensite during the rapid cooling/solidification. The existence of these microscopic segregated solute-rich regions not only softens the as-built alloy, but also augments further austenite reversion during the elevated temperature precipitation heat-treatment cycle [9, 23, 31, 67, 69]. Accordingly, the importance of appropriate AM processing variables is evident since these will govern the volume of retained austenite in the as-built microstructure, and ultimately the part performance. Studies having performed quantitative phase analysis [9, 23, 29, 67] have confirmed a significant amount of retained austinete in the as-built metal, however, are at variance with regards the percentage volume present. Jägle et al. [67] - who used high resolution electron backscatter diffraction (EBSD) scans - estimated a volume fraction of 8.5% $\pm$ 3.56%, whereas Casati et al. [9], Kempen et al. [23], Suryawanshi et al. [29], Yin et al. [30], and Tan et al. [37] performing Reitveld refinements measured 11.38%, 5.8%, 10%, 10.3% and 1.6% respectfully. The observed variability in the literature may indeed be the direct result of the individual fabrication parameters and scan strategies and/or due to material characterization diligence.

In an interesting and recently published study, Bhardwaj et al. [66] quantified the effect of two alternative laser scan strategies on the volume of as-built retained

austenite and found that the scan strategy indeed impacts on the quantity of this phase, and thus the alloy's as-built tensile properties (discussed further in Section 4.3.3). The harmful effect of this austenite phase, which limits the as-built alloy's strengthening capacity, can be greatly diminished by holding the laser heat-input to a minimum, in conjunction with the use of appropriate scanning strategies. Building on Bhardwaj's work, a more comprehensive investigation of process parameter/scan strategy impact on the volume fraction of retained austenite in AM maraging steel 300 would be helpful. Also, the correlation of this phase with the achievable post heat-treated mechanical properties would be a interesting addition.

4.2.2 Precipitate formation in the DMLS material microstructure

When comparing the AM-produced material against its CP counterpart Jägle et al. [8] found no observable difference between the precipitate chemistry, formation-kinetics, morphology, or size. Despite their vastly different processing routes (CP versus AM), precipitates form in the very same way, although the materials exhibit significantly different characteristics with respect to the grain-morphology and size, the texture, and the presence of retained austenite. The alloy's processing history can be held exclusively responsible hence. In an early study by Stanford et al. [3] the authors claim that precipitation took place in MS1 material during the AM build process, as revealed by their microstructural evaluation. Particles of ~20-100nm in size were observed via. scanning electron microscopy (SEM), and the material exhibited a good degree of hardness in the as-built condition (387HV, $\approx$ 39-40HRC). In stark contrast, Jägle et al. [42] reported no evidence of early precipitation or nucleation of solutes in the as-built material despite the alloy's propensity to develop precipitates, and despite AM's unique thermal profile (*intrinsic heat-treatment*). This view is shared by Mutua et al. [18] who declare that the high solidification cooling rates prohibits the formation of precipitates. In more detailed follow-up examinations, Jägle et al. [8] state that early stages of precipitation are limited to

Ti-Ti clustering which constitutes the early formation of Ni_3Ti precipitates. When investigating the size and morphology of precipitates in aged material Jägle et al. [42] found that the particles ranged in size from diameter ~2-11nm depending on their chemistry. Separately, Suryawanshi et al. [29] found the average precipitate size to be ~40nm in length and ~5nm in width. These conclusions put Stanford's observations into question. The works conducted by Jägle are considered to have a greater technical footing as they employed more capable AM equipment, and more appropriate characterization techniques in their assessments. The discrepancies between studies, however, is testament to the level of variation that exists between independent researchers and producers. Selection of equipment, processing parameters, and characterization techniques can provide vastly contrasting results between studies. The current work aims to address the identified issues by (a) following ASTM standardized procedures for test-specimen design and testing; (b) employing AM system supplier's pre-optimized processing parameters and scan strategies during AM fabrication; (c) monitoring anisotropic variation by testing specimens fabricated in three AM build orientations (0°, 45°, 90°); and (d) considering an extensive array of aging heat-treatments to monitor mechanical property and anisotropic variation not previously conducted in the past for this AM material. Furthermore, this work examines the repeatability between EOS EOSINT M280 systems by comparing the material characteristics, microstructures, tensile properties, and anisotropy variation of identical parts fabricated on two alternative machines belonging to and operated by different users.

4.3 Process parameters, laser scan strategies and build defects

4.3.1 Influence of process parameters

Several maraging steel 300 studies have identified the optimum processing parameters as those which provide part relative density $> 99\%$ [27, 29, 31, 56, 86, 88]. According to powder feedstock supplier LPW, a relative density of $> 99.9\%$ is considered the benchmark for near fully dense builds [78]. Experimental results published by Koutney et al. [24] showed that an increase in the laser energy density during AM processing (i.e. from 53.6-65.5 J/mm^3) can lead to enhanced relative density (99.1%-99.9%) and superior mechanical properties (e.g. 16% increase in modulus of elasticity, 3% greater yield strength and 26% increased ductility etc.) in as-built maraging steel 300. Energy density (E_d) is a function of laser power (P), scan speed (v), pitch (scan spacing) (h), and layer-thickness (t) as described by the following equation [16, 18]:

$$E_d = \frac{P}{vht} \tag{4.1}$$

Through a Design of Experiments (DOE) approach, Casalino et al. [16], Campanelli et al. [17], and Mutua et al. [18] lay the groundwork for maximising relative density while signalling the significance of E_d by varying factors P and v, and monitoring the alloy's resulting mean-response in terms of density, hardness, tensile strength, and ductility (% elongation) measurements. The mechanical properties were highly variable due effects of E_d on the resulting relative density which ranged in these studies from 90.9-99.9%. In their work, Mutua et al. [18] provide a graphical process window/schema obtained from their experimental results. The schema relates these influential parameters (P, v, E_d) and clearly identifies a suitable AM-process window for maraging steel 300 fabrication, i.e. regions in which the relationship between these input variables corresponds to alterations in the alloy's relative density, microstructure, and hence the mechanical properties. The authors also showed

that excessively high E_d will lead to porosity, thus, a reduction in the alloy's relative density. The spherically shaped pores observed in this condition were caused by gas entrapment within molten pools. Similarly, Suryawanshi et al. [29] suggest that a sub-optimal combination of process settings, namely laser power (P) and/or lower scan-speed (v) may have been responsible the presence of small spherically shaped pores in their fabricated test specimens. The same authors present contradictory porosity quantifications for alternative evaluation techniques: the Archimedes method (0.5%), and Image Analysis Method (0.7-1.1%). In their reported mechanical properties, an under-performance in terms of the alloy's as-built strength can be observed. Furthermore, the aged (5h at 480°) tensile ductility properties were approximately 40% lower than the guide-values outlined in their material supplier's data sheet [72]. As highlighted earlier, these metallurgical defects can act as stress raisers and potential loci for fracture initiation causing the alloy to fail prematurely.

4.3.2 Influence of the laser scan strategy

Yasa et al. [86] and Becker et al. [27] put forward proposals of laser re-melting (or double exposure) scan-strategies as a solution towards decreasing unwanted porosity. Both studies demonstrated how such scan strategies can provide slight improvements to maraging steel 300's relative density results. In their experiments, Becker et al. [27] selected suitable parameter settings and used these in conjunction with a double exposure scan-strategy to reduce the presence of voids to within 0.3% in the as-built metal (i.e. improving relative density from 99.5% to 99.7%). They scrutinised the effect of laser re-melting by performing tensile tests on specimens built with their longitudinal axis aligned at 0° and 90° to the build-plate. In the reported results, however, the marginal decrease in porosity achieved through laser re-melting (0.2%), is partnered by a considerable increase in tensile property anisotropy (i.e. elasticity modulus, yield strength and ductility). Whilst a single laser exposure scan-strategy produced material exhibiting a certain anisotropy, the secondary pass of the laser resulted in a significantly larger divergence in properties with respect

to the build orientation. The results imply that residual stresses and/or preferred texture (perhaps promoted by this double exposure scan strategy), in conjunction with AM's inherently anisotropic layer-wise macrostructure, may be at the root of the strength divergence. Residual stresses are suspected to be the cause of scatter witnessed in crack growth analysis in the same article. Additionally, when Yasa et al. [86] achieved hardness values 30% higher than the conventionally produced (CP) alloy, they assigned their reasoning to early stage precipitation caused by the process's intrinsic heating. It may be more plausible, however, that this premium hardness derived from compressive surface stresses installed by the double exposure scan strategy. Although tailored scan strategies can be employed to eradicate porosity, the evidence suggests that these thermal processing events have ancillary effects which may adversely affect the performance of produced part. To-date, AM scan-strategy manipulation has played only a supporting or minor role in research concerning maraging steel 300. Accordingly, the AM research and manufacturing community would benefit from a study which would fully characterize the effect of alternative scan-strategies on the microstructural integrity, mechanical performance and anisotropy for this alloy.

4.3.3 Influence of residual stress and texture

Residual stresses in AM-produced alloys are the unfortunate and unavoidable consequence of the short and severe laser-powder interaction times and rapid melt-pool cooling rates [89]. Despite maraging steel's relatively low coefficient of thermal expansion ($\approx 10 \mu\epsilon/^{\circ}C$), residual stresses arise during the build-process due to (i) the severe temperature gradients and localized volume changes induced; and (ii) austenite-to-martensite phase transformation during melt-pool solidification [66, 89]. These stresses are major obstacles among components destined for the aerospace and other high-end industries, which have rigid requirements and specifications, and a strict precision is necessary for their manufacture. High-magnitude residual stresses have led to cases of base-plate separation during the AM cycle [90], or warping/distortion

arising from stress relaxation upon part removal from the build platform [91]. Thin components of non-uniform geometry are especially prone to the latter when differential cooling between the raw-material and the AM system's base-plate metal lead to residual stresses. Upon removal from the build-plate, shrinkage distortions (bowing) are common, caused by disruption to the parts static-equilibrium. Such distortion/stresses can be lessened through connecting the underside of each part to the build platform with an appropriate support structure/scaffolding which functions as a passive heat-sink during manufacturing. The replacement of tensile surface stresses with compressive stresses through shot-peening can assist with the circumvention of premature residual stress related service failures (such as corrosion and fatigue failure) and can enhance the components tribological properties [92]. For that reason shot-peening has been widely adopted in the manufacturing community as a way of improving metallic performance and is a commonly practised post-processing procedure with AM components [20]. As-built residual stresses can also be managed by the selection of suitable process-parameters, i.e. appropriate energy input, the design of laser scanning-strategies and by effectively pre-heating the build-plate in advance of the AM build [21, 27, 93, 94].

Croccolo et al. [13] suggest that due to maraging steel 300's low coefficient of thermal expansion only low magnitude residual stresses arise in from the AM build and are tensile in nature. However there is a difference of opinion with regards the magnitude and sign of the residual stresses that develop. Becker et al. [27] and Bhardwaj et al. [66] showed that rotating the laser scan direction for subsequent build layers during AM build-up had a noticeable impact on the residual stress state in maraging steel 300. In these studies, measurements were performed on the top (free-surface), and base surface (after removal from the build-plate). Two scan strategies, X and XY - as shown in Figure 4.2 - were compared. While both of these studies investigate the influence of the intra-layer laser scan rotation (90°) on surface/near-surface residual stresses, alternative residual stress characterization techniques were employed and these produced conflicting results. In this Figure (Figure 4.2) 'N' represents an ar-

bitrary build layer and subsequent layers are labelled 'N+1' and 'N+2'. Using x-ray diffraction, Bhardwaj et al. [66] detected compressive surface residual stresses for both X and X-Y strategies. Higher magnitude stresses, ≈25% of yield strength (0.25 $\times R_{p0.2}$), were observed in material fabricated using the X scan strategy, whereas the X-Y strategy resulted in slightly lower magnitudes (≈0.2 $\times R_{p0.2}$). This X-Y strategy was also beneficial towards reducing texture, and tensile specimens fabricated using this algorithm achieved higher yield strength and tensile strength, but lower ductility. Interestingly, these mechanical properties observations are believed to be related to a reduced (10%) presence (for this X-Y scan strategy) of retained austenite which reinforces comments made in Section 4.2.1. Unfortunately, the authors don't specify the tensile specimens AM build orientation making it difficult to speculate further on the reported outcomes. Separately, Suryawanshi et al. [29] detected only weak fibre texture in the as-built condition and credited the absence of texture to their use of the X-Y strategy during build-up. They did, however, notice that some grains appeared to be orientated in the laser-scanning direction, which may be a result of melt-pool solidification behaviour, as discussed earlier in section 4.2.1.

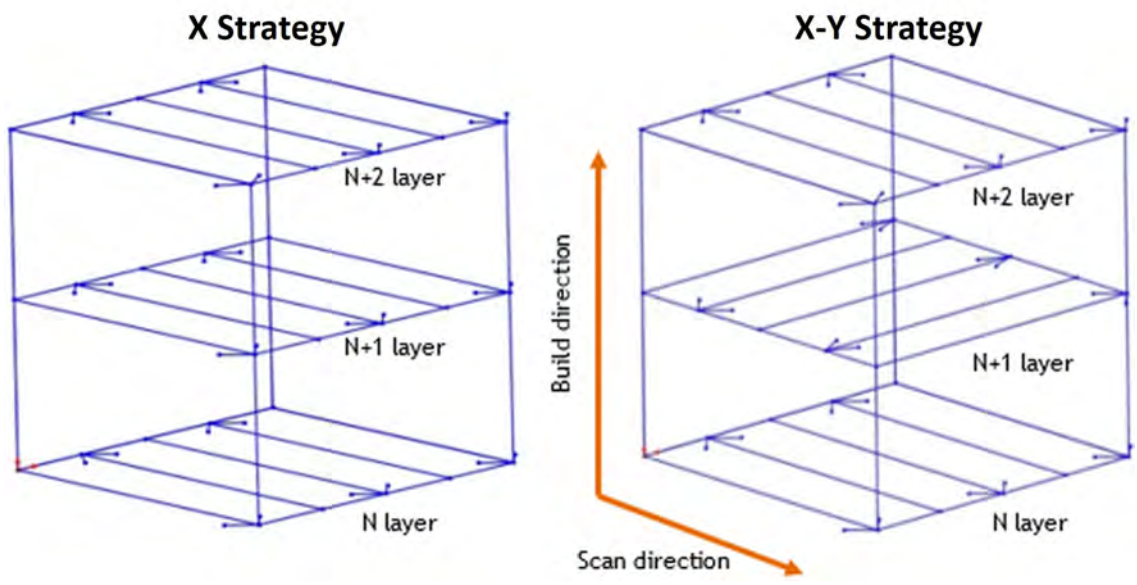

Figure 4.2: Showing the bi-directional (X) and cross-directional (XY) scan strategies used by Becker et al. [27] and Bhardwaj et al. [66] to compare the residual stress state, texture, and mechanical properties in maraging steel 300. 'N' represents an arbitrary build layer and subsequent layers are labelled 'N+1' and 'N+2'.

In contrast to Bhardwaj, Becker et al. [27], who determined near-surface residual stresses using the mechanical *Strain-gage Hole-drilling method* (HDM), discovered $\approx$ 40% higher magnitude stresses approaching yield strength (0.7 $\times R_{p0.2}$) in material that had been fabricated using the X-Y strategy. Moreover, the stresses observed were tensile in nature which is clearly a contradictory finding. The residual stress variation between literature studies suggests there is a need for more comprehensive investigation using appropriate evaluation techniques. Becker et al. [27] do comment that the stress distributions were non-uniform and inconsistent between specimens, and attribute this to the AM process's complex temperature gradients. Earlier work by Casavola et al. [95] employing HDM also observed high-magnitude tensile near-surface stresses (0.7 $\times R_{p0.2}$) in the as-built condition. It is worth noting, however, that one of the fundamental limitations of the HDM method - which relies on the accurate measurement of strains which are caused by localized stress relaxation on the outside of a shallow hole as it is introduced incrementally into the stressed material - is that small experimental errors in strain measurement translate into larger calculated residual stresses. Even in the as-built condition, maraging steel exhibits a high modulus of elasticity (E) ($\approx$160 GPa) and high hardness (Vickers Hardness $\approx$ 350 kg/mm^2), making it a difficult alloy to characterize by sensitive mechanical methods. Nevertheless, it is clear from these studies that the scan strategies play an important role in the development of residual stress and texture in the as-built material.

Maraging steel 300, however, is rarely used in the as-built state, and Becker et al. [27] account for the effectiveness of heat-treatment on residual stress relaxation. The authors demonstrated that by subjecting the material to a post-AM solution anneal, residual stress magnitudes could be relieved by up to 80% and the properties (now akin to those of CP-material) exhibited their most isotropic state (albeit with $\approx$26% reduction in yield strength). The evidence suggests that the solution anneal is undoubtedly effective in reducing the residual stress state, however, this superfluous process-step incurs additional processing cost and complexity and subtracts

from the overall maraging steel 300 AM appeal. As discussed in Section 2.4.1, an aging heat-treatment cycle is the natural route to enhance the alloy's strength capabilities. On its own, however, aging at moderate temperatures (e.g. 440-540°C) seems capable only to provide partial stress relief. Croccolo et al. [20] allege that the standard aging treatment of 6h at 490°C is particularly effective at reducing residual stresses in maraging steel 300, however, a lack of research knowledge regarding stress relaxation by cause of aging make its effectiveness inscrutable. In this context, better comprehension of the link between the alloy's aging heat-treatment and the suppression of factors such as texture and residual stress, which influence mechanical performance and property anisotropy, is required. Such a study could also incorporate alternative scan strategies and build orientations in its appraisal.

4.4 Mechanical properties

As previously noted, non-standardisation of machine-powder variable settings across the AM landscape leads to variations in the microstructural evolution, austenite retention, and presence of defects in fabricated parts. These issues, in conjunction with the use of a assortment of standard/non-standard test-coupon geometries (e.g. flat and cylindrical) and mechanical testing rates in the research literature, have resulted in a spread in the published monotonic properties of AM fabricated maraging steel 300. The influence of the AM build orientation is another aspect influencing the as-built performance of the alloy and requires further investigation. Moreover, a difference of opinion regarding the optimal aging parameters for installing strength and hardness suggests that there is a level of uncertainty with regards heat-treatment selection. For example, EOS (MS1 powder [12]) recommend an aging heat-treatment of 6h at 490°C, whereas Concept Laser (CL50WS powder [72]) and Renishaw (M300 powder [15]) suggest 6-10h at 540°C and 6h at 500°C respectfully.

4.4.1 As-built material properties

The tensile yield strength ($R_{p0.2}$) and elongation at break (A_t) values measured across thirteen (13) research studies conducted on maraging steel 300 are plotted in Figure 4.3 offering a better visualisation of the wide-spread variability observed. For reference, the values published by EOS in their material data sheet (MDS) for MS1 are included on the plot.

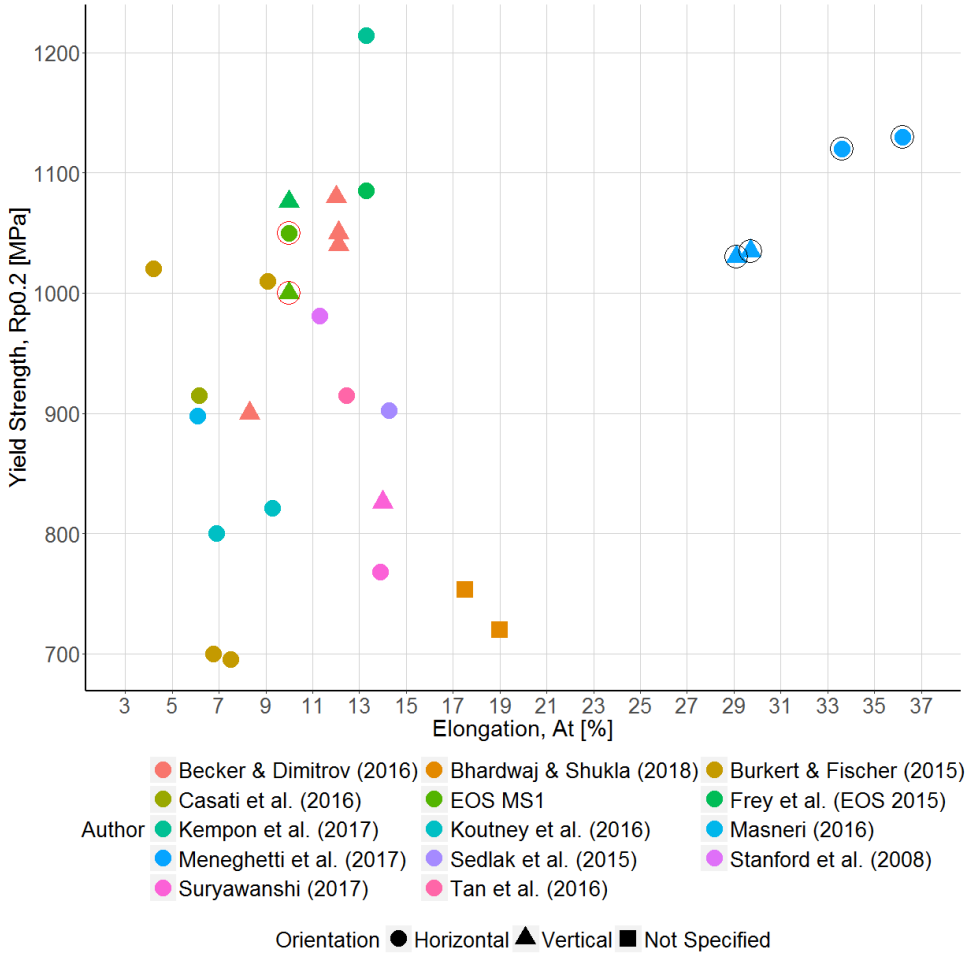

Figure 4.3: Comparison of the as-built yield strength ($R_{p0.2}$) and % elongation (A_t) properties by AM build-orientation for maraging steel 300 test-specimens fabricated using various geometries, processing parameters, scan strategies, and powder feedstock types. The red circled data points are the values published by EOS in their material data sheet for MS1 [12], while circled in black are properties reported by Meneghetti et al. [96]. Both of these groups highlight anisotropic as-built properties since values for the horizontal (circular symbol) and vertically orientated (triangular symbol) test-specimens do not overlap. The square shape symbol is used where the author has not specified the build direction of the tested parts.

As shown, both the EOS [12] data (circled in red) and Meneghetti et al. [96] data

(circled in black) - which report properties for horizontal (0°) and vertical (90°) build orientations - provide evidence that a certain stress and strain anisotropy exists in the as-built metal. There is, however, a lack of consensus between Meneghetti's reported tensile data and their concluding remarks where they comment that there is no difference in terms of mechanical properties between specimen build orientation. It is also worth noting that this particular study reports unusually high elongation properties for the as-built EOS MS1 as shown in Figure 4.3.

4.4.2 Aged material properties

Understandably, the quality of the as-built metal will govern its mechanical performance in the aged condition, and that various combinations of aging time and temperature will give contrasting mechanical properties outcomes in maraging steel 300. Yasa et al. [86] was the first openly published study to examine optimization of the aging heat-treatment of maraging steel 300. The study demonstrated how increased hardness, approximately 10% greater than the CP-alloy, could be achieved in the AM alloy. However, as-expected, ductility and toughness were markedly reduced to values lower than the CP-alloy (AM ductility: $\approx 1.5\%$ versus CP: $\approx 7\%$). Other authors also report lower ductility in the AM-processed and aged material [9, 25, 85, 86]. Casati et al. [9] rationalize AM's comparatively poor ductility and toughness by speculating that the retained austenite at cell boundaries is so fine and well-dispersed, that it prevents any sizeable toughening as further reversion takes place during aging. Certainly, studies covering the conventional welding of maraging steel relate poor weld toughness to high energy inputs which involve prolonged high-temperature exposure and slower cooling rates. This condition can lead to a coarse and segregated structure and encourages precipitation at grain boundaries and thus embrittlement [10].

In a continuation of the work by Yasa et al. [86], the same group of researchers [23] found the best aging parameters, in terms of developing optimum hardness, to be 5h at $480°C$. With this t, T combination, a hardness of 58 HRC was achieved.

Contuzzi et al. [22] accomplished comparable optimum hardness (57 HRC) in his brief conference article, but this was achieved after 15h at 500°C, whereas Mutua et al. [18] identified 5h at 460°C as their optimum.

Casati et al. [9] investigated the effects of a more expansive range of aging parameters (t, T) on the hardness of AM-processed maraging steel 300. The strengthening trend as a function of aging time for the various temperatures revealed the peak hardness for a given t, T combination. These peak conditions were then examined further on tensile test-specimens which were built in the horizontal (0°) orientation. The measured properties reflected the observed changes in the microstructure (i.e. increase in austenite with t, T). The maximum yield strength obtained ($R_{p0.2}$ = 1957±43MPa after 8h at 460°C) is comparable to the typical EOS MS1 achievable value, but EOS specify a different t, T combination ($R_{p0.2}$ = 1990±100 after 6h at 490°C).

It is evident that no two studies have identified an equivalent optimum aging cycle for strength/hardness in the AM-processed alloy. The variety suggests a scepticism about the most appropriate aging parameters, not only in terms of amassing strength and hardness (which has been the focus of these studies in the past), but also in identifying the best combination of t, T to embody ductility and toughness. When increased ductility is sought in MS1, EOS suggest an aging treatment of 6h at 525°C (-600°C) [97], however until now, there has been no published tensile data available for the appraisal of these aging parameters (either from EOS or the research literature). The formulation of a full and robust evaluation of the wide-scale heat-treatment and build orientation influences on the monotonic tensile properties of AM maraging steel, as presented in this study, is therefore much needed.

Anisotropy

The populous presence of blocking precipitates, as well as giving maraging steel outstanding strength and hardness in the aged condition, are also highly effective at concealing anisotropic mechanical behaviour. In that context EOS publish

isotropic data for MS1 in its aged condition [12]. However, a certain stress and strain anisotropy is evident in Suryawanshi et al. [29] and Meneghetti et al. [96] aged yield strength ($R_{p0.2}$) and elongation (A_t) experimental data which are presented in Figure 4.4. As before, this plot intends to highlight a large degree of mechanical properties variation observed within and between literature studies for maraging steel 300 which has been aged to achieve optimal strength. From the data presented, it is worth noting that Suryawanshi et al. [29] downplayed a strength difference (117MPa) between 0° and 90° build orientations as 'marginal', whereas a strain anisotropy of 5% was not highlighted by Meneghetti et al. [96]. Anisotropy can also be observed in Suryawanshi's crack-growth resistance results which show that vertical (90°) specimens display a slightly higher rate of crack-growth than horizontal (0°) specimens, however this too is not highlighted by the authors.

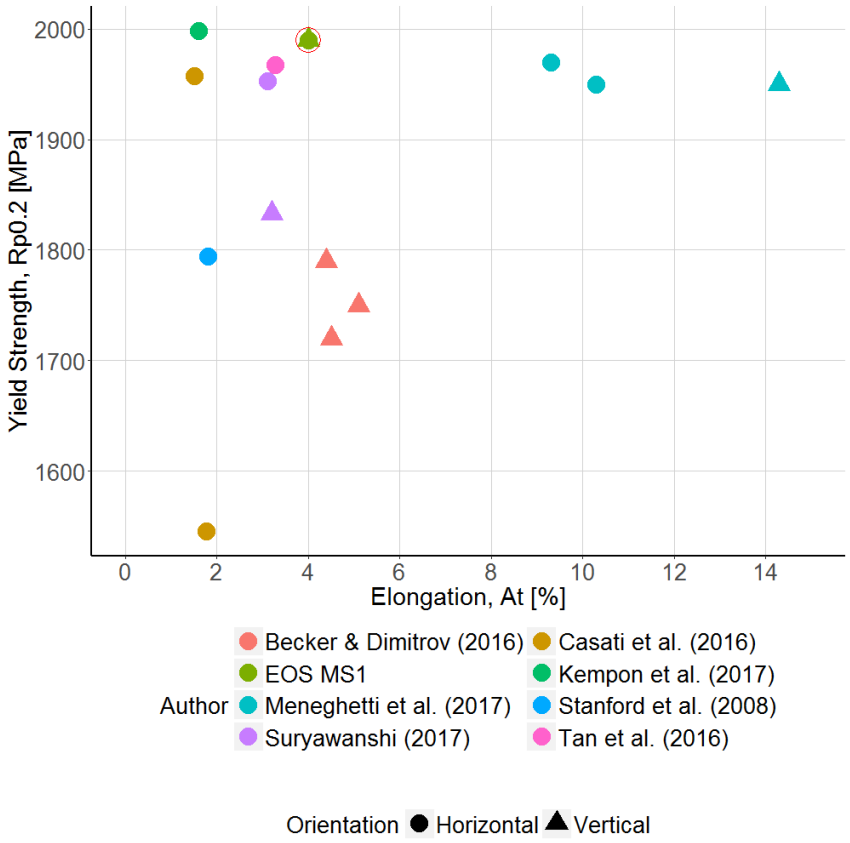

Figure 4.4: Comparison of the aged (for optimal strength) yield strength ($R_{p0.2}$) and % elongation (A_t) properties by AM build-orientation for maraging steel 300 test-specimens fabricated using various geometries, processing parameters, scan strategies, and powder feedstock types. Circled in red are the values published by EOS in their material data sheet for MS1 which indicate isotropic mechanical properties upon aging since horizontal (circular symbol) and vertically orientated (triangular symbol) specimen values overlap.

The direct comparison of stress versus strain ($\sigma - \epsilon$) behaviour between alternative build orientations (i.e. by superimposing the data on a plot) can provide very valuable information on the AM alloy's mechanical response, whereas on their own, the 'fixed value' properties derived from these plots may lead to anisotropic behaviour being overlooked. To-date, however, only one study by Meneghetti et al. [96] provides a visual insight into the anisotropic (elastic and plastic) maraging steel 300 material response by supporting the derived mechanical properties of horizontal and vertically orientated test-coupons with their corresponding superimposed $\sigma - \epsilon$ curves. In this study, both elastic and plastic anisotropy can be observed in the as-built alloy's $\sigma - \epsilon$ plotted paths, however as mentioned above, the derived mechanical properties do not effectively communicate this observation, nor was it highlighted by the authors. They recorded similar derived mechanical property values (elasticity modulus, yield strength, tensile strength and ductility) for specimens fabricated at alternative build orientations (0° and 90°) in both as-built and heat-treated material conditions. Upon aging, the tensile elastic anisotropy previously observed in the as-built $\sigma - \epsilon$ curves is largely reduced. Nonetheless, a slight strength difference between build orientations is reflected in the aged material's plastic response (i.e. between the material's yield point through failure.

Croccolo et al. [20] dedicated to reveal fatigue strength anisotropy in aged MS1 test-specimens grown at three different angles (0°, 45°, and 90°) between specimen's longitudinal axis and the build direction. This experimental study executed a robust fabrication process using the EOSINT M280 AM machine with supplier's (EOS) pre-optimised ParameterSet (*Performance 2.0 for MS1*) to manufacture standardized specimens which were then shot-peened, precipitation hardened (6h at 490°C), and shot-peened once more prior to finish-grinding. This cautious sample preparation sequence, plus the fact that the alloy had been aged to obtain peak strength, rationalizes the results achieved. No significant disparity was observed in the fatigue strength between build-orientations. Still, the 45° and 90° specimens displayed lower fatigue limits, albeit marginal (1.6%, 2.6%), than horizontal specimens. Residual

stresses may be a contributory factor here since it is known that they are positively correlated with increasing build height [94, 98], and suggests that through-thickness, property-altering, residual stresses may remain in the material after the prescribed EOS aging (6h at $490°C$) and shot-peening treatments.

5. Materials and Methods

5.1 Material and fabrication of test samples

Gas-atomized MS1 powder feedstock was used to fabricate test-coupons on two EOS *EOSINT M280* AM systems belonging and operated by different users, denoted as Supplier 1 and Supplier 2. The chemical composition of the raw-material is shown in Table 5.1, which corresponds to US classification 18 Maraging (300), German X3NiCoMoTi 18-9-5, and European 1.2709 [99]. In the same table, the results of the energy dispersive x-ray (EDX) analysis for the main comprising elements, conducted with a Hitachi SU 70 Scanning Electron Microscope (SEM) fitted with an *Oxford Instruments* EDX attachment, are also presented. A close agreement between the Supplier 1 and 2 SEM-EDX values and the EOS published values [12] for MS1 is observed, which also confirms that the powder material used is in line with the manufacturer's (EOS) specifications. A sample of Supplier 1's raw-material was provided, whereas the starting condition of the powder used to fabricated samples from Supplier 2 was not communicated. Supplier 1's sample, which came from a new batch of virgin powder, presented spherical particles typically measuring under $50\mu m$. The SEM morphology and particle size distribution, analysed using a *Malvern Morphologi G3* particle analyser, are shown in Figures 5.1a and 5.1b respectively. The observed median particle size was $36.69\mu m$, and had a standard deviation (SD) of $10.74\mu m$. The median particle circularity (deviation from a perfect circle, where perfect circularity = 1) was 0.956.

A rectangular-shaped tensile test specimen having uniform cross-section at gage and meeting the requirements of the ASTM-E8M standard [100] was selected to

Table 5.1: Chemical composition (%wt) of MS1, the 18Ni (300) grade maraging steel powder supplied by EOS (GmbH) [12] with SEM-EDX analysis results for the main comprising elements.

	Ni	Mo	Co	Ti	Al	Cr	Si	Mn	C	Fe
MS1 [12]	17-19	4.5-5.2	8.5-9.5	0.6-0.8	0.05-0.15	0-0.5	0-0.1	0-0.1	0-0.03	Bal.
Supplier 1-EDX	18.14	5.67	8.94	0.87	-	-	-	-	-	Bal.
Supplier 2-EDX	17.96	5.65	9.08	1.05	-	-	-	-	-	Bal.

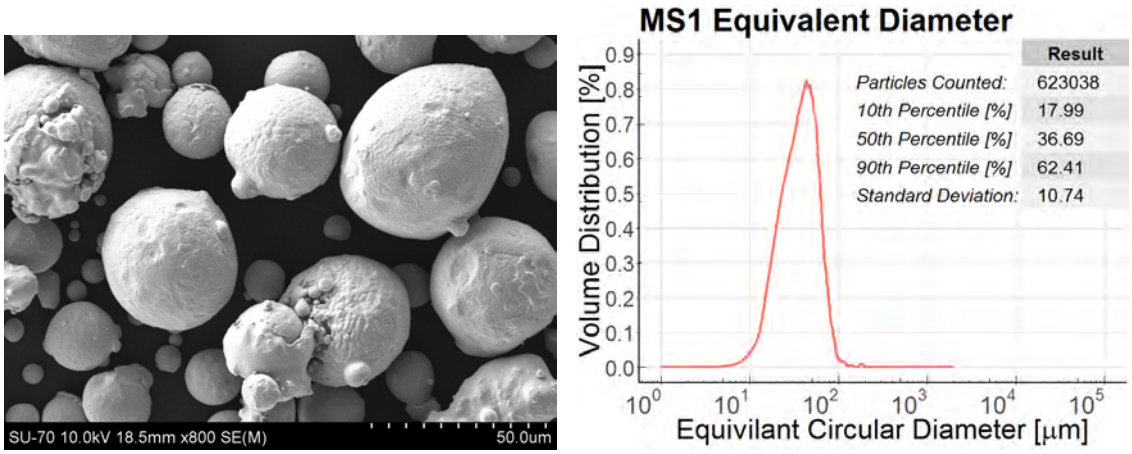

(a) (b)

Figure 5.1: (a) SEM morphology of the virgin MS1 powder, and (b) powder particle size distribution (circular equivalent diameter) with statistical details inset.

allow for both lateral and axial elastic and plastic strain measurements whilst under tensile loading. The finished specimen geometry, dimensions and tolerances are shown in Figure 5.2a. To investigate the influence of build orientation on property anisotropy, test-specimens were fabricated in the Y-Z build plane at three angles (0° (horizontal), 45° (inclined), and 90° (vertical)) between their longitudinal axis and the build platform, as shown in Figure 5.2b. Both EOS *EOSINT M280* systems were equipped with 200W Ytterbium-fibre laser shielded by Nitrogen and were fitted with the manufacturer recommended (for MS1) ceramic re-coater blade. A total of forty-eight (48) samples were fabricated by Supplier 1 (i.e. sixteen (16) test-pieces for each AM orientation) over three consecutive AM builds. Supplier 2 fabricated a smaller batch of twelve (12) samples (i.e. four (4) test-pieces for each AM orientation) in a single AM build.

Both machines were driven by the factory default, undisclosed, and pre-optimized set of parameters *'MS1 Performance 2.0'* which has been developed by the manufacturer for this specific material and machine combination [99]. EOS claims that

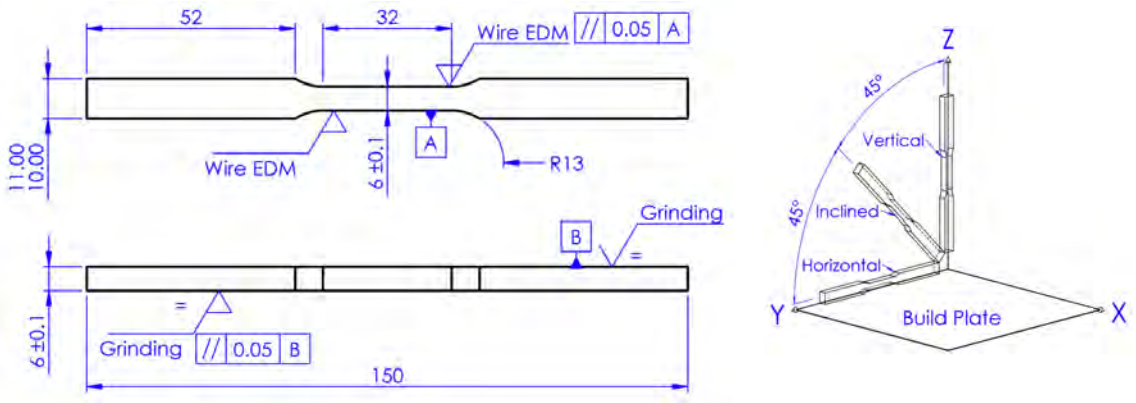

(a) (b)

Figure 5.2: (a) Showing the finish-machined specimen geometry, and (b) the AM build volume coordinate system and test-specimen build orientations.

their set of parameters (*MS1 Performance 2.0*) ensures reliable mechanical properties. This offers a defined part property profile bolstering industry-level repeatability and quality [101]. A vertical support-scaffold connected the under-side of each specimen to the manufacturer's recommended building platform (Steel 1.2083 36mm thick DirectBase TS36P) [99]. This structure played two important roles during the elevated temperature production cycle - (a) it functioned as a passive heat-sink during manufacturing; and (b) it reinforced the 45° inclined specimens against cross-platform re-coater forces and earthward gravitational forces. As shown in Figure 5.3, the AM build leaves visible ridges upon parts' build surfaces and a stair-stepped effect on 45° sloping surfaces which are indicative of the layered fabrication process. High roughness at the surface can augment crack initiation thus leading to premature failure. Furthermore, these ridges hinder the accurate evaluation of gage width and thickness dimensions. Ductility calculations are sensitive to the measurement of gage cross-sectional area, while the ASTM E8M standard exhorts that particular attention be given to the uniformity and quality of surface finish with regards high-strength specimens [100]. For these reasons, a machining allowance of 0.5mm was added to each specimens' face prior to the build to ensure that a uniform and high-quality surface finish, appropriate for the tensile testing of high-strength specimens, could be achieved. This surplus material, which was later machined by single-cycle precision computer numerically controlled (CNC) wire electrical dis-

charge machining (EDM) profiling and surface-grinding operations, had the extra benefit of safeguarding against potential thermally induced distortion.

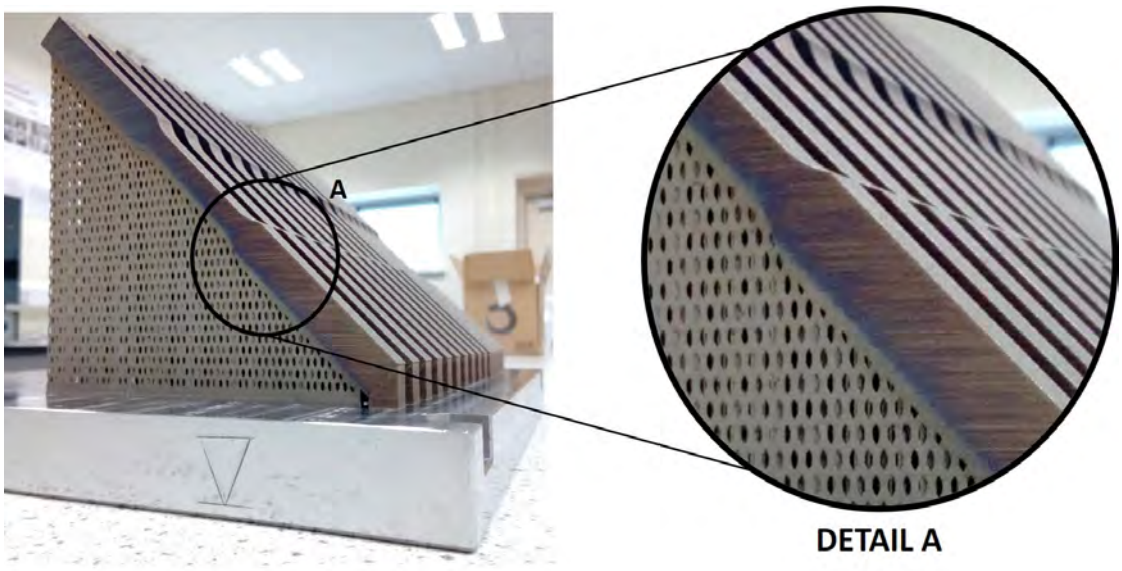

Figure 5.3: DMLS fabricated samples of the 45° build orientation before detachment of the support scaffold from the parts/build-platform. Detail A highlights the presence of distinct surface ridges which are consequent to the layer-wise fabrication process.

As verified by the post-build inspections, the process had achieved strong inter-layer and intra-layer metallic bonding, with a uniform and characteristic ridged surface. The parts were dimensionally accurate, however it is worth noting that a longitudinal shrinkage distortion (bowing) in the AM build direction (Z), to the extent of $\leq$ 0.1mm, was observed in several horizontal (0°) specimens after their removal from the build-plate. This shrinkage, which was rectified in the downstream machining operation, is understood to have been brought about by a build-up of thermal stresses developed between the raw-material and base-plate metal during the heating and cooling cycles over the opening number of layers.

5.2 Heat-treatment

The heat-treatment (aging) was performed in a pre-heated Elite Thermal Systems 120 litre 6kW heavy duty-fan oven (air atmosphere) controlled by dual Eurotherm 3216 PID temperature controllers and cooled slowly in still air at ambient temperature ($23°C$). The experimental heat-treatment plan is shown in Table 5.2, where T

denotes tensile tests and H the Vickers hardness measurements performed for a set of 0°, 45°, 90° specimens. The red font indicates the treatments which were applied to sets of specimens obtained from each M280 machine, and takes into account the EOS recommended heat-treatment for MS1, 6h at 490°C. The black font represents the balance of specimens obtained from Supplier 1. These experimental heat-treatments were selected to validate the EOS recommendations (discussed in Section 4.4.2); to formulate a comprehensive evaluation/comparison of static mechanical properties; and to allow for wide-scale investigation of the anisotropy variation.

Table 5.2: Showing the experimental heat-treatments applied to full-sets of test-specimens (i.e. 0°, 45°, 90°), where the characters *'T'* and *'H'* symbolize a tensile, and/or Vickers Hardness test campaign. The red font indicates the treatments which were applied to sets of specimens obtained from each M280 machine.

Temperature [°C]	**Aging time [hours,h]**											
	As-built	**1h**	**2h**	**3h**	**4h**	**5h**	**6h**	**8h**	**10h**	**12h**	**15h**	**16h**
As-built	T,H	-	-	-	-	-	-	-	-	-	-	-
460°C	-	-	-	-	-	H	T,H	T,H	H	T,H	-	H
490°C	-	-	-	H	T,H	H	T,H	T,H	-	H	-	-
525°C	-	-	-	H	T,H	H	T,H	T,H	H	-	H	-
540°C	-	-	H	-	T,H	H	T,H	T,H	H	-	-	-
600°C	-	T,H	T,H	H	T,H	H	T,H	H	-	-	-	-

5.3 Material characterization methods

5.3.1 Density

Archimedes' Principle density measurements were performed on as-built samples obtained from each DMLS machine, and for each build-orientation, using a *Sartorius Quintix* analytical balance which was fitted with accessory YDK03 density determination kit. The measurement procedure followed the guidelines present in the ASTM B962-17 [102] standard.

Metallographic samples were sectioned and mounted with Buehler Ltd. *PhenoCure* compression mounting compound, and standard finishing steps applied - including polishing with oil based monocrystalline diamond suspension (6μm and 1 μm), *MetaDi* from Buehler Ltd. In each case the sectioned plane was taken perpendicu-

lar to the materials tensile loading axis. Modified Fry's reagent (150mL H_2O; 50mL HCl; 25mL HNO_3; 1g $CuCl_2$) was used to reveal the microstructure which was observed via an *Olympus BX60* Optical light microscope, and *Hitachi SU 70* Scanning Electron Microscope.

5.3.2 Porosity

Porosity was examined via x-ray Computed Tomography (CT) scans, performed using a General Electric *VTOMEX L300, Nanotom S* instrument operating at 180kV, $80\mu A$, $250\mu s$ and with a resolution of $13.4\mu m$. Digital inspection of the porosity network, and a quantitative evaluation of the size and distribution of pores was completed using Thermo Fisher Scientific's *Avizo* software [103].

5.3.3 Hardness

The progress of the aging heat-treatment was evaluated using a *Zwick ZHV* Vickers macro-hardness tester which had been calibrated with a standard test block to the requirements of ASTM E92-17 [104]. Samples were sectioned, mounted, and polished, then indented with a 30kg test force applied perpendicular to the metallographic sample's sectioned plane (i.e. parallel to the AM material's tensile loading axis). Twenty (20) measurements were performed on each test specimen, and the results and test statistics were computed using the R statistical software package [105].

5.3.4 Microstructure

The material's crystal structures were qualitatively analysed (for selective heat-treatments) via a *PANalytical Empyrean Pro* multipurpose x-ray diffractometer (XRD) using Cu Kα radiation. Crystallographic phase identification was achieved using HighScore Plus software.

5.3.5 Mechanical properties

Uniaxial tensile tests were conducted at ambient temperature in a calibrated *Zwick/ Roell (Dartec) M1000/RK* servo-hydraulic closed-loop testing machine equipped with 100kN capacity load cell and fitted with ±100kN fatigue rated hydraulic wedge grips. The test procedure was fully compliant with the ASTM E8M standard [100]. Among other test requirements, this standard prescribes stressing/ straining/ displacement rates for deriving reliable and consistent mechanical properties data. The test was initially controlled (via a 9600 series controller) to the elastic stressing rate of 10.34 MPa/s, using strain control from the extension feedback channel (Epsilon model 3542-025M-050-ST). Upon detection of yield, the test-rate maintained a constant plastic strain rate of $6.25 \times 10^{-4}/s$ controlled via the stroke feedback channel. At the end of the yield (detected from either reaching a 5% increase in stress, or an absolute strain limit of 2%), the test-velocity was commanded by a third rate, the tensile strength (R_m) rate: 0.0068/s. This strain rate was maintained to peak force through failure.

Concurrently, a non-contact full-field displacement measurement was performed using *LaVision's* portable 3D Digital Image Correlation (DIC) apparatus [106]. The apparatus comprised of (i) two 12-bit Imager E-lite CCD-chipped cameras fitted with 35mm lenses, (ii) two gated white light sources each containing twelve linear-configured LEDs, (iii) a *StrainMaster* Controller and data-acquisition unit with integrated analogue-to-digital converter (A/D), and (iv) a dedicated PC complete with *StrainMaster*® processing software. The complete experimental configuration is illustrated in Figure 5.4 (each feature discussed in this section is indicated on this figure).

Each camera was focussed onto the measurement plane providing an overlap region upon the specimen gage surface. The enclosed angle between cameras and the working distance between each camera and the test-specimen was ≈20° and ≈350mm respectively. Using the stereoscopic camera system's in-situ position, a global 3D-coordinate system was derived by means of a precursory calibration step involving a

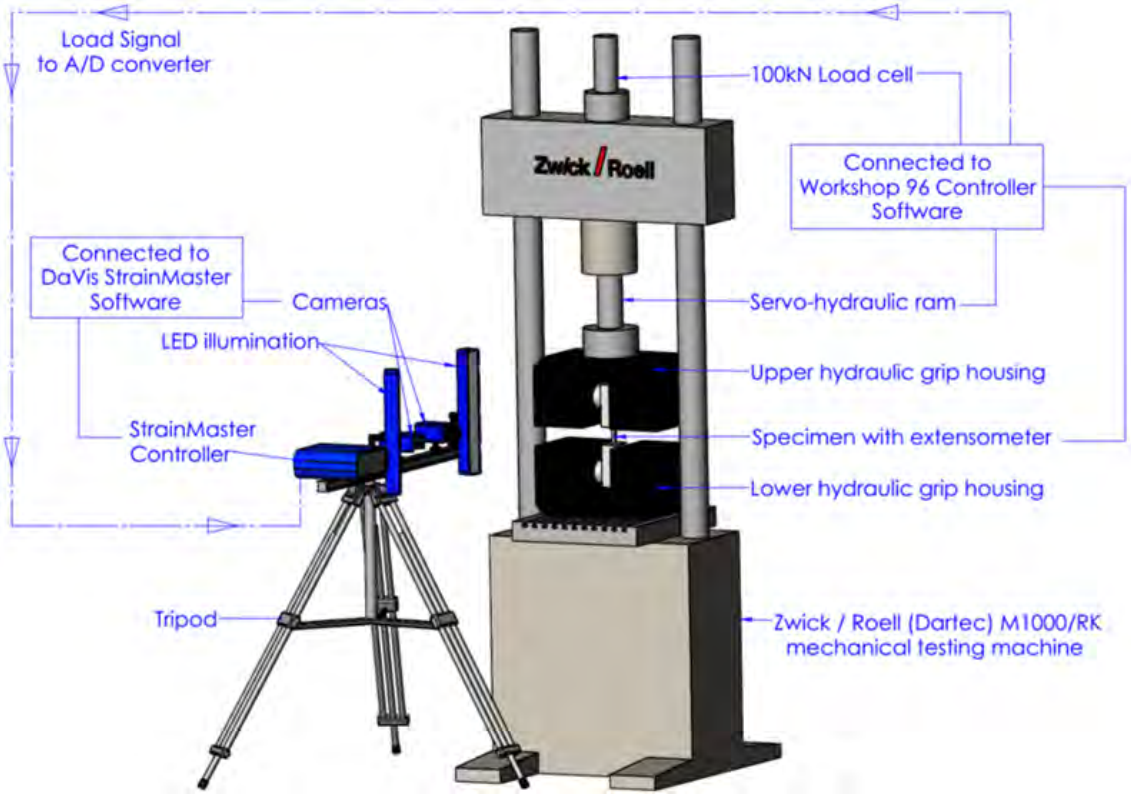

Figure 5.4: Configuration of tensile test set-up including the 3D Digital Image Correlation (DIC) apparatus which allowed concurrent determination of test-specimen width and axial strains.

3D two-level calibration target/plate. This included the generation of a fit mapping function with the calibration plate from which the average deviation of the de-warped calibration target positions to the ideal positions was lower than 0.3 pixel. This corresponds to an excellent fit, and an appropriate basis for the proceeding full-field 3D strain-measurement evaluations [107]. A high-contrast acrylic paint dark 'speckle' pattern (dark black speckles on a bright white background) was applied to the area of interest (i.e. the specimens' gage surface). Special attention was given to achieving a relatively fine pattern scale (for higher spatial resolution) with a non-repeating isotropic distribution. In this study, each subset (or "window") had an area of 37 pixels^2, which translated to approx. 1.75mm^2. The purpose of the speckle pattern is to provide a unique signature pixel arrangement from which the specimen's displacement field can be digitally tracked throughout the tensile test. A sequence of images was captured during each tensile test (i.e. from zero applied load to fracture) at a periodic rate of 5Hz. A displacement vector corresponding to each subset was calculated by the StrainMaster least squares matching algorithm from

a reference (un-deformed) image. The basic result of the DIC analysis was a full-field 3D displacement measurement evaluation containing thousands of measurement points. Poisson (ν) and plastic strain ratios (R-values) were calculated from the DIC determined strain data in accordance with ASTM test methods E132-04 [108] and E517-18 [109]. R-value is the ratio of true width strain (ε_w) to true thickness strain (ε_t), given by Eq. 5.1, with both strains calculated after tensile plastic flow was induced. The R-value was employed to quantify the strain plastic anisotropy (non-uniform transverse straining), which typically is anticipated in AM-fabricated parts.

$$R\ value = \frac{\varepsilon_w}{\varepsilon_t} \tag{5.1}$$

In turn, the individual test-specimen R-values (R_0, R_{45}, and R_{90}), are unified by the parameter ΔR which is used to quantify planar anisotropy (i.e. in the AM Y-Z plane) by Eq. 5.2.

$$\Delta R = \frac{1}{2}(R_0 - 2R_{45} + R_{90}) \tag{5.2}$$

6. Results and Discussion

6.1 As-built material microstructure and density

Representative micrographs are presented for the individual build orientations of parts obtained from each supplier in Figure 6.1. A distinct dissimilarity was observed in the microstructures of the sectioned vertically orientated (90°) parts. As shown in Figures 6.1c and 6.1f, different laser scan strategies were administered by each M280 system during the fabrication process, despite the fact that the MS1 Performance 2.0 set of parameters was used by both suppliers. Supplier 1 specimens were fabricated with a 67° line scan rotation between successive build layers, whereas Supplier 2 specimens display a 90° scan rotation. Other researchers [13, 30] have reported a layer-wise scan rotation angle of 67° when employing MS1 optimized parameters on similar EOS machines. Nevertheless, these limited literature-reported findings do not exclude the existence of strategies with other scan rotation angles (as found in this study).

For clarity, a schematic representation of the administered laser scan strategies for each M280 AM system is shown in Figure 6.2. The set of parameters (*MS1 Performance 2.0*) prescribed uni-direction line-scans with a laser hatch-spacing of $110\mu m$ in each case. The hatch-spacing and line-scan direction remained constant within each AM layer where each line-scan was segmented into stripe divisions of approximately 0.3mm-0.6mm, presumably to prevent excessive localized heat build-up during fabrication. The laser scan-direction was rotated for each consecutive layer as shown in Figure 6.2. The rotation is understood to be beneficial towards homogenizing the AM microstructure. However, the angle of rotation was different for Supplier

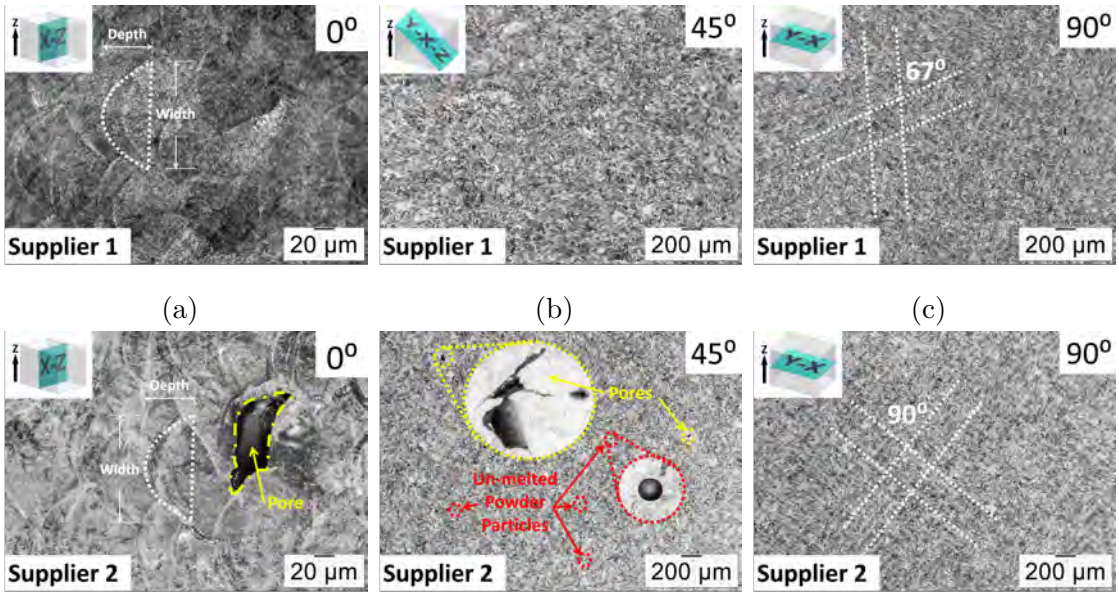

Figure 6.1: Representative optical micrographs of samples fabricated in three build-orientations on two EOSINT M280 systems (Supplier 1 and Supplier 2): (a) and (d) horizontal (0°); (b) and (e) inclined (45°); and (c) and (f) vertical (90°).

1 and 2 (i.e. 67° and 90° respectfully). The reason for this difference between AM systems is unknown, but is perhaps linked to the machines' service interval/history (e.g. through the system maintenance/ software upgrades).

The AM characteristic laser melt tracks and fan-shaped solidification cells are apparent at low magnification in Figures 6.1a and 6.1a. Comparable melt-pool proportions, which are reflective of the applied laser energy input (< 200W), can be observed in the horizontal cross-sections shown in Figures 6.1a and 6.1d. In particular, melt-pool depths 35-55μm corresponding to the applied 40μm layer thickness, and widths 45-70μm suggesting a laser focus diameter of $\approx$ 60μm, were observed. Larger laser focus-diameters (100μm) have been used with higher capacity AM platforms (laser power: 285W) administering equivalent layer-thickness [37]. Supplier 2 micrographs revealed persistent defects in the form of pores and un-melted powder particles as indicated in Figures 6.1d and 6.1e by dotted lines. In connection, inferior density was recorded for Supplier 2 specimens as reported in Table 6.1. Nonetheless, all the reported density values fall within the EOS quoted density range of 8.0-8.1 g/cm^3 [12]. The determined density values (Table 6.1) do not pro-

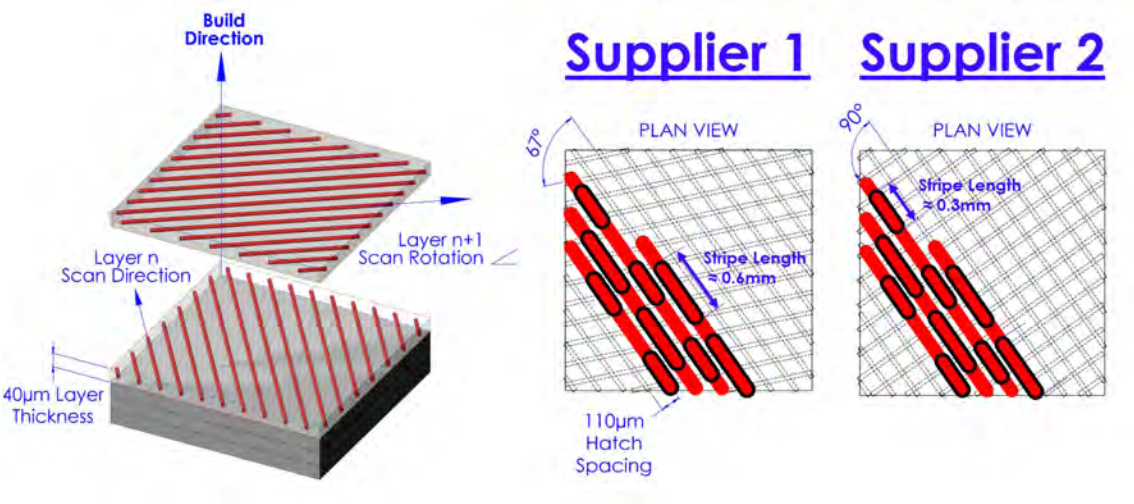

Figure 6.2: Schematic representations of the DMLS laser scan strategies which has been inferred from microstructural observations. Each layer's uni-directional line-scan was divided into short stripes of length 0.3-0.6mm to prevent excessive localized heating. However, a difference in the scan angle is observed for parts obtained from alternative suppliers.

vide sufficient evidence to suggest that part density is influenced by the AM build orientation, however, it is worth noting for the proceeding sections that the Supplier 2 horizontal samples, which exhibited a relatively high degree of porosity in their microstructures, also obtained the lowest overall density values.

Table 6.1: Comparing the density values of maraging steel 300 samples obtained from two EOS M280 DMLS systems for the as-built Horizontal (0°), Inclined (45°), and Vertical (90°) build orientations.

	Density, ρ (g/cm^3)		
	0°	**45°**	**90°**
Supplier 1	8.051	8.050	8.049
Supplier 2	8.028	8.031	8.034

It is believed that the observed microstructural defects (Supplier 2 samples) may be caused by the powder feedstock characteristics, which is consistent with the findings recently reported by Quinn et al. [84]. As discussed in Section 4.1, successive recycling and collection of powder granules following completed AM builds affects the feedstock's morphology, flow-behaviour, packing efficiencies and the interaction between the powder and the laser beam. These factors may have contributed to the porosities and un-melted particles which were observed in the Supplier 2 micrographs. It is, however, noted that the feedstock quality may not be solely responsible for the development of microstructural defects, as the role of the wider (90°) scan

rotation angle has to be examined as well (both separately and in conjunction with the powder quality). To that end, further work is recommended, to fully characterize the effect of alternative scan-strategies on the microstructural integrity and anisotropy of maraging steel 300 parts fabricated with the EOS machines.

Figure 6.3 presents typical high-magnification SEM micrographs for each build-orientation. As shown, the rapid melt-pool cooling rates give rise to various cellular morphologies including fine, coarse, and dendrite cell formations (highlighted on the images by dotted lines). The evolution mechanisms of these growth formations relate to the melt-region thermal flux direction which changes for successive layers and has been discussed in Section 4.2.1. Retained austenite is easily distinguishable in these high magnification images as the bright-colour phase which aggregates at cell boundaries. Also explained in Section 4.2.1, retained austenite occurs when the material cools rapidly from austenite finish (A_f) to ambient temperature, essentially freezing in place solute-rich austenite leaving it untransformed, whereas solute depleted austenite transforms into martensite. The as-built microstructures observed during this investigation compare visually with those reported in the literature [9, 23, 24, 42]

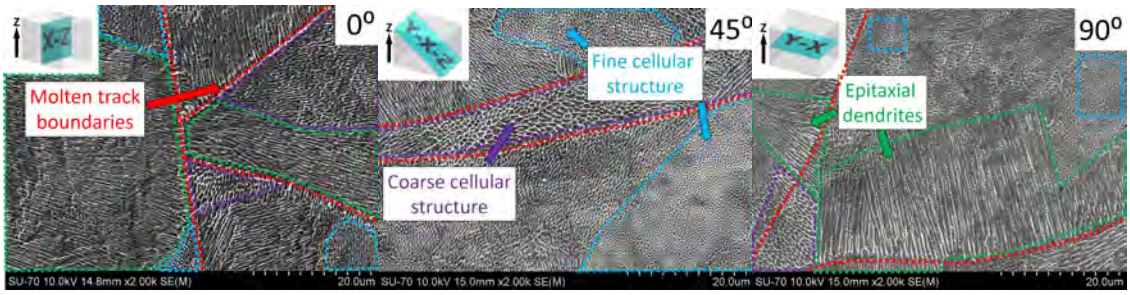

(a) (b) (c)

Figure 6.3: Representative high magnification as-built (SEM) cross-section images of the MS1 microstructure for three-build orientations: (a) horizontal (0°); (b) inclined (45°); and (c) vertical (90°). The SEM images reveal a mesostructure of circular and dendrite cells exhibiting retained austenite at cellular boundaries.

6.2 X-ray CT-scans

The porosity level observed in the Supplier 2 samples mandated a more comprehensive evaluation using x-ray CT-scans. Figure 6.4 presents histograms of the pore size distribution for all three build orientations examined in this study, while the re-constructed scans are presented in Figure 6.5. The scans were performed on as-built material surrounding the tensile specimens' fractured surface. The re-constructed CT-scans and porosity histograms indicate that there is an independent porosity variation due to part orientation within the build volume. The horizontal (0°) sample displayed a lower relative density, and a much greater proportion of larger pores when compared to the inclined (45°) and vertically orientated (90°) samples. The results suggest that the achievable relative density is a function of the powder's quality, and the part's build-platform projected area (i.e. layer-wise cross-sectional area), since the horizontal layers had a significantly larger build-platform projection and were therefore more likely to be affected by powder packing deficiencies during recoating.

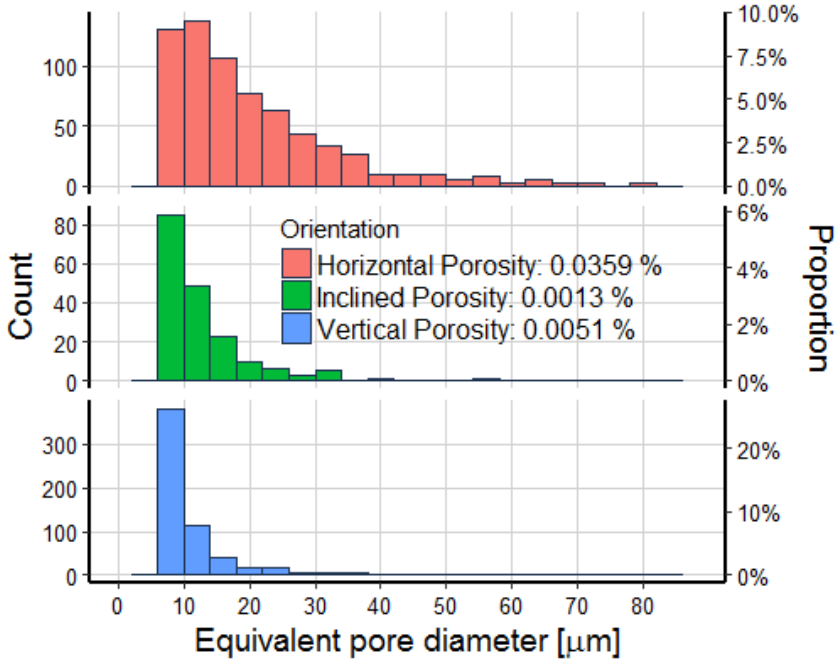

Figure 6.4: Histograms of the pore size distribution in the as-built maraging steel 300 alloy which has been fabricated in three AM build orientations: Horizontal (0°); Inclined (45°); and Vertical (90°).

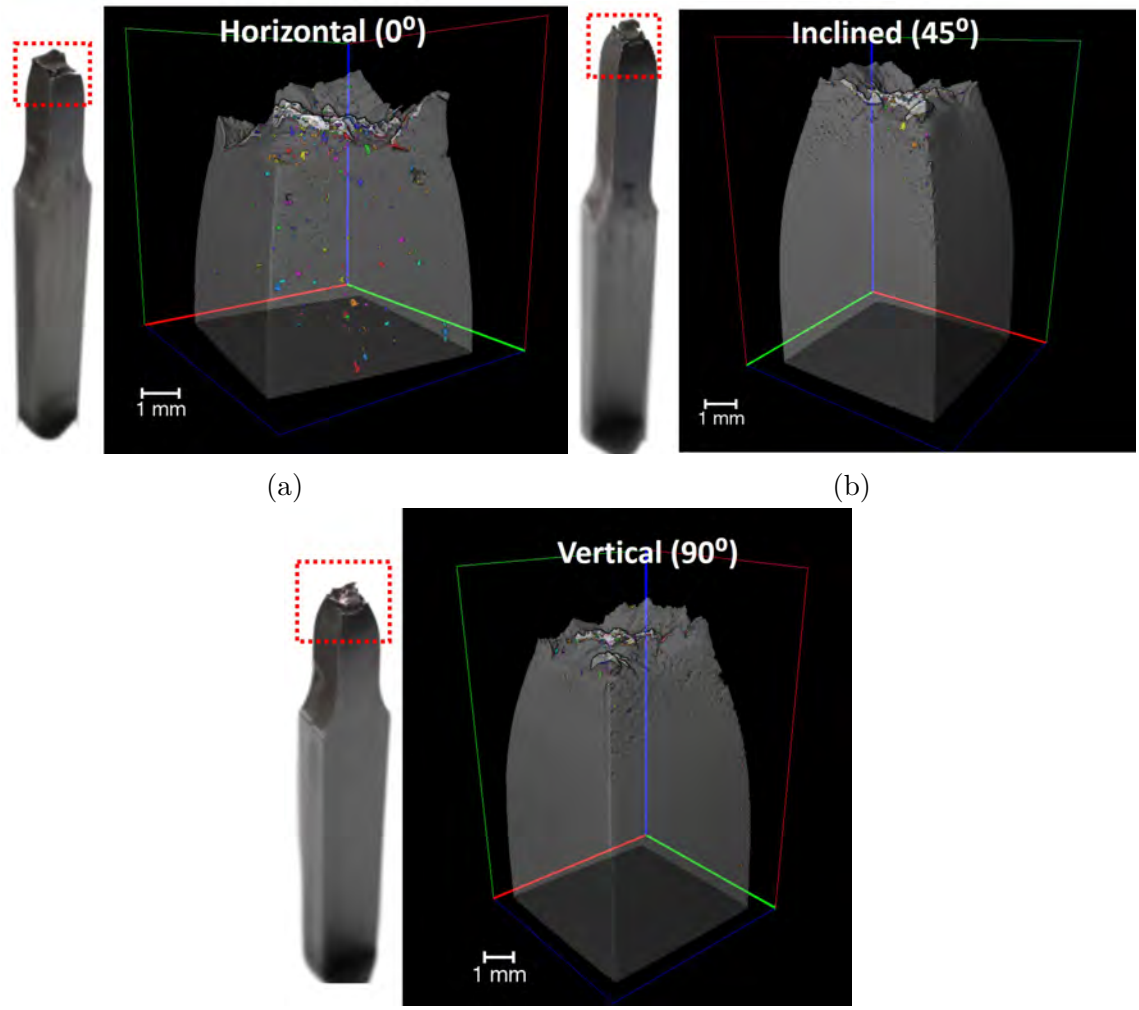

Figure 6.5: Transparent x-ray CT reconstructions showing micro-pores in a volume of DMLS as-built maraging steel 300 (Supplier 2) for build orientations: (a) Horizontal (0°); (b) Inclined (45°); and (c) Vertical (90°).

Although the horizontal (0°) sample exhibited a comparatively large degree of porosity, the relative density of the analysed volume of material remained higher than 99.96% which verifies the alloy's suitability for AM fabrication and welding [8–10]. It is also of note that each of the samples displayed a populous dispersion of sub $\varnothing 40\mu m$ sized defects which is an anticipated finding for this, previously stressed, material.

6.3 Aged material microstructure

Micrographs of the aged alloy, and their corresponding x-ray diffraction (XRD) spectra are presented in Figures 6.6, and 6.7, to demonstrate the effect of aging temperature on the reversion of metastable bcc martensite phase (Fe-α) to fcc austenite (Fe-γ). As explained in Section 2.4.1, the reversion occurs during extended isothermal aging at temperatures which support the dissolution of first-stage metastable Ni_3Mo and Ni_3Ti precipitates ($T > 450$°C). As new Fe_2Mo and/or Fe_7Mo_6 phases nucleate and grow during a second stage development they deplete the matrix of iron, further enhancing the Ni concentration, thus augmenting austenite reversion [4, 5]. At higher temperatures these nucleation sites quickly saturate by diffusion of solute elements from the surrounding lattice. This effect combined with early onset of precipitate coarsening (overaging), causes a reduction in the alloy's strength capabilities, i.e. a softening behaviour. Lower temperatures control/extend precipitate nucleation and growth, suppress austenite reversion, and allow a populous dispersion of small precipitates [4]. For these reasons, the milder aging cycle of 6h at 460°C presents a microstructure (Figure 6.6a) comparable in appearance to that of the as-built metal (Figures 6.3a, 6.3b and 6.3c). Moreover, there is no noticeable phase change observed in the XRD spectra of as-built and 6h at 460°C treatments. As observed in Figure 6.6, the austenite phase develops markedly at temperatures upwards of 490°C, where the bright cellular boundaries loose definition, and the volume fraction of the austenite phase readily increases. This is also reflected in the XRD data (Figure 6.7) where the intensities of Fe-α peaks reduce, and Fe-γ peaks increase with greater aging temperatures.

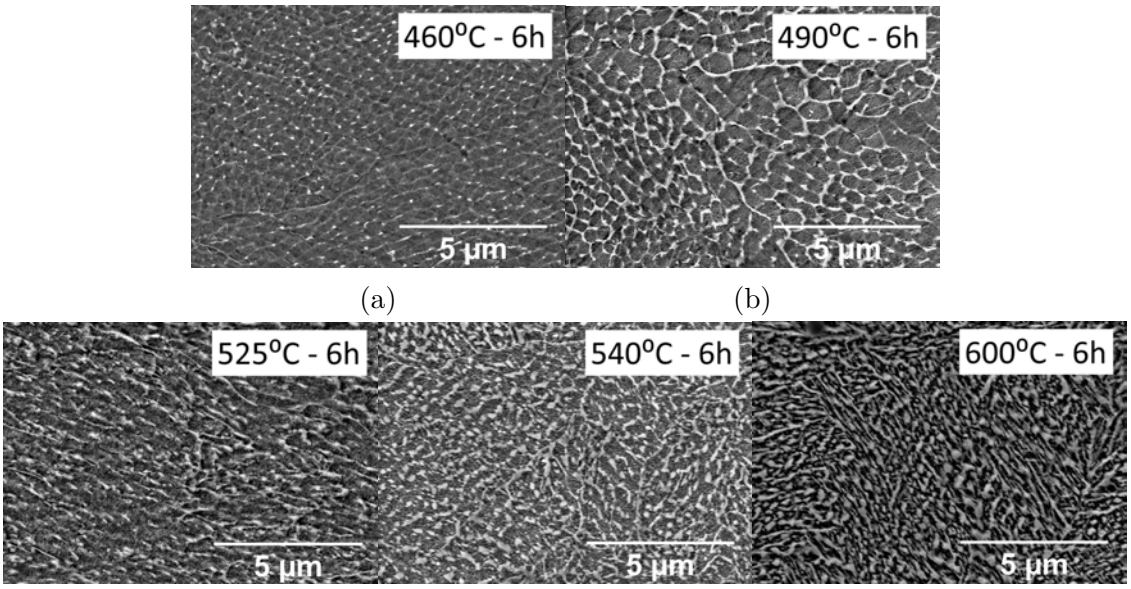

Figure 6.6: SEM micrographs of AM maraging steel 300 aged for 6 hours at various temperatures [(a) 460, (b) 490, (c) 525, (d) 540, (e) 600°C] showing a reversion of austenite at solute rich cell boundaries with increased temperature.

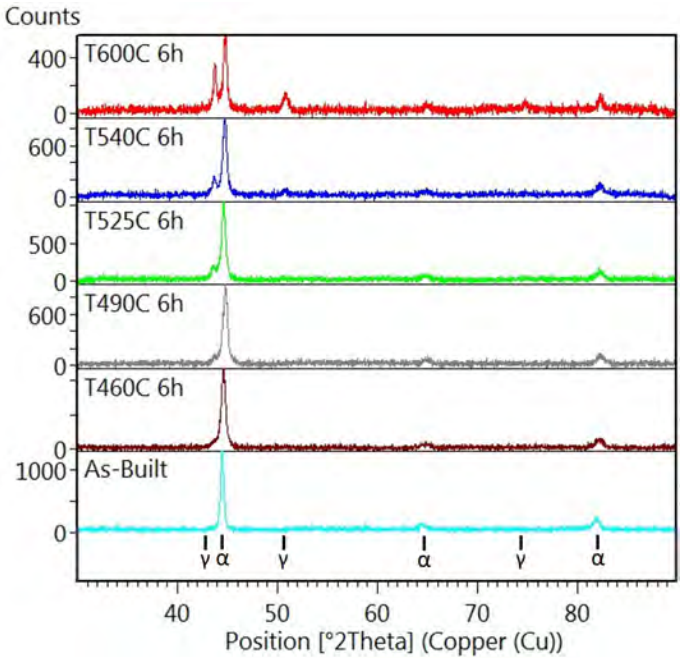

Figure 6.7: XRD spectra for DMLS MS1 as a function of aging temperature. The Fe-α and Fe-γ diffraction positions are highlighted on the plot.

6.4 Mechanical properties

6.4.1 Tensile properties and Vickers hardness

A selection of tensile stress (σ) versus strain (ϵ) curves and Vickers hardness aging curves comparing Supplier 1 versus Supplier 2 data are presented in Figures 6.8, and 6.9 respectively. A full record of the associated mechanical property tensile and hardness data, covering all of the treatments marked in Table 5.2 for both suppliers, is tabulated in Table 6.2. The data convey the extent of mechanical property variation across the as-built build-orientations, and the examined heat-treatments. Significant anisotropy, and an appreciable supplier related variation has been confirmed in both the as-built and aged maraging steel 300 stress-strain curves. In particular, the largest and most obvious strength and ductility divergence can be seen in the as-built inclined (45°) specimens' $\sigma - \epsilon$ curves. Although achieving a 218MPa (22%) superior yield strength ($R_{p0.2}$), the sample fabricated with 67° laser scan rotation (Supplier 1) displayed an unusual σ versus ϵ trajectory. As shown by the solid green curve in Figure 6.8a, an uneven material response during plastic deformation culminated in failure at $\approx 57\%$ less elongation (i.e. an overall reduction of 9.1%) when compared to the Supplier 2 specimen (dashed green curve), which had been fabricated with the 90° laser scan rotation. Remarkably, these samples have comparable hardness values, which indicates that hardness measurements alone can provide insufficient information for the assessment of mechanical properties. Likewise, when analysing the effect of heat-treatment on mechanical anisotropy, Table 6.2 and Figure 6.9 data indicate that hardness measurements are not effective towards revealing and quantifying mechanical anisotropy and helps to explain why similar observations have not been presented in the research literature to-date. Nonetheless, substantial anisotropy is evident in the as-built Vickers hardness measurements for both suppliers (i.e. in Figure 6.9 where the aging time is 0h).

As shown for the hardness measurements in Figure 6.9, even for the low aging temperature (460°C) the greatest percentage of the treatment's peak hardness is

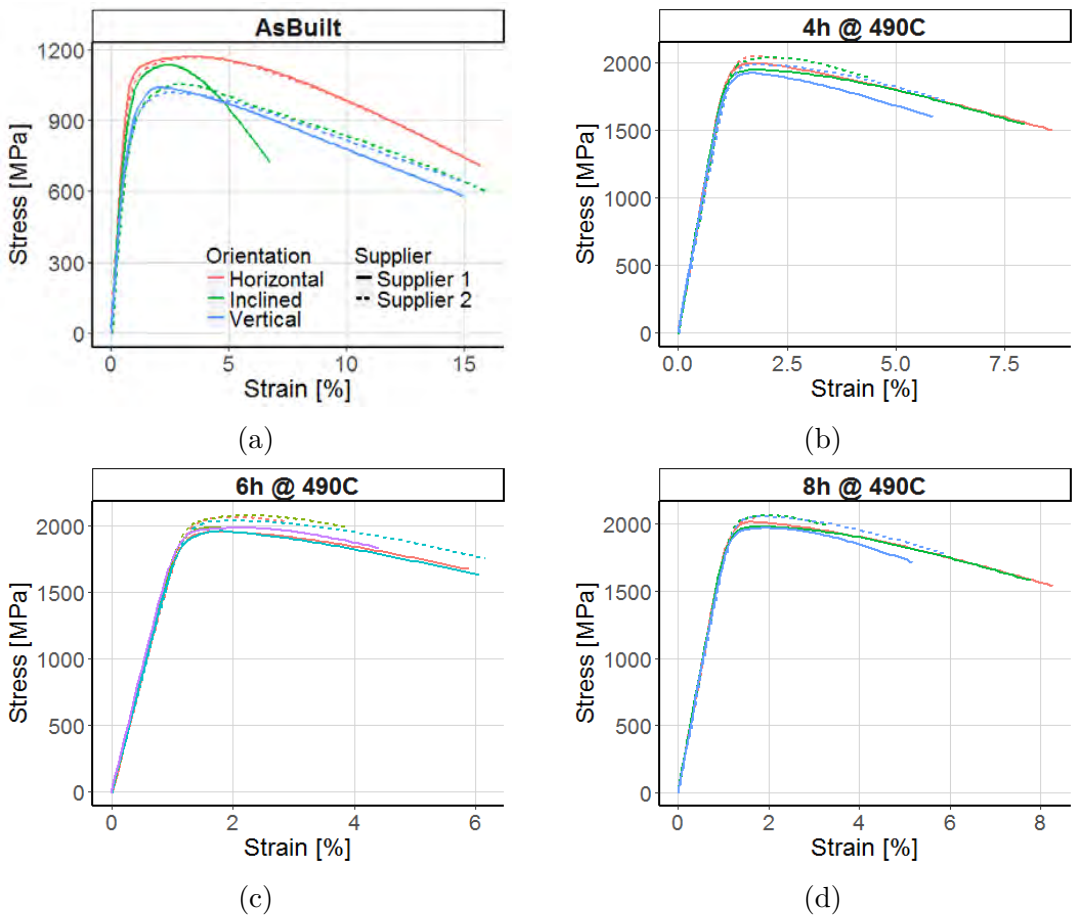

Figure 6.8: Stress (σ) versus strain (ϵ) curves comparing as-built and aged maraging steel 300 test-specimens which have been fabricated on two EOS EOSINT M280 AM machines belonging to and operated by different users.

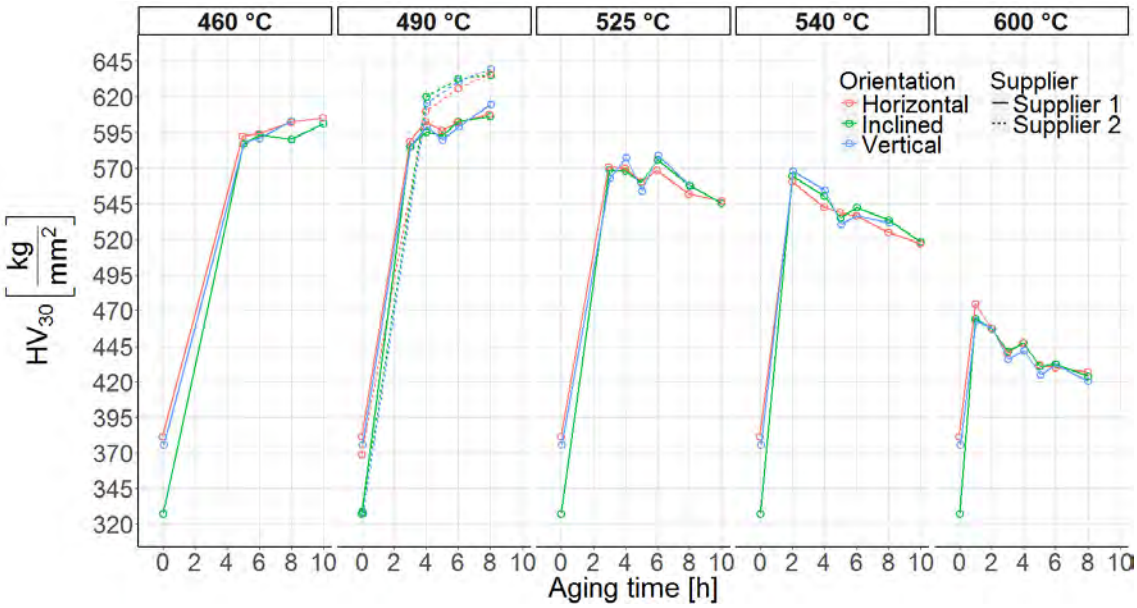

Figure 6.9: Precipitation strengthening curves demonstrating the effect of heat-treatment time and temperature parameters on the attainable hardness and anisotropy of AM MS1 fabricated on two EOS EOSINT M280 machines belonging to and operated by different users.

obtained within the early stages of aging (during underaging). The rate of early-stage hardening is due the populous development of small and coherent first-stage precipitates which shear the passing dislocations [4]. This lower temperature somewhat regulates early-precipitation diffusion kinetics allowing particles to grow by a greater extent before overaging dominates. For this reason, the greater population of particles at lower treatment temperatures provides an enhanced strengthening effect, however, as previously mentioned, the time taken to achieve peak strength/hardness increases alongside. Despite the narrow temperature window, and harmonious strengthening-relationship between $460°C$ and $490°C$, it takes 4h longer for the former to reach its peak-hardness condition.

Both sets of as-built samples exhibited a reduction in modulus of elasticity (E) with increasing build-orientation angle. This may be associated with the microstructural pattern developed during build-up of AM layers, since higher E is achieved when the loading direction is parallel to the build layers. AM's distinct three-dimensional (3D) microstructural pattern, visible in Figure 6.1's micrographs, is brought about by the layer-wise deposition of powder and continuous re-melting/heating of material beneath the melt-pool during build-up.

Overall, Supplier 1 aged specimens having been fabricated with a 67° layer-wise scan rotation and with defect-free microstructures showed higher stiffness and greater strength consistency between build orientations. However, the Supplier 1 group of as-built test-specimens displayed the largest variation across the full range of mechanical properties. For example, the mean and standard deviation (SD) Vickers hardness (HV) with respect to the build orientations was 362HV and 25HV in that order. The mean and SD yield strength ($R_{p0.2}$), and total elongation (At), were 984MPa (with $SD = 89$MPa) and 12% (with $SD = 4.7\%$) respectfully. Higher recorded hardness values were observed jointly in specimens aged at $460°C$ for 12h; and $490°C$ for 8h which measured 609HV (with $SD = 4$HV), and 609HV (with $SD = 5$HV) respectively. Greatest yield strength was 1936MPa (with $SD = 46$MPa) and tensile strength was 2006MPa (with $SD = 36$MPa) for the specimens aged at

460°C for 12h, but there was little mechanical property difference between the 12h at 460°C and 8h at 490°C heat-treatments.

However, as indicated by the aging and $\sigma - \epsilon$ curves, greater strength ($\approx$ 3%) and hardness ($\approx$ 4%) was achieved in the aged Supplier 2 specimens (aged at 490°C for 8h). As with Supplier 1 samples, the strength and hardness continued to rise when the material was aged past the EOS recommended 6h treatment duration. This strength and hardness ascension was accompanied by a reduction in ductility. While in this brittle condition, Supplier 2 samples displayed comparatively erratic and reduced ductility behaviour to those of Supplier 1. Correspondingly, this inferior ductility performance is attributed to the combined consequences of matrix embrittlement due to coarsened precipitates, and the presence of microstructural pores/un-melted particles, which jointly act as sites for crack nucleation [9, 13, 21, 28, 31, 68, 111].

When comparing the experimental mechanical properties against the EOS published data (Table 6.2), both as-built vertical (90°) parts underperformed in terms of elasticity modulus (≈19% lower), and yield strength (≈13% lower). Upon aging, the alloy gained remarkable strength (>87% increase) and hardness (>75% increase), and most mechanical property values fell within the EOS published confidence bands. This maraging steel 300 reflection demonstrates the outstanding effectiveness of the precipitate development towards obstructing and retarding the movement of dislocations in the lattice, but also towards suppressing anisotropic material behaviour. The aging curves show clear evidence of overaging when temperatures exceed 490°C, most noticeably at 600°C where the alloy is heated into the austenite phase transformation zone. This observed loss of hardness is based on Orowan's mechanism of dispersion hardening, where passing dislocations loop around larger and more dispersed stage-two Fe_2Mo and/or Fe_7Mo_6 precipitates [63, 112]. The effectiveness of dislocation hindrance in the overaged specimens is much reduced due to the combined loss of precipitate-lattice coherency, and the increasing sparsity of these blocking particles. Overaged specimens also displayed increased strain-hardening,

Table 6.2: Full set of experimental data retrieved from tensile and Vickers hardness testing of maraging steel 300 produced by DMLS on two EOS EOSINT M280 AM systems belonging to and operated by different users, denoted Supplier 1 and Supplier 2. Elasticity modulus (E); Poisson ratio (ν); Yield strength ($R_{p0.2}$); Tensile strength (R_m); Elongation to fracture (A_t); Reduction in area (Z); and Vickers hardness (HV). EOS reference data [12] are shown with italics fonts.

Data	Heat-Treatment	Orientation	E [GPa]	ν	$R_{p0.2}$ [MPa]	R_m [MPa]	A_t [%]	Z [%]	HV_{30kgf} [kg/mm²]
EOS	*EOS As-Built[12]*	*0°*	*160*±25	-	*1050*±100	*1100*±100	*10*±4	-	*(310-360)*
		90°	*150*±20	-	*1000*±100	*1100*±100	*10*±4	-	*(310-360)*[a]
	EOS Aged[12] 6h @ 490°C	*0°*	*180*±20	-	*1990*±100	*2050*±100	*4*±2	-	*(>513)*
		90°		-				-	
Supplier 1	As-Built	0°	161	0.24	1069	1174	15.7	56	382
		45°	140	0.29	991	1144	6.8	56	327
		90°	122	0.35	892	1057	13.8	62	375
	6h @ 460°C	0°	182	0.33	1961	2004	8.6	33	603
		45°	185	0.31	1895	1963	8.0	28	595
		90°	180	0.32	1875	1928	5.9	24	599
	8h @ 460°C	0°	182	0.33	1961	2004	8.6	33	603
		45°	185	0.31	1895	1963	8.0	28	595
		90°	180	0.32	1875	1928	5.9	24	599
	12h @ 460°C	0°	182	0.33	1961	2004	8.6	33	603
		45°	185	0.31	1895	1963	8.0	28	595
		90°	180	0.32	1875	1928	5.9	24	599
	4h @ 490°C	0°	182	0.33	1961	2004	8.6	33	603
		45°	185	0.31	1895	1963	8.0	28	595
		90°	180	0.32	1875	1928	5.9	24	599
	6h @ 490°C	0°	178	0.40	1901	1958	5.9	19	602
		45°	183	0.28	1925	1984	4.4	10	603
		90°	178	0.28	1893	1958	6.1	22	599
	8h @ 490°C	0°	183	0.34	1969	2020	8.3	32	608
		45°	184	0.29	1930	1993	7.8	29	606
		90°	180	0.32	1912	1978	4.2	21	615
	4h @ 525°C	0°	189	0.33	1811	1882	5.82	35	570
		45°	185	0.29	1811	1878	5.38	30	568
		90°	180	0.3	1797	1885	7.97	23	578
	6h @ 525°C	0°	181	0.34	1768	1844	10.4	32	560
		45°	175	0.32	1747	1818	6.9	29	560
		90°	176	0.31	1741	1816	8.5	31	554
	8h @ 525°C	0°	179	0.34	1729	1811	10.5	36	552
		45°	181	0.31	1714	1802	9.9	33	558
		90°	181	0.32	1723	1816	10.1	30	557
	4h @ 540°C	0°	181	0.34	1700	1769	10.4	37	543
		45°	183	0.32	1697	1778	10.2	38	550
		90°	169	0.30	1656	1744	9.3	33	554
	6h @ 540°C	0°	182	0.26	1661	1736	12.4	38	536
		45°	177	0.29	1666	1746	6.7	19	542
		90°	182	0.31	1640	1724	10.5	31	536
	8h @ 540°C	0°	182	0.31	1625	1701	11.2	41	525
		45°	177	0.29	1620	1705	11.5	37	534
		90°	174	0.31	1579	1666	10.8	33	531
	2h @ 600°C	0°	173	0.32	1326	1440	17.1	49	458
		45°	174	0.29	1312	1425	16.5	53	457
		90°	166	0.29	1290	1405	15.5	51	457
	4h @ 600°C	0°	169	0.31	1267	1387	17.2	49	447
		45°	167	0.27	1263	1382	16.7	49	447
		90°	164	0.30	1253	1368	16.0	49	442
	6h @ 600°C	0°	166	0.33	1214	1338	17.6	50	430
		45°	173	0.26	1211	1335	17.7	50	432
		90°	157	0.33	1172	1303	14.5	54	432
Supplier 2	As-Built	0°	150	0.34	1028	1172	12.9	43	369
		45°	136	0.33	773	1053	15.9	60	329
		90°	120	0.38	853	1035	15.1	60	328
	4h @ 490°C	0°	170	0.29	2006	2050	2.3	6	610
		45°	175	0.27	1977	2047	4.4	12	620
		90°	171	0.31	1929	1996	6.1	14	616
	6h @ 490°C	0°	174	0.30	2004	2070	2.9	7	626
		45°	179	0.31	2004	2080	3.9	5	633
		90°	172	0.34	1981	2047	6.2	21	631
	8h @ 490°C	0°	179	0.38	1998	2047	NA[b]	6	636
		45°	178	0.31	2013	2069	3.4	12	635
		90°	170	0.34	2005	2067	5.5	22	640

[a] Brackets indicate approximate hardness conversion numbers per Table 3, [110];
[b] Fracture occurred before end of yield was reached.

corresponding to the wider dispersion of particles whereby the build-up of subsequent gliding dislocation loops heighten the degree of back-stress in the lattice. The full set of stress (σ) - strain (ϵ) curves displaying this behaviour is provided in Figure 6.10. These overaged AM MS1 properties, not previously reported, may be useful to AM practitioners when good toughness is sought, as indicated by the area under the σ versus ϵ curves.

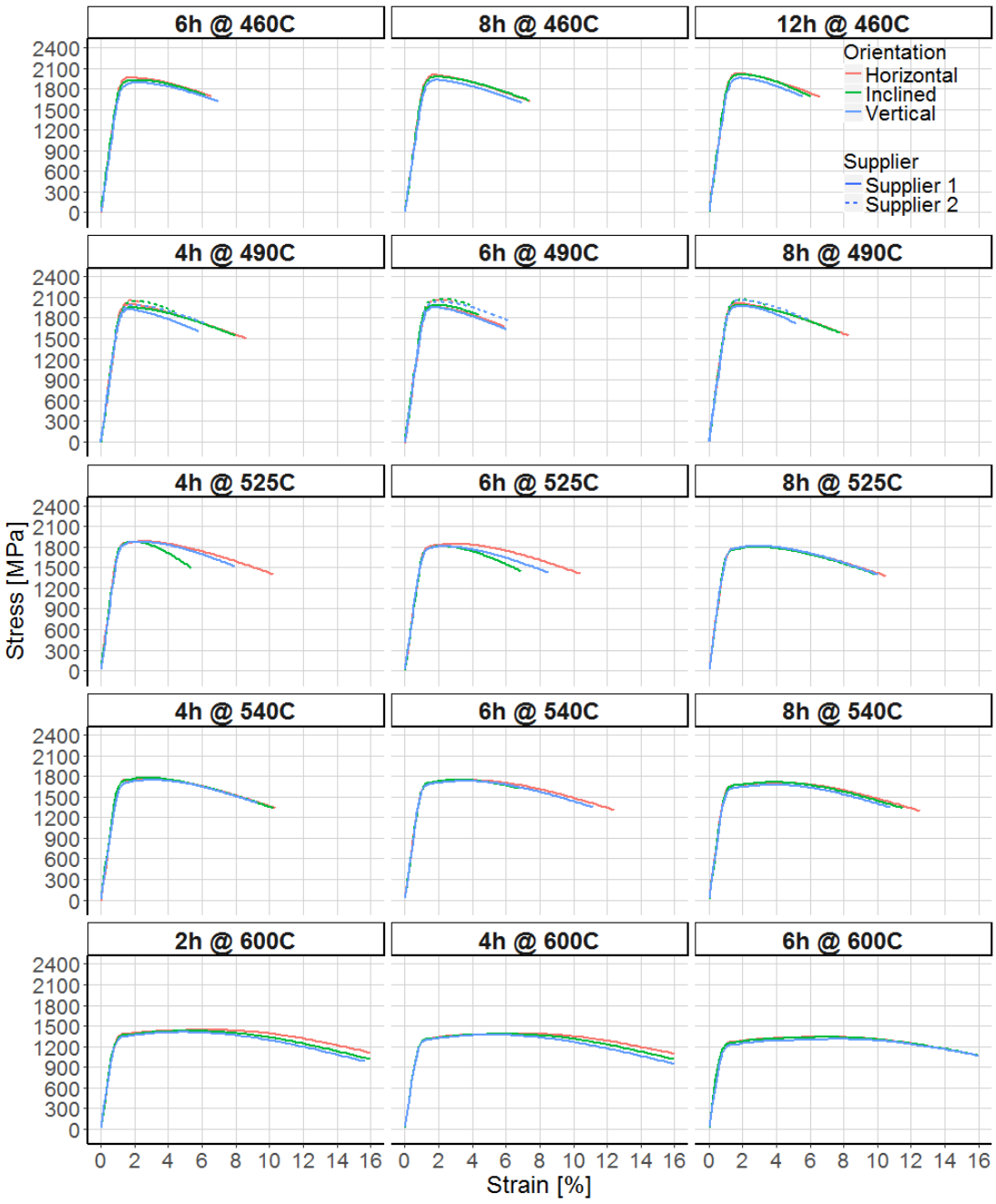

Figure 6.10: Full set of σ-ϵ curves obtained from aged test-specimens. Evidence of overaging (strength reduction) and increased strain hardening behaviour can be seen for this maraging steel 300 alloy as the heat-treatment temperature increases.

To compare the mechanical and anisotropic characteristics between the various heat-treatments, and between samples obtained from either supplier, a relationship between *hardness* (H) and yield strength ($R_{p0.2}$), which is based on similar empirical relationships used for other metals, was devised from the available test data. In particular, the typical linear rule-of-thumb for a broad range of metallic alloys given by Eq. 6.1 [113] has been used.

$$H \approx 3 \times R_{p0.2} \tag{6.1}$$

Where hardness (H), described as the indenter force divided by the projected area of the indent (in MPa) is determined by Eq. 6.2.

$$H = HV_{30} \times 9.81 m/s^2 \tag{6.2}$$

Where HV_{30} represents the Vickers hardness value. The experimental relationships presented in bar-chart form in Figure 6.11, demonstrate the extent of as-built stress anisotropy in the DMLS alloy due to supplier variation and part orientation, reinforcing prior anisotropy observations for the as-built and aged alloy across the range of experimental treatments. The most prominent discrepancies take place between as-built samples obtained from either supplier. This supplier related anisotropy variation may be attributed to the alternative scan strategies employed on either AM machine, and suggests that the scan rotation angle has a significant effect on mechanical anisotropy. Following the application of the aging heat-treatments, the degree of stress anisotropy is dramatically reduced by the presence of hard second phase precipitate particles [114], and Eq. 6.1 is satisfied. Nevertheless, the anisotropy developed during the fabrication process is not fully abolished following aging.

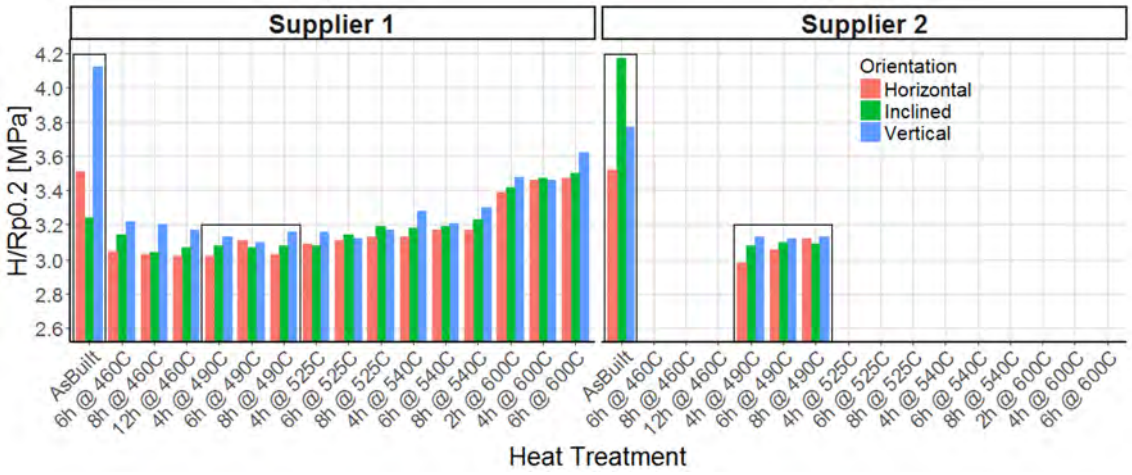

Figure 6.11: Ratio of Hardness (H) to Yield Strength for the as-built and heat-treated maraging steel 300 examined. Common heat treatment plans between Supplier 1 and Supplier 2 are framed (black rectangles) to facilitate easier comparison.

6.4.2 R-values

Further evaluation of plastic anisotropy has been performed via the DIC obtained R-value measurements (calculated using Eq. 5.1), for which a selection of the obtained results are presented in Figure 6.12. The plot confirms (i) the existence of non-uniform transverse straining since $R_{isotropic} = 1$; and (ii) the variation of R-value between AM build orientation angles. Greater R-value variation is observed in Supplier 1 as-built and aged specimens (solid lines) which have been fabricated with the 67° laser-scan strategy. The harmonious and significantly flatter trends observed in Supplier 2 specimens (dashed lines) indicate a uniformity of plastic strain behaviour between build angles and suggests that a 90° scan strategy provides a more homogeneous microstructure. As with the mechanical properties, a significant reduction in plastic strain anisotropy was observed following the application of aging heat-treatments. The precipitation of nanometric dislocation hindering precipitate particles is exclusively responsible hence. Regardless of the scan strategy, build orientation or heat-treatment, all AM fabricated specimens displayed R-values < 1 signifying greater thinning in specimen's thickness direction whilst under tensile loading. This suggests the dominance of a systemic process anisotropy which cannot be abolished simply by aging the AM fabricated alloy. Furthermore, the experimen-

tal findings indicate that the AM induced anisotropy cannot be eliminated through application of the EOS recommended 6h at 490°C heat-treatment. As mentioned previously (Chapter 1), this inherent anisotropy stems from (i) the layer-wise deposition of powder; (ii) planar movement of the heat-source; and (iii) uniaxial movement of the build platform during fabrication. To abolish any fabrication manifested microstructural patterning it may therefore be necessary to perform a solubilization treatment step prior to aging, incurring additional cost, complexity and processing time. This re-crystallisation step has been shown to homogenise the AM maraging steel 300 microstructure by replacing laser scan tracks and melt-pool solidification patterns with slender packets of parallel lath martensite through moderation of the alloy's solidification cooling rates [9, 18, 27, 31].

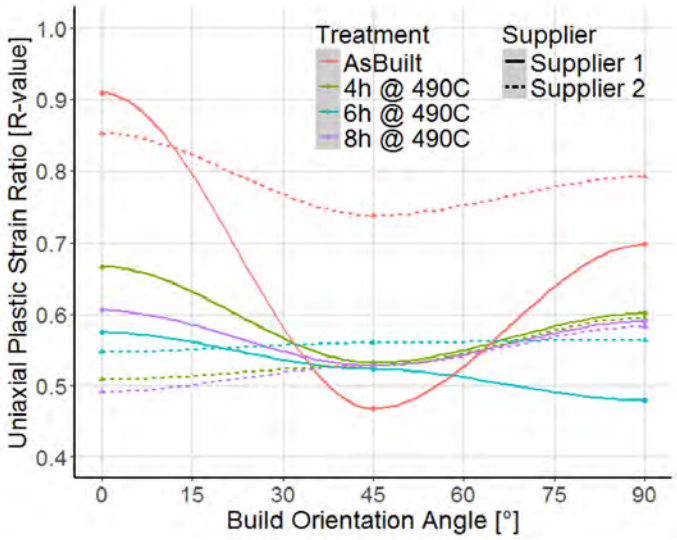

Figure 6.12: Plot of R-values versus build orientation angle, evaluated at 1.5% axial strain. The trend patterns for individual specimens are displayed using local polynomial regression fitting.

6.4.3 Contour maps of mechanical properties

The experimental results indicate that the 6h at 490°C heat-treatment plan is not optimal for the alloy's strength, ductility, hardness, or anisotropy. To address this issue, mean mechanical property values (with respect to the build orientations) from the complete set of experimental results (as outlined in Table 5.2) have been used to construct contour surface plots. In particular, the individual experimental values

were parameterised against the corresponding heat-treatment time and temperature values by implementing bi-variate interpolation onto a grid of the irregularly spaced data using akima interpolation [115]. A version of the akima algorithm which uses bi-linear spline interpolation was chosen for this purpose. This in turn permitted the representation of a smooth surface of z values distributed at assigned x (aging time) and y (aging temperature) grid positions. An equally spaced grid composing 100×100 tiles was selected to provide high resolution and contrast with later imaging functions. The akima algorithm's resulting structures were suitable for input into high performance imaging functions (ggplot2 [116]) using the R statistical processing software [105] - principally *raster*, which represents colour, and *contour*, which joins points of equal magnitude. This methodology was applied to each of the important response variables ($R_{p0.2}$, R_m, At, HV, and ΔR-values) to create the contour maps displayed in Figure 6.13.

The discrete time and temperature combinations at which the response variables have been experimentally evaluated are clearly marked on each of the the contour maps. It must be emphasised that the gradients in between these measurement points have been smoothly fitted to the data using the akima algorithm (spline interpolation), and are therefore not absolute values. While this form of interpolation uses low degree polynomials which help to minimise overfitting/modelling error, these plots should act as a guide rather than conveying definitive material outputs. The constructed contour maps can serve as a very practical tool in terms of tailoring the output of the EOS MS1 material either for research or part production purposes. For example, they can provide informed heat-treatment selection when particular mechanical properties and anisotropy limits are required for an AM part. Moreover, the contour maps can be further enriched with supplementary experimental data, in-turn increasing the reliability and validity of this heat-treatment selection tool.

Figure 6.13 clearly communicates that the chosen aging parameters correspond to significantly different achievable mechanical properties in DMLS MS1. Remarkable strength and hardness can be installed by underaging the alloy between 460-

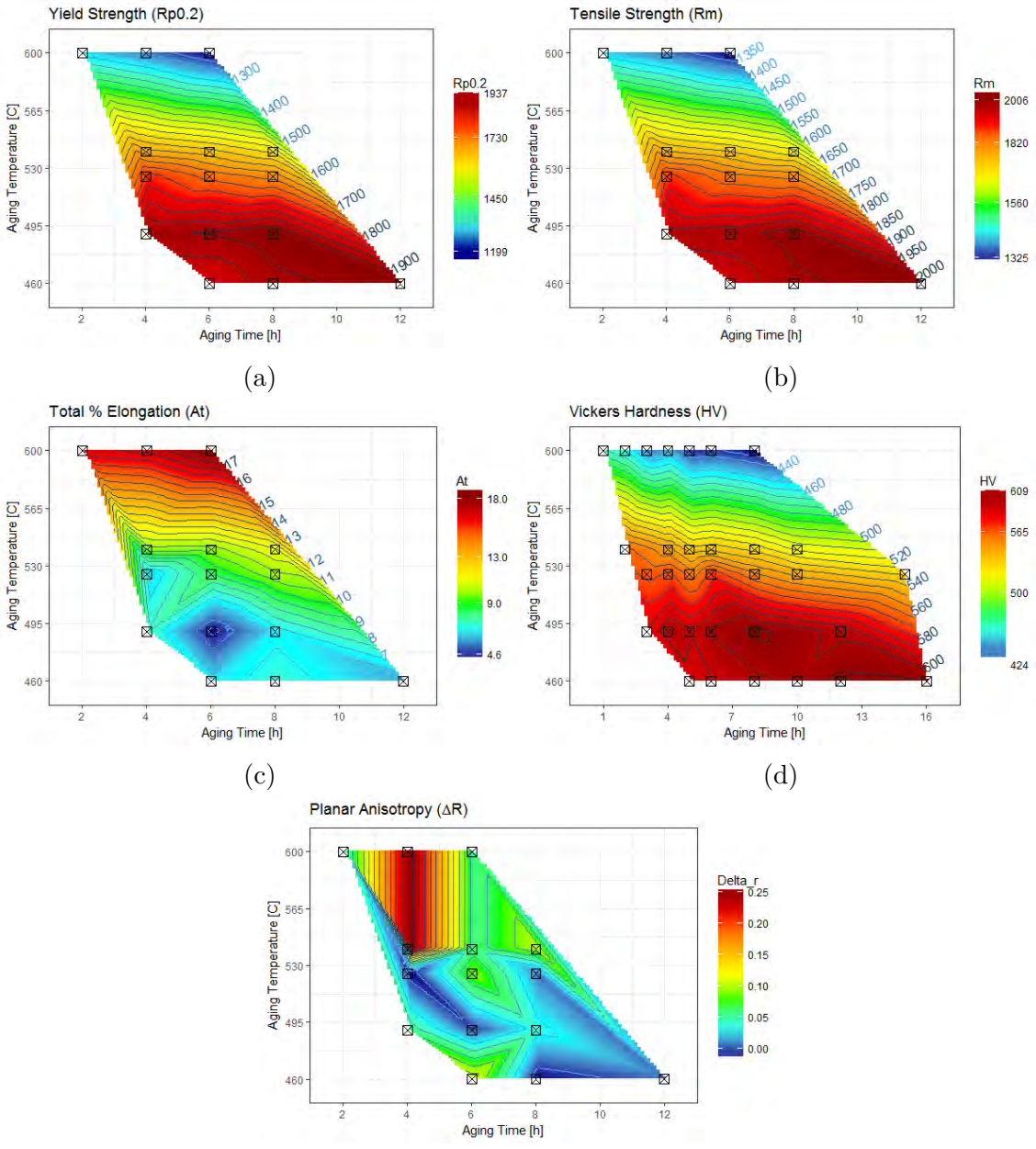

Figure 6.13: Interpolated smooth surface contour plots of experimentally determined (marked) AM MS1 properties (a) Yield strength ($R_{p0.2}$); (b) Tensile strength (R_m); (c) Total % Elongation (At); (d) Vickers hardness (HV); and (e) Planar anisotropy (ΔR) evaluated at 1.5% axial strain.

$525°C$ (see Figures 6.13a, 6.13b, and 6.13d), however, ductility (and toughness) are markedly reduced in this condition (see Figure 6.13c). When increased ductility is sought, the alloy can be aged at temperatures above $525°C$, though a loss of strength and hardness can be expected as overaging and austenite reversion rapidly take hold. The ΔR contour plot for R-values evaluated at 1.5% axial strain is shown in Figure 6.13e. ΔR, calculated using Equation 5.2, represents an overall measure of the variation of R-value in the Y-Z build plane (planar anisotropy) where for an isotropic material: $\Delta R = 0$. For AM materials, non-zero values of ΔR could be an indicator of preferred texture / alignment of the micro-structure due to the laser scanning pattern (especially in the distribution of second phases such as inclusions) / the presence of residual stresses [114]. The contour plot highlights that the range of ΔR variation is low across all treatments ($<$0.25 at 1.5% axial strain). Planar anisotropy is minimised in the underaged to peak-aged condition. It is understood that the populous presence of small precipitates effectively conceals non-uniform transverse straining by blocking gliding dislocations in this stiff and brittle condition. Comparatively, a greater degree of planar anisotropy can be observed in the overaged and austenitized material, where a lattice with fewer blocking obstacles, and a higher volume fraction of ductile Fe-γ, sees ΔR deviate from zero.

7. Conclusions

As AM technology continues to mature, more is expected of the functional parts produced, with special attention towards achieving metallurgical soundness by tackling the factors which influence mechanical performance. However, the deficit of process knowledge concerning such factors is forestalling the technology's widespread advancement into the engineering arena, since industrial entities seeking to produce high-value AM components which are destined for use in demanding engineering applications expect high-quality and consistent process outputs. Accordingly, this research study investigates inconsistencies in the mechanical characteristics and plastic anisotropy levels in identical EOSINT M280 fabricated maraging steel 300 (MS1) test-coupons that have been supplied by two AM facilities. The effect of three AM build-orientations (0°,45°, and 90°) on the as-built plastic anisotropy of these parts has been thoroughly examined, and the alloy's mechanical performance and plastic strain behaviour has been monitored through an array of strengthening heat-treatment plans to identify the combinations of time and temperature which can diminish anisotropy. In doing so, a broad collection of mechanical properties, material characteristics, and plastic anisotropy levels for these additively manufactured standard test-specimens have been evaluated and discussed in this novel experimental investigation. The important conclusions are summarized as follows:

1. Considerable anisotropy has been confirmed in as-built MS1;

2. Appreciable microstructural dissimilarities affecting mechanical performance and anisotropy have been observed in as-built maraging steel 300 samples obtained from alternative suppliers;

3. The AM laser scan strategy, and in particular the scan rotation angle between AM build layers, had a profound effect on the strength, ductility and anisotropy (transverse strain behaviour) developed in the as-built alloy;

4. Microstructural porosities and un-fused powder particles observed in one group of samples led to reduced plasticity and erratic fracture behaviours in aged samples;

5. The AM component's relative density is affected by unfavourable powder feedstock characteristics (size and morphology), and the part's cross-sectional projection onto the build-platform;

6. Plastic anisotropy can be reduced significantly through application of a dislocation hindering precipitation heat-treatment, however, a degree of transverse strain anisotropy is likely to remain due to the AM material's fabrication history;

7. The 6h at $490°C$ heat-treatment plan is not optimal in terms of strength, hardness, ductility and anisotropy properties for the DMLS MS1. A proposition of 8h at $490°C$ is offered where optimal design strength ($R_{p0.2}$ >1900 MPa) is sought, whereas the 8h at $525°C$ aging plan offers a good isotropic compromise between design strength ($R_{p0.2}$ >1700 MPa), and ductility ($A_t \approx 10\%$);

8. Heat-treatment parameters can be tailored to meet strength/ ductility/ anisotropy design requirements by using the obtained mechanical properties contour maps;

9. The relationships between the constructed contour maps, and in particular the connection of discrete data points regarding these, can serve AM engineers beyond acting as visualisation aids for heat-treatment selection. With some further development, these contour maps have potential usefulness as a predictive and interpretive tool for optimising the AM process output as well as informing the material selection process for mechanical component design;

10. The as-built and overaged specimens showed higher levels of planar anisotropy compared to that of the underaged and peak-aged condition;

11. Hardness measurements alone are not effective towards quantifying anisotropy in DMLS maraging steel 300.

8. Recommendations and Future Work

Some suggestions for future work are given as follows:

Influence of the feedstock quality and laser scan-strategies: An investigation into the influence of powder recycling on the presence of microstructural defects, and the mechanical and physical properties of maraging steel 300, has not been previously reported. Moreover, the condition of the starting material, in conjunction with alterations to the input variable of the laser scan-strategy (e.g. the intra-layer scan rotation angle etc.), has not been examined. These investigations are therefore proposed, and it is suggested to hold constant the (pre-optimized) process parameters of layer-thickness, scan-speed, hatch-spacing, laser-power etc. so that the input variables (powder quality, scan strategy) are exclusively responsible for the observed changes in the as-built material's response (i.e. the presence of microstructural pores and un-melted particles, and the alloy's mechanical and physical properties);

Suppression of as-built plastic anisotropy through parameter and scan strategy manipulation: Sufficient research knowledge exists on the process parameter selection which will enable the fabrication of near full-density ($> 99.9\%$) maraging steel 300 parts. However, as has been verified by this study, the use of alternative laser scan strategies will influence the fabricated part's plastic strain behaviour with respect to the AM build orientation. A study with the objective of minimizing the as-built plastic anisotropy in maraging steel 300, through laser scan strategy manipulation, is therefore suggested. This optimization study could use the same experimental methodology as the current work (tensile testing in conjunc-

tion with DIC displacement analysis) to harvest tensile and plastic strain data from as-built samples fabricated at 0°, 45°, and 90° build orientations. Following this, the planar anisotropy data obtained from the individual scan strategies examined, could be visualised using interpolated contour maps similar to those presented in Section 6.4.3. Indeed, a series of contour plots could be produced from the obtained dataset covering a range of tensile plastic straining (e.g. 1.5 - 10%), thus providing clear understanding of as-built material's plastic anisotropy characteristics due to scan strategy manipulation;

Retained Austenite: A complimentary extension of the above-mentioned investigations would include accurate quantifications of the percentile volume of retained austenite in the as-built microstructure. As highlighted in Section 4.2.1, the laser scan strategy is suspected to affect the volume of retained austenite in AM processed maraging steel 300, and this phase has an ancillary effect on the achievable mechanical properties in the aged condition. Thus, the correlation between the volume of retained austenite and the achievable pre and post heat-treated mechanical properties is also recommended;

Residual stress and texture: It has been identified in Section 4.3.3 that the influence of the laser scan strategy on preferred texture generation and the as-built residual stress state in maraging steel 300 remains an open question requiring detailed quantitative analyses through employing appropriate and accurate evaluation techniques. Furthermore, it is not clear whether the alloy's typical heat-treatment parameters are capable to suppress texture and residual stress in the aged material. To that end, a dedicated experimental study reporting on these critical matters, and their influence on the anisotropic mechanical behaviour of the fabricated part, is suggested;

Mapping and optimisation of the mechanical properties: The interpolated contour maps presented in the current work (Figure 6.13) provide a means of tailor-

ing the material outputs (mechanical properties and anisotropy) through informed heat-treatment selection. A follow-up research project is suggested for the development of a mechanical properties' optimization tool for AM engineers in industry, research centres and academia working with maraging steel 300. This tool, which would require the development of a mathematical model, computer code and software application, would draw from a database of experimentally determined material properties and characteristics, and be used to tailor the output of the AM process. Using this predictive tool in conjunction with the data collected from studies such as this, and from investigations performed by the wider AM community (e.g. test data gathered by other investigators using EOS AM technology globally), would allow AM engineers to tailor the alloy's mechanical properties and performance outputs (e.g. strength, ductility, and anisotropy etc.) based on known and experimentally verified input variables (e.g. process parameters, scan-strategies, and heat-treatments etc.). Furthermore, the tool could be extended later to include other aspects influencing mechanical performance - such as the scan strategy influences (i.e. residual stress, texture) - as this data becomes available. A generalised methodology, applicable to other AM metals, is expected as an additional outcome of this research.

References

[1] J.R. Davis, ed. *Alloying: Understanding the Basics*. ISBN: 978-0-87170-744-4. Ohio, USA: ASM International, 2001.

[2] A.M. Hall and C.J. Slunder. *The Metallurgy, Behaviour, and Application of the 18-percent Nickel Maraging Steels*. Survey 20000828 057. SP-5051. NASA, 1968. URL: http://www.dtic.mil/dtic/tr/fulltext/u2/a382105.pdf (visited on 09/01/2017).

[3] M. Stanford, K. Kibble, M. Lindop, D. Mynors, and C. Durnall. "An investigation into fully melting a maraging steel using Direct Metal Laser Sintering (DMLS)". In: *Special Edition Metal Forming Conference 2008*. Metal Forming Conference. Vol. 2. 79. 2008, pp. 847–852.

[4] Wei. Sha and Zhanli. Guo. *Maraging Steels, Modelling of Microstructure, Properties and Applications*. ISBN: 978-1-84569-686-3. Cambridge UK: Woodhead Publishing, 2009.

[5] ASM International. *ASM Handbook Volume 4: Heat Treating*. Vol. 4. Ohio USA: ASM International, 1991.

[6] F. Tariq, N. Naz, and Rasheed A. B. "Effect of Cyclic Aging on Mechanical Properties and Microstructure of Maraging Steel 250". In: *Journal of Materials Engineering and Performance* 19.7 (Oct. 2010), pp. 1005–1014. ISSN: 1544-1024. DOI: 10.1007/s11665-009-9583-7. URL: https://doi.org/10.1007/s11665-009-9583-7.

[7] L. M. Kleiner and Yu. N. Simonov. "Structure and properties of low-carbon martensitic steels". In: *Metal Science and Heat Treatment* 41.8 (Aug. 1999), pp. 366–368. ISSN: 1573-8973. DOI: 10.1007/BF02474887. URL: https://doi.org/10.1007/BF02474887.

[8] Eric A. Jägle, Zhendong Sheng, Liang Wu, Lin Lu, Jeroen Risse, Andreas Weisheit, and Dierk Raabe. "Precipitation Reactions in Age-Hardenable Alloys During Laser Additive Manufacturing". In: *JOM* 68.3 (Mar. 2016), pp. 943–949. ISSN: 1543-1851. DOI: 10.1007/s11837-015-1764-2. URL: https://doi.org/10.1007/s11837-015-1764-2.

[9] R. Casati, J.N. Lemke, A. Tuissi, and M. Vedani. "Aging Behaviour and Mechanical Performance of 18-Ni 300 Steel Processed by Selective Laser Melting". In: *Metals* 6.9 (2016). ISSN: 2075-4701. DOI: 10.3390/met6090218. URL: http://www.mdpi.com/2075-4701/6/9/218.

[10] F.H. Lang and N. Kenyon. *WRC Bulletin: Welding of Maraging Steels*. Technical Report 159. USA: Welding Research Council, 1971.

[11] EOS. *Materials for Metal Additive Manufacturing*. EN. Electro Optical Systems, 2017. URL: https://www.eos.info/material-m (visited on 10/28/2017).

[12] EOS. *EOS MaragingSteel MS1*. Material data sheet EOSINT M280 EOSINT M270. Weil: Electro Optical Systems (EOS), 2011. 6 pp. URL: http://ip-saas-eos-cms.s3.amazonaws.com/public/1af123af9a636e61/042696652ecc69142c8518dc772dc113/EOS_MaragingSteel_MS1_en.pdf (visited on 06/22/2017).

[13] D. Croccolo, M. De Agostinis, S. Fini, G. Olmi, F. Robusto, K.S. Ciric, A. Vranic, and N. Bogojevic. "Fatigue Response of As-Built DMLS Maraging Steel and Effects of Aging, Machining, and Peening Treatments". In: *Metals* 8.7 (2018). ISSN: 2075-4701. DOI: 10.3390/met8070505. URL: http://www.mdpi.com/2075-4701/8/7/505.

[14] M. Frey, M. Shellabear, and L. Thersson. *Mechanical Testing of DMLS Parts*. White Paper. Electro Optical Systems (EOS), 2015. URL: http://www.fabricadeprototipos.com/links/DMLS/link2_ensaiosmecanicos.pdf.

[15] Renishaw. *Maraging steel M300 powder for Additive manufacturing*. Data sheet. UK: Renishaw, 2017. 2 pp. URL: http://resources.renishaw.com/en/download (visited on 07/04/2018).

[16] G. Casalino, S.L. Campanelli, N. Contuzzi, and A.D. Ludovico. "Experimental investigation and statistical optimisation of the selective laser melting process of a maraging steel". In: *Optics and Laser Technology* 65 (2015), pp. 151–158. ISSN: 0030-3992. DOI: https://doi.org/10.1016/j.optlastec.2014.07.021. URL: http://www.sciencedirect.com/science/article/pii/S0030399214002011.

[17] Sabina L. Campanelli, N. Contuzzi, and Antonio D. Ludovico. "Manufacturing of 18 Ni Marage 300 Steel Samples by Selective Laser Melting". In: *Advances in Materials and Processing Technologies*. Vol. 83. Advanced Materials Research. Trans Tech Publications, Jan. 2010, pp. 850–857. DOI: 10.4028/www.scientific.net/AMR.83-86.850.

[18] J. Mutua, S. Nakata, T. Onda, and Z.C. Chen. "Optimization of selective laser melting parameters and influence of post heat treatment on microstructure and mechanical properties of maraging steel". In: *Materials and Design* 139 (2018), pp. 486–497. ISSN: 0264-1275. DOI: https://doi.org/10.1016/j.matdes.2017.11.042. URL: http://www.sciencedirect.com/science/article/pii/S0264127517310730.

[19] K. Monkova, I. Zetkova, L. Kučerová, M. Zetek, P. Monka, and M. Daňa. "Study of 3D printing direction and effects of heat treatment on mechanical properties of MS1 maraging steel". In: *Archive of Applied Mechanics* (May 2018), pp. 1–14. ISSN: 1432-0681. DOI: 10.1007/s00419-018-1389-3. URL: https://doi.org/10.1007/s00419-018-1389-3.

[20] D. Croccolo, M. De Agostinis, S. Fini, G. Olmi, A. Vranic, and S. Ciric-Kostic. "Influence of the build orientation on the fatigue strength of EOS maraging steel produced by additive metal machine". In: *Fatigue and Fracture of Engineering Materials and Structures* 39.5 (2016), pp. 637–647. ISSN: 1460-2695. DOI: 10.1111/ffe.12395. URL: http://dx.doi.org/10.1111/ffe.12395.

[21] T. Burkert and A. Fischer. "The effects of heat balance on the void formation within marage 300 processed by selective laser melting". In: *International Solid Freeform Fabrication Symposium*. TX: University of Texas, 2015, pp. 745–757. URL: http://sffsymposium.engr.utexas.edu/sites/default/files/2015/2015-61-Burkert.pdf (visited on 11/25/2017).

[22] N. Contuzzi, S. Campanelli, G. Casalino, and A. Ludovico. "Effect of Heat Treatment on Selective Laser Melted Steel Parts". In: *Annals of DAAAM for 2010 & Proceedings of the 21st International DAAAM Symposium*. Ed. by B. Katalinic. 21 vols. 1. Vienna, Austria, EU: DAAAM International, 2010, pp. 1–2. ISBN: 978-3-901509-73-5. URL: www.daaam.info/Downloads/Pdfs/proceedings/...2010/24802_Symp_1_head.pdf (visited on 08/28/2017).

[23] K. Kempen, E. Yasa, L. Thijs, J.-P. Kruth, and J. Van Humbeeck. "Microstructure and mechanical properties of Selective Laser Melted 18Ni-300 steel". In: *Physics Procedia* 12 (2011). Lasers in Manufacturing 2011 - Proceedings of the Sixth International WLT Conference on Lasers in Manufacturing, pp. 255–263. ISSN: 1875-3892. DOI: http://dx.doi.org/10.1016/j.phpro.2011.03.033. URL: http://www.sciencedirect.com/science/article/pii/S187538921100112X.

[24] D. Koutney, L. Panteljev, J. Tomes, and D. Palousek. "Comparison of selective laser melting of 18NI maraging steel by PXL and M2 cusing". In: *MM (Modern Machinery) Science Journal* (6 Dec. 2016), pp. 1590–1596. DOI: 10.17973/MMSJ.2016_12_2016191. URL: http://www.mmscience.eu/december-2016.html (visited on 11/29/2017).

[25] C. Tan, K. Zhou, X. Tong, Y. Huang, J. Jing, W. Ma, F. Li, and T. Kuang. "Microstructure and Mechanical Properties of 18Ni-300 Maraging Steel Fabricated by Selective Laser Melting". In: *6th International Conference on Advanced Design and Manufacturing Engineering (ICADME 2016)*. Atlantis Press, 2016, pp. 404–410. URL: http://www.atlantis-press.com/php/download_paper.php?id=25862785 (visited on 08/19/2017).

[26] J. Sedlak, D. Rican, M. Piska, and L. Rozkosny. "Study of Materials Produced by Powder Metallurgy Using Classical and Modern Additive Laser Technology". In: *Procedia Engineering* 100 (2015). Part of Special issue 25th DAAAM International Symposium on Intelligent Manufacturing and Automation, 2014, pp. 1232–1241.

[27] T.H. Becker and D. Dimitrov. "The achievable mechanical properties of SLM produced Maraging Steel 300 components". In: *Rapid Prototyping Journal* 22.3 (2016), pp. 487–494. DOI: 10.1108/RPJ-08-2014-0096. eprint: https://doi.org/10.1108/RPJ-08-2014-0096. URL: https://doi.org/10.1108/RPJ-08-2014-0096.

[28] R. Casati, J. Lemke, and M. Vedani. "Microstructural and Mechanical Properties of As Built, Solution Treated and Aged 18 Ni (300 grade) Maraging Steel Produced by Selective Laser Melting". In: *La Metallurgia Italiana* (2017), pp. 11–20. URL: http://www.aimnet.it/la_metallurgia_italiana/2017/gennaio/Casati.pdf (visited on 11/08/2017).

[29] J. Suryawanshi, K.G. Prashanth, and U. Ramamurty. "Tensile, fracture, and fatigue crack growth properties of a 3D printed maraging steel through selective laser melting". In: *Journal of Alloys and Compounds* 725.Supplement C (2017), pp. 355–364. ISSN: 0925-8388. DOI: https://doi.org/10.1016/j.jallcom.2017.07.177. URL: http://www.sciencedirect.com/science/article/pii/S0925838817325537.

[30] S. Yin, C. Chen, X. Yan, X. Feng, R. Jenkins, P. O'Reilly, M. Liu, H. Li, and R. Lupoi. "The influence of aging temperature and aging time on the mechanical and tribological properties of selective laser melted maraging 18Ni-300 steel". In: *Additive Manufacturing* 22 (2018), pp. 592–600. ISSN: 2214-8604. DOI: https://doi.org/10.1016/j.addma.2018.06.005. URL: http://www.sciencedirect.com/science/article/pii/S2214860418302999.

[31] Yuchao. Bai, Yongqiang. Yang, Di. Wang, and Mingkang. Zhang. "Influence mechanism of parameters process and mechanical properties evolution mechanism of maraging steel 300 by selective laser melting". In: *Materials Science and Engineering: A* 703.Supplement C (2017), pp. 116–123. ISSN: 0921-5093. DOI: https://doi.org/10.1016/j.msea.2017.06.033. URL: http://www.sciencedirect.com/science/article/pii/S0921509317307979.

[32] Dirk Herzog, Vanessa Seyda, Eric Wycisk, and Claus Emmelmann. "Additive manufacturing of metals". In: *Acta Materialia* 117.Supplement C (2016), pp. 371–392. ISSN: 1359-6454. DOI: https://doi.org/10.1016/j.actamat.2016.07.019. URL: http://www.sciencedirect.com/science/article/pii/S1359645416305158.

[33] B. Klahn C.and Leutenecker and M. Meboldt. "Design Strategies for the Process of Additive Manufacturing". In: *Procedia CIRP* 36 (2015). CIRP 25th Design Conference Innovative Product Creation, pp. 230–235. ISSN: 2212-8271. DOI: https://doi.org/10.1016/j.procir.2015.01.082. URL: http://www.sciencedirect.com/science/article/pii/S2212827115008938.

[34] S.P. Moylan and J.A. Slotwinski. "Assessment of Guidelines for Conducting Round Robin Studies in Additive Manufacturing". In: *2014 ASPE Spring Topical Meeting–Dimensional Accuracy and Surface Finish in Additive Manufacturing*. Vol. 57. NIST. Berkelye, CA, Apr. 2014.

[35] S.P. Moylan, J. Land, and A.M. Possolo. "Additive Manufacturing Round Robin Protocols: A Pilot Study". In: *Proceedings of the Solid Freeform Fabrication Symposium*. Solid Freeform Fabrication Symposium. Austin, TX: NIST, Aug. 2015.

[36] B. Ahuja, A. Schaub, D. Junker, M. Karg, F. Tenner, R. Plettke, M. Merklein, and M. Schmidt. "A round robin study for leaser beam melting in a metal powder bed". English. In: *South African Journal of Industrial Engineering* 27.2 (2016), pp. 30–42. ISSN: 1012-277X. DOI: http://dx.doi.org/10.7166/27-2-1201. URL: http://journals.co.za/content/indeng/27/2/EJC193268.

[37] C. Tan, K. Zhou, W. Ma, P. Zhang, M. Liu, and T. Kuang. "Microstructural evolution, nanoprecipitation behavior and mechanical properties of selective laser melted high-performance grade 300 maraging steel". In: *Materials and Design* 134 (2017), pp. 23–34. ISSN: 0264-1275. DOI: https://doi.org/10.1016/j.matdes.2017.08.026. URL: http://www.sciencedirect.com/science/article/pii/S0264127517307724.

[38] J.R. Davis, ed. *ASM Specialty Handbook: Tool Materials*. ASM International, 2005. ISBN: 9780871705457.

[39] Inco. *18 per cent maraging steels. Engineering properties*. Tech. rep. 4419. International Nickel Company, 1976. 30 pp.

[40] E.P. Abrahamson. *Processing and Properties on 18Ni Maraging Steel by Powder Metallurgy*. Tech. rep. AD 758439. AMMRC TR 73-4. MA,USA: Army Materials and Mechanics Research Center, Feb. 1973.

[41] A. Shekhter, H. I. Aaronson, M. R. Miller, S. P. Ringer, and E. V. Pereloma. "Effect of aging and deformation on the microstructure and properties of Fe-Ni-Ti maraging steel". In: *Metallurgical and Materials Transactions A* 35.3 (Mar. 2004), pp. 973–983. ISSN: 1543-1940. DOI: 10.1007/s11661-004-0024-9. URL: https://doi.org/10.1007/s11661-004-0024-9.

[42] E.A. Jägle, P.P. Choi, J. Van Humbeeck, and D. Raabe. "Precipitation and austenite reversion behavior of a maraging steel produced by selective laser melting". In: *Journal of Materials Research* 29.17 (2014), pp. 2072–2079. DOI: 10.1557/jmr.2014.204. URL: https://www.cambridge.org/core/services/aop-cambridge-core/content/view/S0884291414002040.

[43] T.B. Sercombe. "Sintering of freeformed maraging steel with boron additions". In: *Materials Science and Engineering: A* 363.1 (2003), pp. 242–252. ISSN: 0921-5093. DOI: https://doi.org/10.1016/S0921-5093(03)00645-2. URL: http://www.sciencedirect.com/science/article/pii/S0921509303006452.

[44] C. Casavola, S.L. Campanelli, and C. Pappalettere. "Experimental Analysis of Residual Stresses in the Selective Laser Melting Process". In: *Proceedings of the XIth International Congress and Exposition*. Society for Experimental Mechanics Inc. Orlando, Florida, June 2008.

[45] T. Wohlers and Gornet. T. *History of Additive Manufacturing*. White Paper. Wohlers Associates, 2014. 34 pp. URL: http://wohlersassociates.com/history2014.pdf (visited on 11/02/2017).

[46] C. Altwood, M. Ensz, D. Greene, M. Griffith, L. Harwell, D. Reckaway, T. Romero, E. Schlienger, and J. Smugersky. "Laser Engineered Net Shaping (LENS(TM)): A Tool for Direct Fabrication of Metal Parts". In: *Laser Materials Processing*. Section E. ICALEO '98. Orlando, Florida, Nov. 1998, pp. 1–7. URL: https://www.osti.gov/biblio/1549-laser-engineered-net-shaping-lens-tm-tool-direct-fabrication-metal-parts.

[47] T. DebRoy et al. “Additive manufacturing of metallic components – Process, structure and properties”. In: *Progress in Materials Science* 92 (2018), pp. 112–224. ISSN: 0079-6425. DOI: https://doi.org/10.1016/j.pmatsci.2017.10.001. URL: http://www.sciencedirect.com/science/article/pii/S0079642517301172.

[48] J.O. Milewski. *Additive Manufacturing of Metals: From Fundamental Technologh to Rocket Nozzles, Medical Implants, and Custom Jewelry*. 258. Springer Series in Material Science. Cham, Switzerland: Springer, Cham, 2017. DOI: https://doi.org/10.1007/978-3-319-58205-4.

[49] Renishaw. *Digging Deep with Wassara*. Case Study H-5800-4015-01. UK: Renishaw, 2018. URL: http://www.renishaw.com/en/digging-deep-with-wassara--43252.

[50] E. Bassoli, A. Gatto, N.T. Sewell, and D. Johns. “On the effects of build orientation in powder-fed Additive Layer Manufacture of steel 316L”. In: *Innovative Developments in Design and Manufacturing. Advanced research in virtual and rapid prototyping*. 4TH International Conference on Advanced Research and Rapid Prototyping. (Liberia, Portugal). Ed. by Bartolo et al. CRC Press, 2010, pp. 263–268. ISBN: 9781439859216.

[51] L.N. Carter, C. Martin, P.J. Withers, and M.M. Attallah. “The influence of the laser scan strategy on grain structure and cracking behaviour in SLM powder-bed fabricated nickel superalloy”. In: *Journal of Alloys and Compounds* 615.Supplement C (2014), pp. 338–347. ISSN: 0925-8388. DOI: https://doi.org/10.1016/j.jallcom.2014.06.172. URL: http://www.sciencedirect.com/science/article/pii/S092583881401528X.

[52] D. Appleyard. “Powering up on powder technology”. In: *Metal Powder Report* 70.6 (2015), pp. 285–289. ISSN: 0026-0657. DOI: https://doi.org/10.1016/j.mprp.2015.08.075. URL: http://www.sciencedirect.com/science/article/pii/S0026065715005184 (visited on 10/06/2017).

[53] D. Scott. *Add It Up: 5 Industrial Additive Manufacturing Trends for 2017*. Autodesk, 2017. URL: https://www.autodesk.com/redshift/industrial-additive-manufacturing-trends/ (visited on 10/05/2017).

[54] Sunpreet Singh, Seeram Ramakrishna, and Rupinder Singh. “Material issues in additive manufacturing: A review”. In: *Journal of Manufacturing Processes* 25.Supplement C (2017), pp. 185–200. ISSN: 1526-6125. DOI: https://doi.org/10.1016/j.jmapro.2016.11.006. URL: http://www.sciencedirect.com/science/article/pii/S152661251630161X.

[55] Grand-View-Research. *3D Metal Printing Market Analysis By Product (Titanium, Nickel, Steel, Aluminum), By Application (Aerospace and Defense, Automotive, Medical and Dental), By Form (Powder, Filament), By Region, By Country, And Segment Forecasts, 2014 - 2025*. Annual Report 4312495. Research and Markets, May 2017. 90 pp. URL: https://www.researchandmarkets.com/research/j37c7h/3d_metal_printing (visited on 10/05/2017).

[56] E. Yasa, J. Deckers, J.P. Kruth, M. Rombouts, and J. Luyten. "Experimental investigation of Charpy impact tests on metallic SLM parts". In: *Innovative Developments in Design and Manufacturing Advanced Research in Virtual and Rapid Prototyping*. 2009, pp. 217–214. URL: https://lirias.kuleuven.be/bitstream/123456789/224820/2/Yasa_VRAP_2009_submitted.pdf (visited on 11/24/2017).

[57] William E. Frazier. "Metal Additive Manufacturing: A Review". In: *Journal of Materials Engineering and Performance* 23.6 (June 2014), pp. 1917–1928. ISSN: 1544-1024. DOI: 10.1007/s11665-014-0958-z. URL: https://doi.org/10.1007/s11665-014-0958-z.

[58] Thomas Niendorf, Stefan Leuders, Andre Riemer, Hans Albert Richard, Thomas Tröster, and Dieter Schwarze. "Highly Anisotropic Steel Processed by Selective Laser Melting". In: *Metallurgical and Materials Transactions B* 44.4 (Aug. 2013), pp. 794–796. ISSN: 1543-1916. DOI: 10.1007/s11663-013-9875-z. URL: https://doi.org/10.1007/s11663-013-9875-z.

[59] S.L. Campanelli, N. Contuzzi, A. Angelastro, and A.D. Ludovico. In: *New Trends in Technologies: Devices, Computer, Communication and Industrial Systems*. IntechOpen, 2010. Chap. 13. Capabilities and Performances of the Selective Laser Melting Process, pp. 233–252. URL: https://www.intechopen.com/download/pdf/12285.

[60] K. Kunze, T. Etter, J. Grässlin, and V. Shklover. "Texture, anisotropy in microstructure and mechanical properties of IN738LC alloy processed by selective laser melting (SLM)". In: *Materials Science and Engineering: A* 620.Supplement C (2015), pp. 213–222. ISSN: 0921-5093. DOI: https://doi.org/10.1016/j.msea.2014.10.003. URL: http://www.sciencedirect.com/science/article/pii/S0921509314012362.

[61] C.U. Brown and A. Donmez. *NIST Advanced Manufacturing Series. Microstructure Analysis for Additive Manufacturing: A Review of Existing Standards*. Report 100-3. NIST, 2016. 27 pp. DOI: 10.6028/NIST.AMS.100-3.

[62] T. Etter, K. Kunze, F. Geiger, and H. Meidani. "Reduction in mechanical anisotropy through high temperature heat treatment of Hastelloy X processed by Selective Laser Melting (SLM)". In: *IOP Conference Series: Materials Science and Engineering* 82.1 (2015), p. 012097. URL: http://stacks.iop.org/1757-899X/82/i=1/a=012097.

[63] G.E. Dieter. *Mechanical Metallurgy*. New York USA: McGraw-Hill, 1961.

[64] Lore Thijs, Karolien Kempen, Jean-Pierre Kruth, and Jan Van Humbeeck. "Fine-structured aluminium products with controllable texture by selective laser melting of pre-alloyed AlSi10Mg powder". In: *Acta Materialia* 61.5 (2013), pp. 1809–1819. ISSN: 1359-6454. DOI: https://doi.org/10.1016/j.actamat.2012.11.052. URL: http://www.sciencedirect.com/science/article/pii/S1359645412008592.

[65] B. AlMangour, D. Grzesiak, and J.M. Yang. "Rapid fabrication of bulk-form TiB2/316L stainless steel nanocomposites with novel reinforcement architecture and improved performance by selective laser melting". In: *Journal of Alloys and Compounds* 680 (2016), pp. 480–493. ISSN: 0925-8388. DOI: https://doi.org/10.1016/j.jallcom.2016.04.156. URL: http://www.sciencedirect.com/science/article/pii/S0925838816311355.

[66] T. Bhardwaj and M. Shukla. "Effect of laser scanning strategies on texture, physical and mechanical properties of laser sintered maraging steel". In: *Materials Science and Engineering: A* 734 (2018), pp. 102–109. ISSN: 0921-5093. DOI: https://doi.org/10.1016/j.msea.2018.07.089. URL: http://www.sciencedirect.com/science/article/pii/S0921509318310244.

[67] E.A. Jägle, Z. Sheng, P. Kurnsteiner, S. Ocylok, A. Weisheit, and D. Raabe. "Comparison of Maraging Steel Micro- and Nanostructure Produced Conventionally and by Laser Additive Manufacturing". In: *Materials* 10 (2017). ISSN: 1996-1944. DOI: 10.3390/ma10010008. URL: http://www.mdpi.com/1996-1944/10/1/8.

[68] U.K. Viswanathan, G.K. Dey, and V. Sethumadhavan. "Effects of austenite reversion during overageing on the mechanical properties of 18 Ni (350) maraging steel". In: *Materials Science and Engineering: A* 398.1 (2005), pp. 367–372. ISSN: 0921-5093. DOI: https://doi.org/10.1016/j.msea.2005.03.074. URL: http://www.sciencedirect.com/science/article/pii/S0921509305003576.

[69] C.R. Shamantha, R. Narayanan, K.J.L. Iyer, V.M. Radhakrishnan, S.K. Seshadri, S. Sundararajan, and S. Sundaresan. "Microstructural changes during welding and subsequent heat treatment of 18Ni (250-grade) maraging steel". In: *Materials Science and Engineering: A* 287.1 (2000), pp. 43–51. ISSN: 0921-5093. DOI: https://doi.org/10.1016/S0921-5093(00)00838-8. URL: http://www.sciencedirect.com/science/article/pii/S0921509300008388.

[70] H. Leitner, M. Schober, R. Schnitzer, and S. Zinner. "Strengthening behavior of Fe–Cr–Ni–Al–(Ti) maraging steels". In: *Materials Science and Engineering: A* 528.15 (2011), pp. 5264–5270. ISSN: 0921-5093. DOI: https://doi.org/10.1016/j.msea.2011.03.058. URL: http://www.sciencedirect.com/science/article/pii/S092150931100342X.

[71] U.K. Viswanathan, R. Kishore, and M.K. Asundi. "Effect of Therml Cycling on the Mechanical Properties of 350-Grade Maraging Steel". In: *Mwtallurgical and Materials Transactions*. A 27 (Mar. 1996), pp. 757–761.

[72] Concept Laser. *CL 50WS Hot Work Steel 1.2709 Powder*. Material data sheet. DE: Concept Laser, 2016. 2 pp. URL: https://www.concept-laser.de/fileadmin//user_upload/Datasheet_CL_50WS.pdf (visited on 08/15/2018).

[73] 3D Systems. *LaserForm Maraging Steel (B). for ProX DMP 200 and 300 Direct Metal Printers*. Material Product Data Sheet. US: 3D Systems, 2017. 1 p. URL: https://www.3dsystems.com/materials/maraging-steel (visited on 09/19/2017).

[74] Oerlikon. *Maraging Steel (C300) Type Powder for Additive Manufacturing*. Material Product Data Sheet. Switzerland, 2017. 1 p. URL: https://www.oerlikon.com/metco/en/ (visited on 09/19/2017).

[75] LPW. *Powder Range. Metal powders from LPW*. Material data sheet. UK: LPW, 2016. 12 pp. URL: http://www.lpwtechnology.com/wp-content/uploads/2016/11/LPW_Powders_Brochure.pdf (visited on 09/19/2017).

[76] 3TRPD. *Maraging Steel 1.2709 (Source EOS)*. Material Specification. UK: 3TRPD, 2012. 1 p. URL: http://www.3trpd.co.uk/wp-content/uploads/2013/03/maraging-steel-1-2709-2012.pdf (visited on 09/19/2017).

[77] Sandvik Materials Technology. *Sandvik Osprey Metal Powders*. Tech. rep. UK: Sandvik Materials Technology, Sept. 2010. URL: https://www.materials.sandvik/globalassets/global/downloads/products_downloads/metal_powders/s-po009-ps-eng-09.2010.pdf.

[78] LPW Technology. *Case Study: Maraging Steel - The Effects of Alloy Chemistry on Processability*. Case Study. LPW, Aug. 2017. URL: https://www.lpwtechnology.com/wp-content/uploads/2017/08/Case-Study-M300.pdf.

[79] LPW Technology. *Case Study: The impact of powder variability on Additive Manufacturing build quality*. Case Study. LPW, May 2018. URL: https://www.lpwtechnology.com/wp-content/uploads/2018/05/Case-Study-12-ALSi10Mg-Final.pdf.

[80] A.T. Sutton, C.S. Kriewall, M.C. Leu, and J.W. Newkirk. "Powders for Additive Manufacturing Processes: Characterization Techniques and Effects on Part Properties". In: *Proceedings of the 26th Annual International Solid Freeform Fabrication Symposium*. Solid Freeform Fabrication 2016. 2016.

[81] K. Kempen. "Expanding the Materials Palette for Selective Laser Melting of Metals". Dissertation. KU Leuven – Faculty of Engineering Science, Mar. 2015.

[82] C. Masneri. "Microstructural and mechanical properties of maraging steel parts produced by selective laser melting". MA thesis. Politecnico Milano, 2016.

[83] Renishaw. *Investigating the effects of multiple re-use of Ti6Al4V powder in additive manufacturing (AM)*. White Paper. Renishaw, 2016. URL: http://resources.renishaw.com/en/details/white-paper-investigating-the-effects-of-multiple-powder-re-use-in-am--83164.

[84] P.T. Quinn, S.M. O'Halloran, J. Lawlor, and R. Raghavendra. "Characterization of Recycled Powders and Resulting Properties Derived From Additive Manufacturing". In: *Preliminary Proceedings: 35th International Manufacturing Conference (IMC35)*. Dublin Institute of Technology. June 2018, pp. 8–11.

[85] S. Hoeges, C.T. Schade, and R. Causton. *Development of a Maraging Steel Powder for Additive Manufacturing*. Report. 2015.

[86] D. Bourdil, ed. *Microstructure and Mechanical Properties of Maraging Steel 300 After Selective Laser Melting*. Solid Freeform Fabrication Symposium. (Texas, Aug. 12, 2010). USA, Aug. 2010, pp. 383–396. URL: https://sffsymposium.engr.utexas.edu/Manuscripts/2010/2010-32-Yasa.pdf (visited on 08/08/2017).

[87] S. Morito, H. Tanaka, R. Konishi, T. Furuhara, and T. Maki. "The morphology and crystallography of lath martensite in Fe-C alloys". In: *Acta Materialia* 51.6 (2003), pp. 1789–1799. ISSN: 1359-6454. DOI: https://doi.org/10.1016/S1359-6454(02)00577-3. URL: http://www.sciencedirect.com/science/article/pii/S1359645402005773.

[88] I. Tolosa, F. Garciandía, F. Zubiri, F. Zapirain, and A. Esnaola. "Study of mechanical properties of AISI 316 stainless steel processed by "selective laser melting", following different manufacturing strategies". In: *The International Journal of Advanced Manufacturing Technology* 51.5 (Nov. 2010), pp. 639–647. ISSN: 1433-3015. DOI: 10.1007/s00170-010-2631-5. URL: https://doi.org/10.1007/s00170-010-2631-5.

[89] R. Glaser, R. Goel, M. Hewitt, F. Meng, P. Wang, and R. Yan. *3D Printing Alloys*. Report. US: Northwestern University, 2015. URL: https://canvas.northwestern.edu/files/2229202/download?download_frd=1&verifier=N8bi8oUaRn08EPsKLapRweNJAdhdKg2PH0jtJdIJ (visited on 10/28/2017).

[90] Z. Liu, C.K. Chua, K.F. Leong, K. Kempen, L. Thijs, E. Yasa, J. Van-Humbeeck, and J-P. Kruth. "A preliminary investigation on selective laser melting of M2 high speed steel". In: *Innovative Developments in Virtual and Physical Prototyping*. Vol. 1. International Conference on Advanced Research in Virtual and Rapid Prototyping (VRAP). Leiria, Portugal: Taylor & Francis group, 2012, pp. 339–346. ISBN: 978-0-203-18141-6. URL: https://core.ac.uk/download/pdf/34477951.pdf (visited on 11/25/2017).

[91] I. Yadroitsava and I. Yadroitsev. "Residual Stress in Metal Specimens Produced by Direct Metal Laser Sintering". In: *Annual International Solid Freeform Fabrication Symposium*. TX, 2015, pp. 614–625. URL: http://sffsymposium.engr.utexas.edu/sites/default/files/2015/2015-49-Yadroitsev.pdf.

[92] B. AlMangour and J.M. Yang. "Improving the surface quality and mechanical properties by shot-peening of 17-4 stainless steel fabricated by additive manufacturing". In: *Materials and Design* 110.Supplement C (2016), pp. 914–924. ISSN: 0264-1275. DOI: https://doi.org/10.1016/j.matdes.2016.08.037. URL: http://www.sciencedirect.com/science/article/pii/S0264127516311005.

[93] I. Yadroitsev and I. Yadroitsev. "Residual Stress in Metal Specimens Produced by Direct Metal Laser Sintering". In: *International Solid Freeform Fabrication Symposium*. TX: University of Texas, 2015, pp. 614–625. URL: https://sffsymposium.engr.utexas.edu/sites/default/files/2015/2015-49-Yadroitsev.pdf (visited on 11/25/2017).

[94] Peter Mercelis and Jean-Pierre Kruth. "Residual stresses in selective laser sintering and selective laser melting". In: *Rapid Prototyping Journal* 12.5 (2006), pp. 254–265. DOI: 10.1108/13552540610707013. eprint: https://doi.org/10.1108/13552540610707013. URL: https://doi.org/10.1108/13552540610707013.

[95] C. Casavola, S.L. Campanelli, and C. Pappalettere. "Preliminary investigation on distribution of residual stress generated by the selective laser melting process". In: *The Journal of Strain Analysis for Engineering Design* 44.1 (2009), pp. 93–104. DOI: 10.1243/03093247JSA464. eprint: https://doi.org/10.1243/03093247JSA464. URL: https://doi.org/10.1243/03093247JSA464.

[96] G. Meneghetti, D. Rigon, D. Cozzi, W. Waldhauser, and M. Dabala. "Influence of build orientation on static and axial fatigue properties of maraging steel specimens produced by additive manufacturing". In: *Procedia Structural Integrity* 7 (2017). 3rd International Symposium on Fatigue Design and Material Defects, FDMD 2017, pp. 149–157. ISSN: 2452-3216. DOI: https://doi.org/10.1016/j.prostr.2017.11.072. URL: http://www.sciencedirect.com/science/article/pii/S2452321617304262.

[97] EOS. *Machine and software parameters EOSINT M 280*. EN. Parameter Sheet. Made available to EOSINT M280 machine owners by request to EOS (not published). Electro Optical Systems (EOS), 2015.

[98] P. Edwards and M. Ramulu. "Fatigue performance evaluation of selective laser melted Ti–6Al–4V". In: *Materials Science and Engineering: A* 598 (2014), pp. 327–337. ISSN: 0921-5093. DOI: https://doi.org/10.1016/j.msea.2014.01.041. URL: http://www.sciencedirect.com/science/article/pii/S0921509314000720.

[99] EOS. *EOSINT M 280. Status: December 2010*. Technical Description. Electro Optical Systems (GmbH), 2010. 33 pp. URL: https://webbuilder5.asiannet.com/ftp/2684/TD_M280_en_2011-03-29.pdf.

[100] ASTM. *ASTME8/E8M-16a: Standard Test Methods for Tension Testing of Metallic Materials*. Test Standard. West Conshohocken: ASTM, 2016. DOI: 10.1520/E0008_E0008M-16A. URL: http://www.astm.org/cgi-bin/resolver.cgi?E8E8M-16a. PA.

[101] F. Pfefferkorn and J. Wielhammer. *Open and Flexible: EOS Part Property Management Provides both Individualization and Standardization*. White Paper. EOS (gmbh), 2013. 12 pp. URL: https://cdn3.scrvt.com/eos/public/7e99ba072eca9ad8/294354957693f78ddb4787d3959e7057/ppm_whitepaper.pdf (visited on 11/02/2017).

[102] ASTM. *ASTMB962-17: Standard Test Methods for Density of Compacted or Sintered Powder Metallurgy (PM) Products Using Archimedes' Principle*. Test Standard. West Conshohocken: ASTM, 2017. PA.

[103] ThermoScientific. *Thermo Scientific Avizo Software 9*. User's Guide 9. Berlin, DE: ThermoScientific, 2018.

[104] ASTM. *ASTME92-17: Standard Test Methods for Vickers Hardness and Knoop Hardness of Metallic Materials*. Test Standard. West Conshohocken: ASTM, 2017. URL: https://www.astm.org/Standards/E92.htm. PA.

[105] R Core Team. *R: A Language and Environment for Statistical Computing*. Tech. rep. Vienna, Austria: R Foundation for Statistical Computing, 2014. URL: http://www.R-project.org/.

[106] LaVision. *Full Field Strain Measurement*. Subject Guide. Germany: La Vision GmbH, 2014. URL: http://www.lavision.de/en/applications/materials-testing/stereo-dic/index.php (visited on 12/07/2017).

[107] LaVision. *StrainMaster: Product Manual for DaVis 8.3*. Manual 1003017. Page total: 122. DE: LaVision, 2017.

[108] ASTM. *ASTME132-04: Standard Test Method for Poisson's Ratio at Room Temperature*. Test Standard. West Conshohocken: ASTM, 2004. DOI: 10.1520/E0132-04. URL: http://www.astm.org/cgi-bin/resolver.cgi?E132-04. PA.

[109] ASTM. *ASTME517-18: Standard Test Method for Plastic Strain Ratio r for Sheet Metal*. Test Standard. West Conshohocken: ASTM, 2018. DOI: 10.1520/E0517-18. URL: https://www.astm.org/Standards/E517.htm. PA.

[110] ASTM. *ASTME140-07: Standard Hardness Conversion Tables for Metals Relationship Among Brinell Hardness, Vickers Hardness, Rockwell Hardness, Superficial Hardness, Knoop Hardness, and Scleroscope Hardness*. Test Standard. West Conshohocken: ASTM, 2007. DOI: 10.1520/E0140-07. URL: http://www.astm.org/cgi-bin/resolver.cgi?E140-07. PA.

[111] R. Branco, J.D.M. Costa, F. Berto, S. M. J. Razavi, J. A. M. Ferreira, C. Capela, L. Santos, and F. Antunes. "Low-Cycle Fatigue Behaviour of AISI 18Ni300 Maraging Steel Produced by Selective Laser Melting". In: *Metals* 8.32 (2018). ISSN: 2075-4701. DOI: 10.3390/met8010032. URL: http://www.mdpi.com/2075-4701/8/1/32.

[112] W.F. Smith and J. Hashemi. *Foundations of Materials Science and Engineering*. 3rd ed. ISBN 0-07-240233-4. New York USA: McGraw-Hill, 2004.

[113] M. Ashby and D.R.H. Jones. *Engineering Materials 2: An Introduction to Microstructures, Processing and Design*. ISBN: 9780080468631. New York USA: Butterworth-Heinemann, 2005.

[114] B. Hutchinson. "Critical Assessment 16: Anisotropy in metals". In: *Materials Science and Technology* 31.12 (2015), pp. 1393–1401. DOI: 10.1179/1743284715Y.0000000118. eprint: https://doi.org/10.1179/1743284715Y.0000000118. URL: https://doi.org/10.1179/1743284715Y.0000000118.

[115] Hiroshi Akima and Albrecht Gebhardt. *akima: Interpolation of Irregularly and Regularly Spaced Data*. R package version 0.6-2. 2016. URL: https://CRAN.R-project.org/package=akima.

[116] Hadley Wickham. *ggplot2: Elegant Graphics for Data Analysis*. Springer-Verlag New York, 2016. ISBN: 978-3-319-24277-4. URL: http://ggplot2.org.

[117] l. Kucerova and I. Zetkova. "Metallography of 3D Printed 1.2709 Tool Steel". In: *Manufacturing Technology* 16.1 (2016), pp. 140–144.

[118] N. Takata, R. Nishida, A. Suzuki, M. Kobashi, and M. Kato. "Crystallographic Features of Microstructure in Maraging Steel Fabricated by Selective Laser Melting". In: *Metals* 8.440 (2018). Special Issue Additive Manufacturing of Ferrous Materials. ISSN: 2075-4701. DOI: 10.3390/met8060440. URL: http://www.mdpi.com/2075-4701/8/6/440.

[119] V.A. Popovich, E.V. Borisov, A.A. Popovich, V.Sh. Sufiiarov, D.V. Masaylo, and L. Alzina. "Functionally graded Inconel 718 processed by additive manufacturing: Crystallographic texture, anisotropy of microstructure and mechanical properties". In: *Materials & Design* 114.Supplement C (2017), pp. 441–449. ISSN: 0264-1275. DOI: https://doi.org/10.1016/j.matdes.2016.10.075. URL: http://www.sciencedirect.com/science/article/pii/S026412751631382X.

Appendix A. Article 1

Process Phenomena Influencing the Tensile and Anisotropic Characteristics of Additively Manufactured Maraging Steel

Barry Mooney[a], Kyriakos I. Kourousis[a], Ramesh Raghavendra[b]

[a] *School of Engineering, University of Limerick, Ireland, V94 T9PX*
[b] *South Eastern Applied Materials Research Centre (SEAM), Waterford Institute of Technology, Ireland, X91 TX03*

Abstract
The tensile mechanical properties and anisotropy levels of identical test-coupons, fabricated from maraging steel 300 (MS300) using two alternative EOS EOSINT M280 Additive Manufacturing (AM) systems, have been examined. The mechanical performance variations resulting from process differences between the two suppliers and the part's build volume orientation (0°, 45°, 90°) are investigated. Significant microstructural discrepancies, affecting mechanical performance, plasticity and anisotropy levels, have been observed in the as-built samples obtained from the two suppliers. A difference in the angle of the laser scan strategy, in conjunction with unfavourable powder feedstock characteristics, are understood to have had a profound influence on the plasticity and anisotropy divergences observed in the AM MS300 alloy. Plastic anisotropy levels can be largely reduced through application of aging heat-treatments, however, a degree of transverse strain anisotropy is likely to remain due to the AM alloy's fabrication history.

Keywords: additive manufacturing, 3D printing, maraging steel, anisotropy, heat treatment, strength, ductility.

Preprint submitted to Materials Science & Engineering: A *July 19, 2018*
In Review Manuscript *December 5, 2018*

Introduction

Maraging steel 300 (MS300) is a high-strength Fe-Ni based alloy which, in powder form, is used widely as a feedstock for laser additive manufacturing (AM). MS1 is one such powder developed by EOS for their *Direct Metal Laser Sintering* (DMLS) sys-

tems. The alloy's high-strength, combined with its agreeableness to laser-synthesis, facilitates the rapid production of geometrically complex structures which have load-bearing capabilities and can easily achieve high-density and chemically homogeneous microstructures [8, 9, 13]. As AM technology matures, it is progressively becoming a viable option for serial production of structure-critical engineering components [32, 33]. Key to this successful advancement is a clear understanding of the factors which influence the metallurgical soundness of the produced parts. An important aspect for the serial production of AM parts is the ability to achieve consistent and repeatable mechanical properties outputs for identical parts produced on alternative machines, however, very limited published research exists on the repeatability of mechanical behaviour in AM-produced metals [24, 34–36]. Indeed, there is variation in the EOS-reported as-built MS1 mechanical properties for identical test-coupons fabricated on EOS DMLS equipment [12, 14], but also among MS300 properties reported in the open literature for contrasting test-coupon geometries which have been fabricated on EOS and other metal AM systems [3, 19, 26][9, 18, 21, 23, 24, 27, 29, 37]. The spread of the as-built tensile properties reported across these studies (i.e. elasticity modulus (E): 150-194 GPa [12, 27]; yield strength ($R_{p0.2}$): 768-1214 MPa [23, 29]; tensile strength (R_m): 1010-1325 MPa [27, 29]; and elongation to fracture (A_t): 6.1-14.3 % [9, 26]) is a measure of the variability observed. This highlights the need for a deeper understanding of the factors that affect the reproducibility of AM parts, since engineers seeking to use this advantageous technology for structure-critical designs require a greater control of the achievable mechanical properties.

In this paper, we examine the material characteristics, microstructures, tensile properties, and anisotropy variation of identical MS300 test-coupons which have been fabricated in three build orientations (0°, 45°, and 90°), on two EOS EOSINT M280 AM machines belonging and operated by different users. For this purpose, the relationship between the AM process phenomena and the resulting mechanical properties, including plastic anisotropy, has been investigated.

Material and methods

Fabrication of samples

Test coupons were fabricated from MS1 powder feedstock on two EOS *EOSINT M280* AM systems belonging and operated by different users, denoted as Supplier 1 and Supplier 2. Both AM systems were controlled using the EOS-predefined set of parameters *MS1 Performance 2.0*, which administers $40\mu m$ layer-thickness and has been optimized by EOS for the fabrication of MS1 components. The chemical composition of the MS1 material is presented in Table A.1, along with the results of the energy dispersive X-ray (EDX) analysis, which were obtained with a *Hitachi SU 70* scanning electron microscope (SEM), fitted with an *Oxford Instruments* EDX attachment. A close agreement between the Supplier 1 and 2 SEM-EDX values and the EOS published values [12] for MS1 is observed, which also confirms that the powder material used is in line with the manufacturer's (EOS) specifications.

Table A.1: Chemical composition (%wt) of MS1, the 18Ni (300) grade maraging steel powder supplied by EOS (GmbH) [12] with SEM-EDX analysis results for the main comprising elements.

	Ni	**Mo**	**Co**	**Ti**	**Al**	**Cr**	**Si**	**Mn**	**C**	**Fe**
MS1 [12]	17-19	4.5-5.2	8.5-9.5	0.6-0.8	0.05-0.15	0-0.5	0-0.1	0-0.1	0-0.03	Bal.
Supplier 1-EDX	18.14	5.67	8.94	0.87	-	-	-	-	-	Bal.
Supplier 2-EDX	17.96	5.65	9.08	1.05	-	-	-	-	-	Bal.

Four sets of test specimens, orientated at three angles [0° (horizontal), 45° (inclined), and 90° (vertical)] between their longitudinal axis and the build platform, were produced on each machine. This facilitated an investigation of the influence of build orientation on property anisotropy. For this purpose, a rectangular-shaped tensile test specimen having uniform cross-section at gage and meeting the requirements of the ASTM-E8M standard [100] was selected. The finished specimen geometry, dimensions and tolerances are shown in Figure A.1a. This specimen design allowed for the measurement of both lateral and axial elastic and plastic strains whilst under tensile loading. A machining allowance of 0.5mm was included to ensure that a uniform and high-quality surface finish, appropriate for the tensile testing of high-strength

specimens [100], could be achieved. After the AM build, the DMLS parts were processed through a single-cycle precision computer numerically controlled (CNC) wire electrical discharge machining (EDM) profiling and surface-grinding operations.

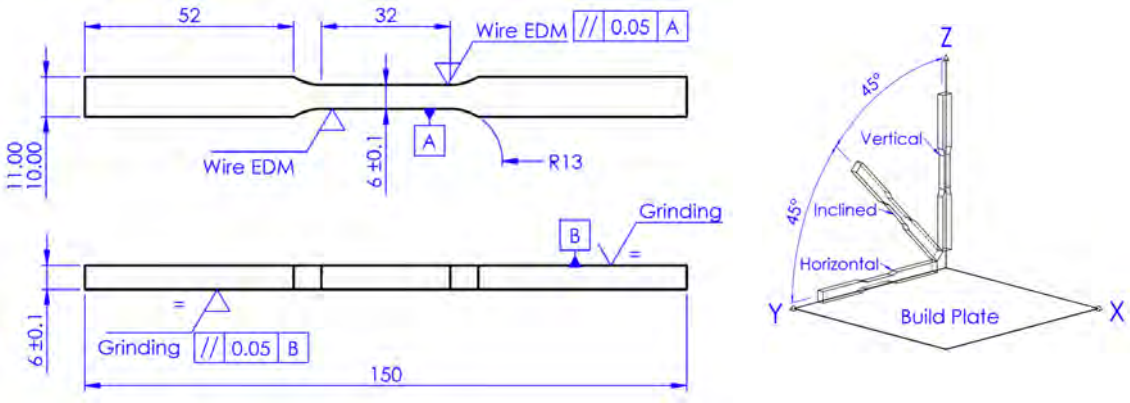

(a) (b)

Figure A.1: (a) Showing the finish-machined specimen geometry, and (b) the AM build volume coordinate system and test-specimen build orientations.

Heat-treatment

High strength is achieved in MS300 through a second phase precipitation of intermetallic compounds (Ni_3Ti, Ni_3Mo, Fe_2Mo and Fe_7Mo_6) for which a disperse concentration of fully dissolved hardening elements in solid solution is necessary [4, 28, 42]. In contrast to conventionally produced MS300, and by reason of the rapid cooling rates (circa 10^3 to 10^8 $K.s^{-1}$), the DMLS process provides a solid solution with full potential for precipitation strengthening [28]. EOS therefore recommend a straightforward isothermal aging heat-treatment of 6 hours at $490°C$ [12] which allows a populous dispersion of dislocation hindering precipitates to form, and leads to the alloy's characteristic high strength (circa 2,000 MPa) and hardness.

In this study, three sets of specimens obtained from each M280 machine, were aged at $490°C$ for durations 4, 6 and 8 hours (h), while the remaining two sets were kept in the as-built condition. The aging parameters were chosen to investigate the influence of heat-treatment on mechanical properties and anisotropy levels, and to validate the EOS recommendation.

Characterization

Archimedes' Principle density measurements were performed on as-built samples obtained from each DMLS machine, and for each build-orientation, using a *Sartorius Quintix* analytical balance which was fitted with accessory YDK03 density determination kit. The measurement procedure followed the guidelines present in the ASTM B962-17 [102] standard.

Metallographic samples were obtained from arbitrary sections of the fractured coupon's grip-ends, then mounted with phenolic compound, and polished using standard finishing steps. The sectioned plane was taken perpendicular to the materials tensile loading axis in each case, and the etched microstructure (150mL H_2O; 50mL HCl; 25mL HNO_3; 1g $CuCl_2$) was then inspected using an *Olympus BX60* Optical microscope.

Porosity was examined via X-ray Computed Tomography (CT) scans, performed using a General Electric *VTOMEX L300, Nanotom S* instrument operating at 180kV, $80\mu A$, $250\mu s$ and with a resolution of $13.4\mu m$. Digital inspection of the porosity network, and a quantitative evaluation of the size and distribution of pores was completed using Thermo Fisher Scientific's *Avizo* software [103].

Vickers hardness indents were applied perpendicular to the metallographic sample's sectioned plane using a *Zwick ZHV* hardness tester which had been calibrated with a standard test block to the requirements of ASTM E92-17 [104]. Twenty (20) measurements were performed on each of the mounted and polished samples, and the results and test statistics were computed using the R statistical software package [105].

Tensile testing was conducted at room-temperature in a *Zwick/Roell (Dartec) M1000/RK* servo-hydraulic testing machine equipped with 100kN capacity load cell and fitted with ±100kN fatigue rated hydraulic wedge grips. The test procedure was fully compliant with the ASTM E8M standard [100]. Among other test requirements, this standard prescribes stressing/ straining/ displacement rates for deriving reliable and consistent mechanical properties data. The test was initially controlled

(via a 9600 series controller) to the elastic stressing rate of 10.34 MPa/s, using strain control from the extension feedback channel (Epsilon model 3542-025M-050-ST). Upon detection of yield, the test-rate maintained a constant plastic strain rate of $6.25 \times 10^{-4}/s$ controlled via the stroke feedback channel. At the end of the yield (detected from either reaching a 5% increase in stress, or an absolute strain limit of 2%), the test-velocity was commanded by a third rate, the tensile strength (R_m) rate: 0.0068/s. This strain rate was maintained to peak force through failure.

Concurrently, a non-contact full-field displacement measurement was performed using *LaVision's* portable 3D Digital Image Correlation (DIC) apparatus complete with *StrainMaster* software [106]. This involved the application of a non-repeating isotropic acrylic speckle pattern (dark black speckles on a bright white background) onto the gage surface of the specimen and capturing a sequence of images throughout each tensile test at a periodic rate of 5Hz (i.e. from zero applied load until fracture). The purpose of the speckle pattern is to provide a unique signature pixel arrangement from which the specimen's displacement field can be digitally tracked throughout the tensile test. Poisson (ν) and plastic strain ratios (R-values) were calculated from the DIC determined strain data in accordance with ASTM test methods E132-04 [108] and E517-18 [109]. R-value is the ratio of true width strain (ε_w) to true thickness strain (ε_t), given by Eq. A.1, with both strains calculated after tensile plastic flow was induced.

$$R\ value = \frac{\varepsilon_w}{\varepsilon_t} \tag{A.1}$$

The R-value was employed to quantify the strain plastic anisotropy (non-uniform transverse straining), which typically is anticipated in AM-fabricated parts. The complete experimental configuration is illustrated in Figure A.2 (each feature discussed in this section is indicated on this figure).

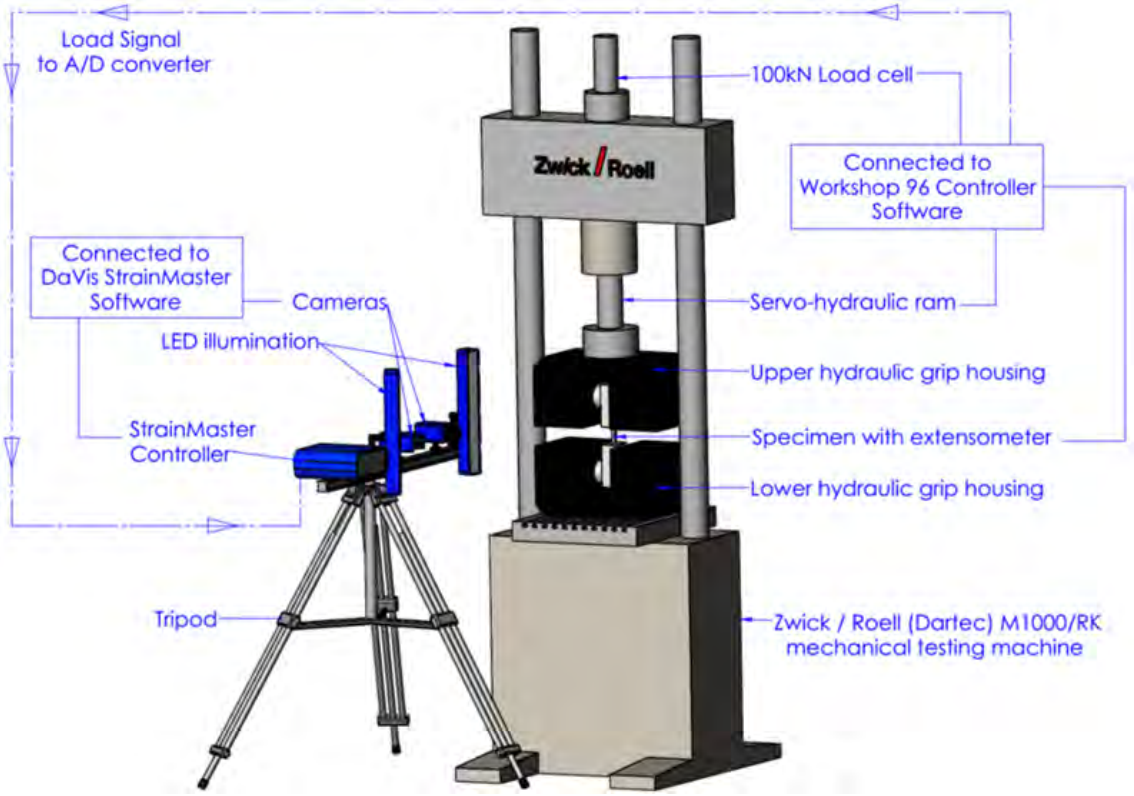

Figure A.2: Configuration of tensile test set-up including the 3D Digital Image Correlation (DIC) apparatus which allowed concurrent determination of test-specimen width and axial strains.

Results and discussion

Microstructures and density

Representative micrographs are presented for the individual build orientations of parts obtained from each supplier in Figure A.3. A distinct dissimilarity was observed in the microstructures of the sectioned vertically orientated (90°) parts. As shown in Figures A.3c and A.3f, different laser scan strategies were administered by each M280 system during the fabrication process, despite the fact that the MS1 Performance 2.0 set of parameters was used by both suppliers. Supplier 1 specimens were fabricated with a 67° line scan rotation between successive build layers, whereas Supplier 2 specimens display a 90° scan rotation. Other researchers [13, 30] have reported a layer-wise scan rotation angle of 67° when employing MS1 optimized parameters on similar EOS machines. Nevertheless, these limited literature-reported findings do not exclude the existence of strategies with other scan rotation angles

(as found in this study).

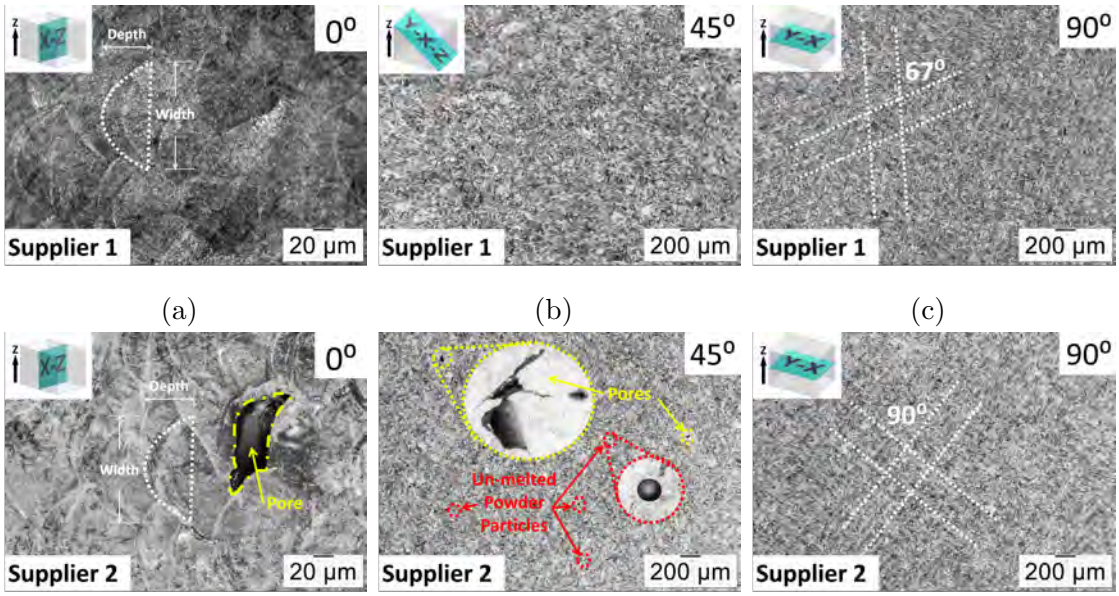

Figure A.3: Representative optical micrographs of samples fabricated in three build-orientations on two EOSINT M280 systems (Supplier 1 and Supplier 2): (a) and (d) horizontal (0°); (b) and (e) inclined (45°); and (c) and (f) vertical (90°).

Comparable melt-pool proportions, which are reflective of the applied laser energy input (< 200W), can be observed in the horizontal cross-sections shown in Figures A.3a and A.3d. In particular, melt-pool depths 35-55μm corresponding to the applied 40μm layer thickness, and widths 45-70μm suggesting a laser focus diameter of $\approx$ 60μm, were observed. Supplier 2 micrographs revealed persistent defects in the form of pores and un-melted powder particles as indicated in Figures A.3d and A.3e by dotted lines. In connection, inferior density was recorded for Supplier 2 specimens as reported in Table A.2. Nonetheless, all the reported density values fall within the EOS quoted density range of 8.0 - 8.1 g/cm^3 [12]. The determined density values (Table A.2) do not provide sufficient evidence to suggest that part density is influenced by the AM build orientation, however, it is worth noting for the proceeding sections that the Supplier 2 horizontal samples, which exhibited a relatively high degree of porosity in their microstructures, also obtained the lowest overall density values.

It is believed that the observed microstructural defects may be caused by the pow-

Table A.2: Comparing the density values of MS300 samples obtained from two EOS M280 DMLS systems for the as-built Horizontal (0°), Inclined (45°), and Vertical (90°) build orientations.

	Density, ρ (g/cm^3)		
	0°	**45°**	**90°**
Supplier 1	8.051	8.050	8.049
Supplier 2	8.028	8.031	8.034

der feedstock characteristics, which is consistent with the findings recently reported by Quinn et al. [84]. In particular, smaller spherical granules permit high packing efficiencies and are readily consumed during recoating. Contrastingly, larger granules are more likely to get pushed cross-platform into the system's collection chamber. Therefore, successive recycling and collection of powder granules following completed AM builds increases the percentile volume of larger and agglomerated powder particles in the feedstock [84]. When used in subsequent AM builds, the affected powder will impede flow behaviour due to inter-particle friction during the recoating process, lead to reduced packing efficiencies, and interact differently with the laser-beam [80]. These factors may have contributed to the porosities and unmelted particles which were observed in the Supplier 2 micrographs. Accordingly, the importance of appropriate powder sieving and quality control techniques is evident, since these will influence the feedstock characteristics, and ultimately induce microstructural defects in AM fabricated alloys. It is, however, noted that the feedstock quality may not be the sole responsible for the development of microstructural defects, as the role of the wider (90°) scan rotation angle has to be examined as well (both separately and in conjunction with the powder quality). To that end, further work is planned, to fully characterise the effect of alternative scan-strategies on the microstructural integrity and anisotropy of MS300 parts fabricated with the EOS machines.

X-ray CT-scans

The porosity level observed in the Supplier 2 samples mandated a more comprehensive evaluation using X-ray CT-scans. The re-constructed scans are presented in

Figure A.4, while Figure A.5 presents histograms of the pore size distribution for all three build orientations examined in this study. The scans were performed on as-built material surrounding the fractured surface to help identify if a coalescence of pores led to crack initiation. While no evidence of this was found, there appears to be independent porosity variation due to part orientation within the build volume. The horizontal (0°) sample displayed a lower relative density, and a much greater proportion of larger pores when compared to the inclined (45°) and vertically orientated (90°) samples. The results suggest that the achievable relative density is a function of the powder's quality, and the part's build-platform projected area (i.e. layer-wise cross-sectional area), since the horizontal layers had a significantly larger build-platform projection and were therefore more likely to be affected by powder packing deficiencies during recoating.

Although the horizontal (0°) sample exhibited a comparatively large degree of porosity, the relative density of the analysed volume of MS300 material remained higher than 99.96% which verifies the alloy's suitability for AM fabrication and welding [8–10]. It is also of note that each of the samples displayed a populous dispersion of sub $‰40\mu m$ sized defects which is an anticipated finding for this, previously stressed, material.

Mechanical properties

Tensile stress (σ) versus strain (ϵ) curves, Vickers hardness aging curves, and their associated mechanical property values are presented in Figures A.6, A.7a, and Table B.4 respectively. Significant anisotropy, and an appreciable supplier related variation has been confirmed in both the as-built and aged MS300 stress-strain curves. In particular, the largest and most obvious strength and ductility divergence can be seen in the as-built inclined (45°) specimens' $\sigma - \epsilon$ curves. Although achieving a 218MPa (22%) superior yield strength ($R_{p0.2}$), the sample fabricated with 67° laser scan rotation (Supplier 1) displayed an unusual σ versus ϵ trajectory. As shown by the solid green curve in Figure A.6a, an uneven material response during

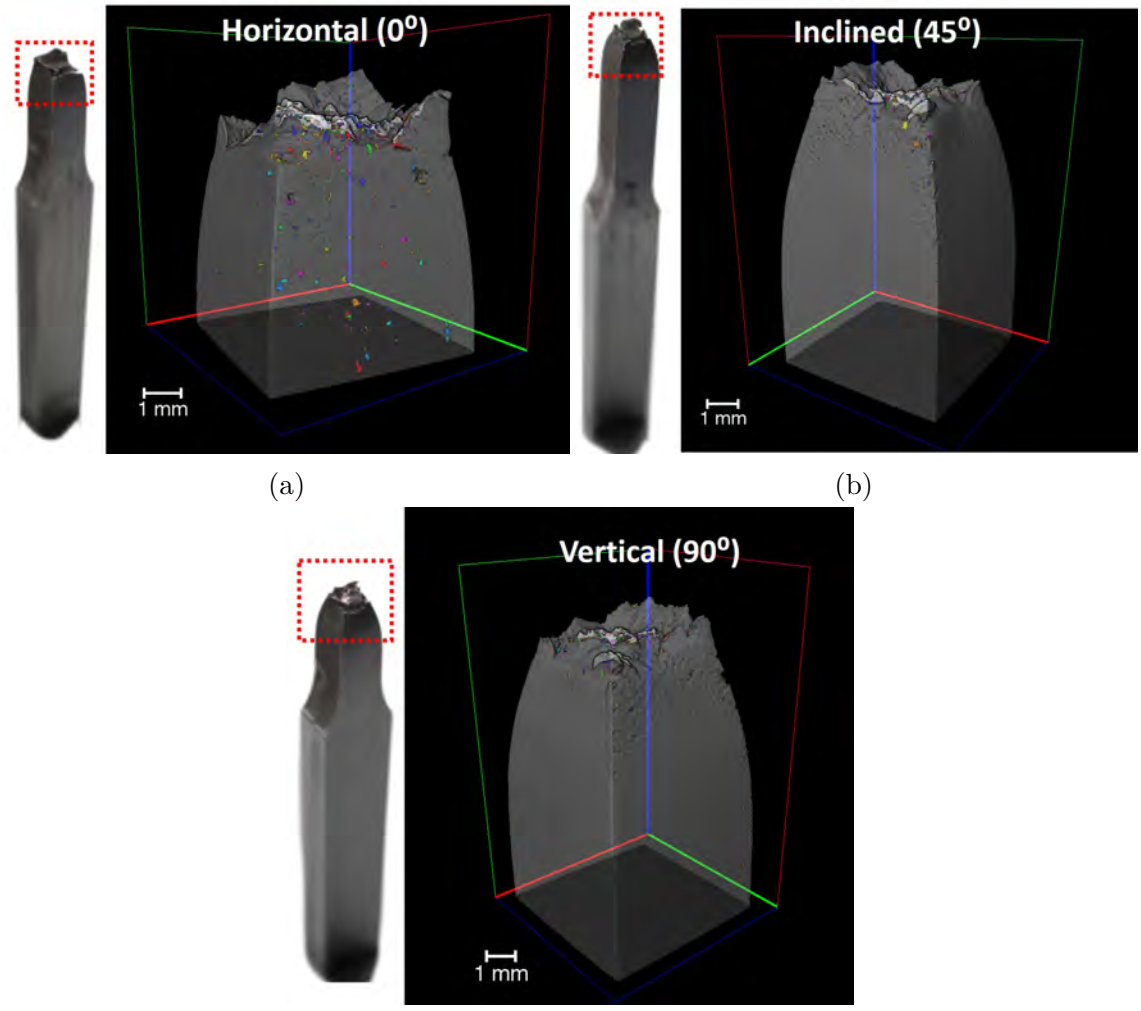

(a) (b)

(c)

Figure A.4: Transparent X-ray CT reconstructions showing micro-pores in a volume of DMLS as-built MS300 for build-orientations: (a) Horizontal (0°); (b) Inclined (45°); and (c) Vertical (90°).

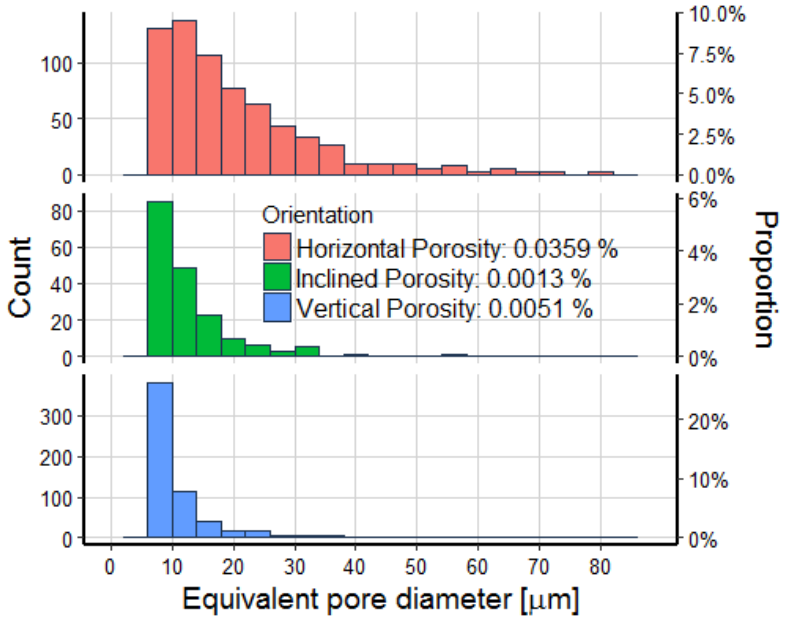

Figure A.5: Histograms of the pore size distribution in the as-built MS300 alloy which has been fabricated in three AM build-orientations: Horizontal (0°); Inclined (45°); and Vertical (90°).

plastic deformation culminated in failure at ≈ 57% less elongation (i.e. a reduction of 9.1%) when compared to the Supplier 2 specimen (dashed green curve), which had been fabricated with the 90° laser scan rotation. Remarkably, these samples have comparable hardness values, which indicates that hardness measurements alone can provide insufficient information for the assessment of the mechanical properties. This also explains why similar observations have not been reported in the AM MS300 research literature to-date.

Both sets of as-built samples exhibited a reduction in modulus of elasticity (E) with increasing build-orientation angle. This may be associated with the microstructural pattern developed during build-up of AM layers, since higher E is achieved when the loading direction is parallel to the build layers. AM's distinct three-dimensional (3D) microstructural pattern, visible in Figure A.3's micrographs, is brought about by the layer-wise deposition of powder and continuous re-melting/heating of material beneath the melt-pool during build-up.

Overall, Supplier 1 specimens having been fabricated with a 67° layer-wise scan rotation showed higher stiffness and greater strength consistency between build orientations. However, as indicated by the aging and $\sigma - \epsilon$ curves, greater strength and

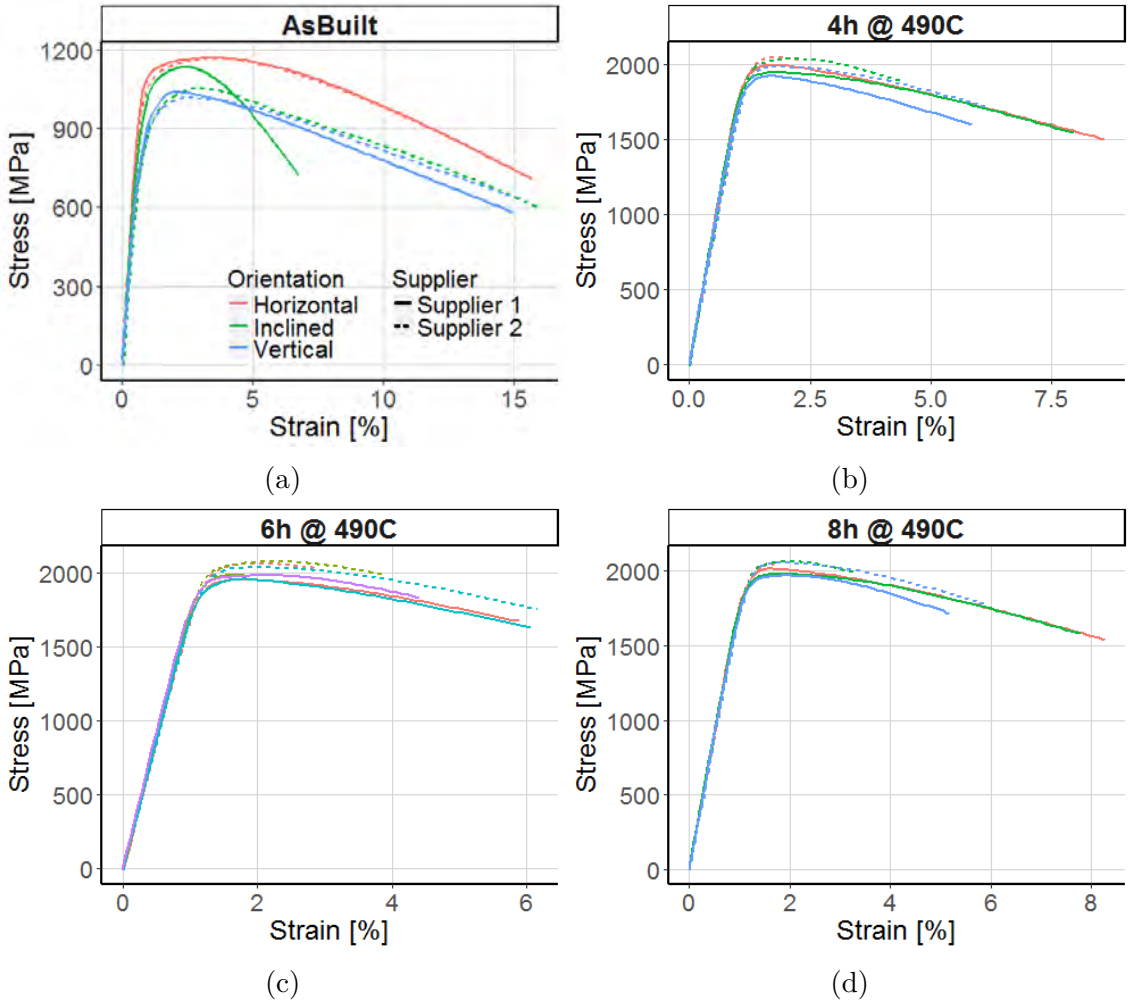

Figure A.6: Stress (σ) versus strain (ϵ) curves comparing as-built and aged MS300 test-specimens which have been fabricated on two EOS EOSINT M280 AM machines belonging and operated by different users.

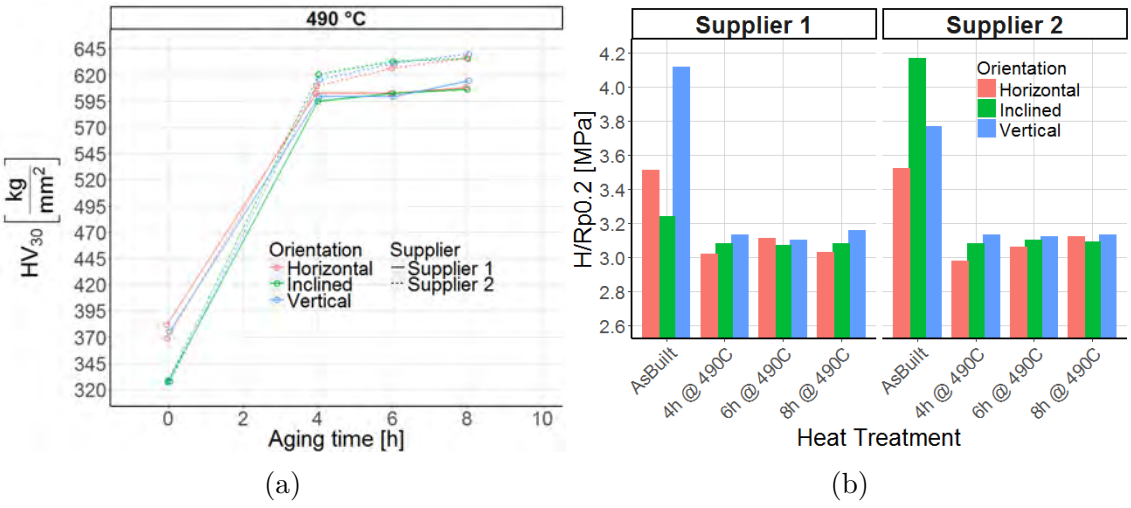

Figure A.7: (a) Precipitation strengthening curves; and (b) Ratio of Hardness (H) to Yield Strength for the as-built and heat-treated MS300 examined.

Table A.3: Mechanical properties data retrieved from tensile and Vickers hardness testing of MS300 produced by DMLS (Elasticity modulus (E); Poisson ratio (ν); Yield strength ($R_{p0.2}$); Tensile strength (R_m); Elongation to fracture (A_t); Reduction in area (Z); and Vickers hardness (HV)). EOS reference data [12] are shown with italics fonts.

Data	Heat-Treatment	Orientation	E [GPa]	ν	$R_{p0.2}$ [MPa]	R_m [MPa]	A_t [%]	Z [%]	HV_{30kgf} [kg/mm²]
EOS	***EOS As-Built[12]***	***0°***	*160*±25	-	*1050*±100	*1100*±100	*10*±4	-	*(310-360)*
		90°	*150*±20	-	*1000*±100	*1100*±100	*10*±4	-	*(310-360)*[a]
	EOS Aged[12] 6h @ 490°C	***0°***	*180*±20	-	*1990*±100	*2050*±100	*4*±2	-	*(>513)*
		90°		-				-	
Supplier 1	**As-Built**	**0°**	161	0.24	1069	1174	15.7	56	382
		45°	140	0.29	991	1144	6.8	56	327
		90°	122	0.35	892	1057	13.8	62	375
	4h @ 490°C	**0°**	182	0.33	1961	2004	8.6	33	603
		45°	185	0.31	1895	1963	8.0	28	595
		90°	180	0.32	1875	1928	5.9	24	599
	6h @ 490°C	**0°**	178	0.40	1901	1958	5.9	19	602
		45°	183	0.28	1925	1984	4.4	10	603
		90°	178	0.28	1893	1958	6.1	22	599
	8h @ 490°C	**0°**	183	0.34	1969	2020	8.3	32	608
		45°	184	0.29	1930	1993	7.8	29	606
		90°	180	0.32	1912	1978	4.2	21	615
Supplier 2	**As-Built**	**0°**	150	0.34	1028	1172	12.9	43	369
		45°	136	0.33	773	1053	15.9	60	329
		90°	120	0.38	853	1035	15.1	60	328
	4h @ 490°C	**0°**	170	0.29	2006	2050	2.3	6	610
		45°	175	0.27	1977	2047	4.4	12	620
		90°	171	0.31	1929	1996	6.1	14	616
	6h @ 490°C	**0°**	174	0.30	2004	2070	2.9	7	626
		45°	179	0.31	2004	2080	3.9	5	633
		90°	172	0.34	1981	2047	6.2	21	631
	8h @ 490°C	**0°**	179	0.38	1998	2047	NA[b]	6	636
		45°	178	0.31	2013	2069	3.4	12	635
		90°	170	0.34	2005	2067	5.5	22	640

[a] Brackets indicate approximate hardness conversion numbers per Table 3,[110];
[b] Fracture occurred before end of yield was reached.

hardness was achieved in the aged Supplier 2 specimens. The strength and hardness of samples from each supplier continued to rise when the material was aged past the EOS recommended 6h treatment duration. This strength and hardness ascension was accompanied by a reduction in ductility. While in this brittle condition, Supplier 2 samples displayed comparatively erratic and reduced ductility behaviour to those of Supplier 1. Correspondingly, this inferior ductility performance is attributed to the combined consequences of matrix embrittlement due to coarsened precipitates, and the presence of microstructural pores/un-melted particles, which jointly act as sites for crack nucleation [9, 13, 21, 28, 31, 68, 111].

When comparing the experimental mechanical properties against the EOS published data (Table B.4), both as-built vertical (90°) parts underperformed in terms of elasticity modulus (≈19% lower), and yield strength (≈13% lower). Upon aging, the alloy gained remarkable strength (>87% increase) and hardness (>75% increase), and most mechanical property values fell within the EOS published confidence bands. This MS300 reflection demonstrates the outstanding effectiveness of the precipitate development towards obstructing and retarding the movement of dislocations in the lattice, but also towards suppressing anisotropic material behaviour.

To compare the mechanical and anisotropic characteristics of samples from either supplier, a relationship between *hardness* (H) and yield strength ($R_{p0.2}$), which is based on similar empirical relationships used for other metals, was devised from the available test data. In particular, the typical linear rule-of-thumb for a broad range of metallic alloys given by Eq. A.2 [113] has been used.

$$H \approx 3 \times R_{p0.2} \tag{A.2}$$

Where hardness (H), described as the indenter force divided by the projected area of the indent (in MPa) is determined by Eq.3.

$$H = HV_{30} \times 9.81 m/s^2 \tag{A.3}$$

Where HV_{30} represents the Vickers hardness value. The experimental relationships, presented in Figure A.7b, demonstrate the extent of as-built stress anisotropy in the DMLS alloy due to supplier variation and part orientation. The most prominent discrepancies take place between as-built samples obtained from either supplier. This supplier related anisotropy variation may be attributed to the alternative scan strategies employed on either AM machine, and suggests that the scan rotation angle has a significant effect on mechanical anisotropy. Following the application of the aging heat-treatments, the degree of stress anisotropy is dramatically reduced by the presence of hard second phase precipitate particles [114], and Equation A.2 is satisfied. Nevertheless, the anisotropy developed during the fabrication process is not fully abolished following aging.

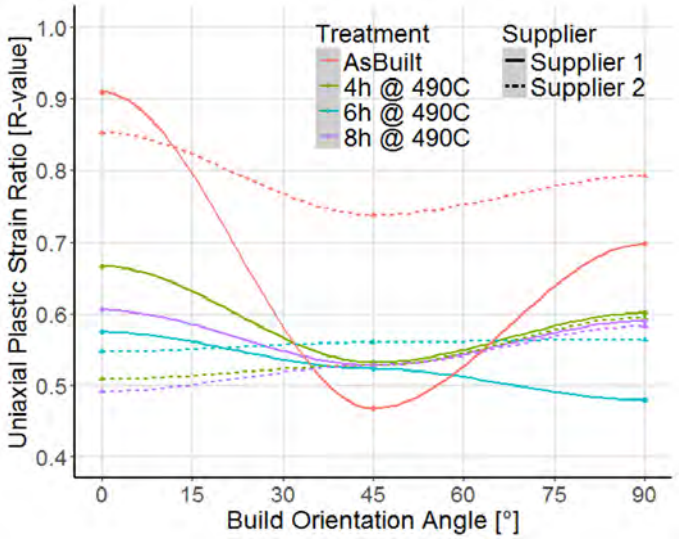

Figure A.8: Plot of R-values versus build orientation angle, evaluated at 1.5% axial strain. The trend patterns for individual specimens are displayed using local polynomial regression fitting.

Further evaluation of plastic anisotropy has been performed via the DIC obtained R-value measurements, for which the obtained results are presented in Figure A.8. The plot confirms (i) the existence of non-uniform transverse straining since $R_{isotropic} = 1$; and (ii) the variation of R-value between AM build orientation angles. Greater R-value variation is observed in Supplier 1 as-built and aged specimens (solid lines) which have been fabricated with the 67° laser-scan strategy. The harmonious and significantly flatter trends observed in Supplier 2 specimens (dashed lines) indicate a uniformity of plastic strain behaviour between build angles and suggests that a

90° scan strategy provides a more homogeneous microstructure. Regardless of the scan strategy, build orientation or heat treatment, all AM fabricated specimens displayed R-values < 1 signifying greater thinning in specimen's thickness direction whilst under tensile loading. This suggests the dominance of a systemic process anisotropy which cannot be abolished simply by aging the AM fabricated alloy. This inherent anisotropy stems from (i) the layer-wise deposition of powder; (ii) planar movement of the heat-source; and (iii) uni-axial movement of the build platform during fabrication. To abolish any fabrication manifested microstructural patterning it may therefore be necessary to perform a solubilization treatment step prior to aging. This re-crystallisation step has been shown to homogenise the AM MS300 microstructure by replacing laser scan tracks and melt-pool solidification patterns with slender packets of parallel lath martensite through moderation of the alloy's solidification cooling rates [9, 18, 27, 31]. However, such circumstances incur additional processing cost, complexity, and time, which subtracts from the overall AM MS300 appeal.

Conclusions

The deficit of process knowledge concerning the factors which influence the mechanical performance of AM metals is forestalling the technology's widespread advancement into the engineering arena, since components destined for use in demanding engineering applications have rigid requirements and specifications, and a strict precision is necessary for their manufacture. Accordingly, this research article investigates inconsistencies in the mechanical characteristics and plastic anisotropy levels in identical EOSINT M280 fabricated MS300 test-coupons that have been supplied by two AM facilities. Three build orientations (0°,45°, and 90°) are investigated, and the alloy's performance has been monitored in the as-built and aged conditions (4h, 6h and 8h at $490°C$). The important conclusions are summarized as follows:

1. Considerable microstructural dissimilarities affecting mechanical performance

and anisotropy have been observed in as-built MS300 samples obtained from alternative suppliers;

2. The AM laser scan strategy, and in particular the scan rotation angle between AM build layers, had a profound effect on the strength, ductility and anisotropy (transverse strain behaviour) developed in the as-built alloy;

3. Microstructural porosities and un-fused powder particles observed in one group of samples led to reduced plasticity and erratic fracture behaviours in aged MS300 samples;

4. The AM component's relative density is affected by unfavourable powder feedstock characteristics (size and morphology), and the part's cross-sectional projection onto the build-platform;

5. Plastic anisotropy can be reduced significantly through application of a dislocation hindering precipitation heat-treatment, however, a degree of transverse strain anisotropy is likely to remain due to the AM material's fabrication history.

Appendix B. Article 2

Plastic Anisotropy of Additively Manufactured Maraging Steel: Influence of the Build Orientation and Heat Treatments

Barry Mooney[a], Kyriakos I. Kourousis[a], Ramesh Raghavendra[b]

[a] *School of Engineering, University of Limerick, Ireland, V94 T9PX*
[b] *South Eastern Applied Materials Research Centre (SEAM), Waterford Institute of Technology, Ireland, X91 TX03*

Abstract

This experimental study investigates the combined effect of the three primary Additive Manufacturing (AM) build orientations (0°, 45°, and 90°) and an extensive array of heat treatment plans on the plastic anisotropy of maraging steel 300 (MS1) fabricated on the EOSINT M280 Direct Metal Laser Sintering (DMLS) system. The alloy's microstructure, hardness, tensile properties and plastic strain behaviour have been examined for various strengthening heat-treatment plans to assess the influence of the time and temperature combinations on plastic anisotropy and mechanical properties (e.g. strength, ductility). A comprehensive visual representation of the material's overall mechanical properties, for all three AM build orientations, against the various heat treatment plans is offered through time - temperature contour maps. Considerable plastic anisotropy has been confirmed in the as-built condition, which can be reduced by aging heat-treatment, as verified in this study. However, it has identified that a degree of transverse strain anisotropy is likely to remain due to the AM alloy's fabrication history, a finding that has not been previously reported in the literature. Moreover, the heat treatment plan (6h at 490°C) recommended by the DMLS system manufacturer has been found not to be the optimal in terms of achieving high strength, hardness, ductility and low anisotropy for the MS1 material. With the use of the comprehensive experimental data collected and analysed in this study, and presented in the constructed contour maps, the alloy's heat treatment parameters (time, temperature) can be tailored to meet the desired strength/ductility/anisotropy design requirements, either for research or part production purposes.

Keywords: additive manufacturing, 3D printing, maraging steel, anisotropy, heat treatment, strength, ductility.

Preprint submitted to Additive Manufacturing *September 3, 2018*
In Review Manuscript *December 5, 2018*

Introduction

Structure-critical metallic components, produced by additive manufacturing (AM), are expected to display a high degree of isotropy. The dependence of mechanical properties on orientation, known as *anisotropy*, is a consequence of the metal's fabrication history which places limitations on the design of the part. Maraging steels possess the mechanical properties which give them engineering significance in applications where high-strength, toughness and ductility (at high-hardness), and dimensional stability are required [1–3]. Based on the binary Fe-Ni primary phase system, the highly-alloyed steel is strengthened by finely dispersed precipitates, which block movement of dislocations/defects within the crystal lattice. The dispersion of secondary phase alloying elements (Mo, Co, Ti and Al), mobilized through a straightforward and relatively expeditious aging heat-treatment, leads to an exceptional combination of strength and toughness [2, 6–8]. Maraging steel's low-carbon soft martensitic matrix is mostly free from interstitial alloying elements, which rank it as an excellent candidate for synthesis by AM and welding [1, 8–10]. The 18Ni (300) grade[1], or slight modifications thereof, has been used in AM, and is retailed commercially in powder form under several aliases. The quality assured *MS1* is one such powder supplied by EOS [11]. This powder has been suitably refined for EOS's powder-bed AM systems and processing techniques, which have retained the historical proprietary name *Direct Metal Laser Sintering* (DMLS). Another, commonly used, term for this process is Selective Laser Melting (SLM), since the technique employs a high-powered laser-beam energy source to fully melt powder particles into a high density, and chemically homogeneous composition. Driven by computer aided design (CAD) data, the laser's scanning strategies can be used to achieve layer-wise growth of imaginative, and relatively unconstrained geometries [11, 12].

[1]One of the four commercial maraging steel grades developed by Inco, where each grade was optimised in terms of strength and toughness. The *300* designation represents the grade's yield strength in ksi units [39]

It is the alloy's outstanding properties and heat-treatment expediency in conjunction with the AM process's shaping efficiency that give DMLS produced maraging steel 300 such appeal. These factors allow for a much-accelerated fabrication route than conventionally manufactured (CM) parts, and thus offsets the high acquisition cost of the alloy, as well as the process costs. DMLS built maraging steel 300, however, has a major drawback amongst its CM counterpart. The mechanical properties are known to be anisotropic due to an inherent sensitivity with regards to how a part is orientated within the AM build volume [12, 14, 15]. This anisotropy is manifested through the fabrication process where large thermal gradients during melt-pool solidification, combined with the layer-wise deposition of the powder, planar movement of the heat source, and uniaxial movement of the build-plate, make it difficult to homogenize the microstructure and mechanical properties of the as-built metal. A mesostructure of fine solidification cells, unique to the powder processing method and consequent to the powder granule melt dynamics, is coupled with continuous re-melting/heating of material beneath the melt-pool during build-up causes a distinct three-dimensional (3D) microstructural pattern to form. This results in mechanical properties which vary with direction and causes the material to exhibit anisotropic mechanical properties. Furthermore, the state of anisotropy can be exacerbated by ancillary process defects, such as residual stresses, and porosity, and a number researchers have investigated the effect of AM processing parameters to improve the build quality of maraging steel 300 [16–18].

As indicated by EOS in the MS1 material data sheet (MDS) [12], the material becomes isotropic following application of a specified aging heat-treatment (6h at $490°C$), however, the MDS is not sufficient to characterize the material performance for engineering designs and products, since it covers only the primary build orientations (0°, 90°), and comes from a single source (EOS). The effectiveness of both the AM fabrication and heat-treatment procedure can only be measured by the extent to which the as-built and treated component behaves under mechanical loading, yet very limited published research [19, 20] exists concerning the build orientation

influence on mechanical behaviour of AM-produced maraging steel 300. Croccolo et al. [20], who investigated the dependence of build orientation relative to the build plane (0°, 45°, and 90°) on the high-cycle fatigue life of EOS M280 produced MS1 specimens in the aged (6h at 490°C) condition only, found no substantial difference on the fatigue properties. Recently, Monkova et al. [19] examined the tensile properties of EOS MS1 fabricated at 0°, 45°, and 90°, and contrary to the EOS published MDS [12] they observed no significant orientation dependence in the tensile stress-strain behaviour for as-built, solution heat-treated (1h at 820°C), and aged (6h at 490°C) material. Other available test-data is mainly limited to static testing (tensile, and/or hardness) of maraging steel 300 fabricated in one [3, 8, 9, 16, 21–26], or two [14, 18, 27–29] of the primary AM build orientations. The most comprehensive of these studies in terms of the reported mechanical properties is [9], which monitors the effect of an array of aging heat-treatments on the static properties of AM fabricated maraging steel 300. While the study presents a broad range of hardness results, only very limited tensile properties are reported (i.e. for the as-built and five other peak-aged heat-treatment conditions). Furthermore, only the horizontal (0°) build-orientation is considered. Authors Yin et al. [30] and Bai et al. [31] and Mutua et al. [18] also present hardness and tensile data for horizontal specimens tested under a narrow array of aging treatments. In these studies, however, non-characteristic fluctuations/variations in the AM alloy's elasticity and plasticity behaviour can be observed. While explanations for these abnormalities are not asserted, they may indeed be introduced during the fabrication process and/or during the material characterization process (e.g. due to the tensile test rates employed). Nevertheless, these irregularities mandate a more comprehensive and detailed experimental analysis of AM maraging steel 300 monotonic behaviour. So far, the effect of aging heat-treatment on stress and strain anisotropy for this particular material has not been previously addressed, and there have been no reported findings on strain anisotropy for parts fabricated at various build orientations (i.e. 0°, 45°, and 90°). Moreover, the availability of tensile properties for AM fabricated maraging steel 300

for the primary build orientations (0°, and 90°) is limited. Other significant work has been performed to-date in characterizing the microstructure [25, 29, 31, 37, 117, 118], precipitation reactions [8, 42], and austenite reversion behaviours [9, 23, 37, 86] with several of these studies reporting similar microstructures in maraging steel 300 having been produced on a range of AM machines under varying process parameters.

Since it is necessary to consider the material's multiaxial mechanical properties during the process of mechanical component design, the lack of orientation dependence data presents challenges for engineers when it comes to utilising the highly advantageous AM technology for their engineering designs and products. In order to address the aforementioned research literature gaps, in this work, we report a comprehensive experimental analysis of maraging steel 300 mechanical properties and plastic anisotropy behaviour. In doing so, we take into account both the effect of three AM build-orientations (0°, 45°, and 90°), as well as a large array of heat-treatment plans (combinations of time, and temperature) to allow for a wide-scale investigation of anisotropic variation, not previously conducted in the past for this AM material. Plastic anisotropy describes an uneven response of the alloy's plastic properties (or flow-strain relationships) with respect to the AM build orientations, and has been quantified in this investigation by the *R-value* parameter. R-value is the ratio of true width-to-thickness plastic strains, and this parameters allows an examination of the alloy's tendency to strain non-uniformly by consequence of the test-coupon's build-orientation. The full mapping of AM fabricated maraging steel 300 mechanical properties for all three build orientations, in conjunction with their respective R-values has not previously been reported in the literature, and can serve as a very practical tool for AM engineers and researchers wishing to tailor the output of the EOS MS1. This novel experimental work is particularly focused on providing a means of AM maraging steel 300 heat-treatment selection to meet individual strength/ ductility/ anisotropy engineering design requirements, and intends to act as a guide project for other AM manufactured metals exhibiting anisotropy.

Material and methods

Material and AM process

Gas-atomized MS1 powder feedstock supplied by EOS was used. The chemical composition of the raw-material is shown in Table B.1, which corresponds to US classification 18 Maraging (300), German X3NiCoMoTi 18-9-5, and European 1.2709 [99]. In the same table, the results of the energy dispersive x-ray (EDX) analysis, conducted with a Hitachi SU 70 Scanning Electron Microscope (SEM), for the main comprising elements are also presented. The powder presented spherical particles typically measuring under $50\mu m$. The SEM morphology and particle size distribution, analysed using a *Malvern Morphologi G3* particle analyser, are shown in Figures B.1a and B.1b respectfully. The observed median particle size was $36.69\mu m$, and had a standard deviation (SD) of $10.74\mu m$. The median particle circularity (deviation from a perfect circle, where perfect circularity = 1) was 0.956.

Table B.1: Chemical composition (%wt) of MS1, the 18Ni (300) grade maraging steel powder supplied by EOS [12] with SEM-EDX analysis results for the main comprising elements (EDX sampling area: $\approx 10\mu m^2$).

	Ni	**Mo**	**Co**	**Ti**	**Al**	**Cr**	**Si**	**Mn**	**C**	**Fe**
MS1 [12]	17-19	4.5-5.2	8.5-9.5	0.6-0.8	0.05-0.15	0-0.5	0-0.1	0-0.1	0-0.03	Bal.
SEM-EDX	18.14	5.67	8.94	0.87	-	-	-	-	-	Bal.

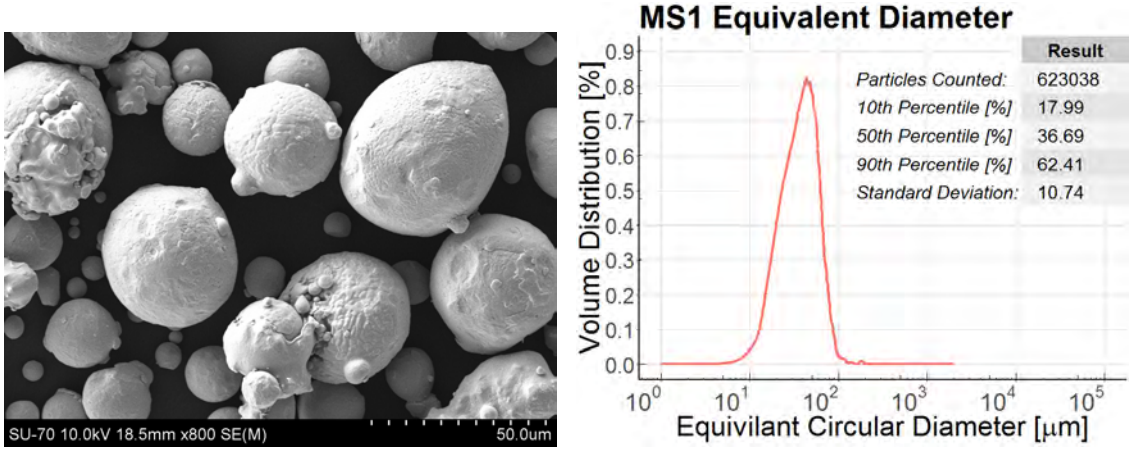

(a) (b)

Figure B.1: (a) SEM morphology of the MS1 powder, and (b) powder particle size distribution (circular equivalent diameter) with statistical details inset.

A rectangular-shaped tensile test specimen, meeting the requirements of the ASTM E8M standard [100], was selected to allow for both lateral and axial elastic and plastic strain measurements whilst under tensile loading. The test specimen geometry, dimensions and tolerances are shown in Figure B.2a. Test-specimens having a uniform cross-section at gage, were fabricated at SEAM, IE using the EOS *EOSINT M280* system within an atmosphere of inert Nitrogen over the course of three consecutive AM builds. The M280 was equipped with 200W Ytterbium-fibre laser and was fitted with the manufacturers recommended (for MS1) ceramic re-coater blade. To investigate the influence of build orientation on property anisotropy, test-specimens were fabricated in the Y-Z build plane at three angles (0° (horizontal), 45° (inclined), and 90° (vertical)) between their longitudinal axis and the build platform, as shown in Figure B.2b. A total of forty-eight (48) samples were fabricated (i.e. sixteen (16) test-pieces for each AM orientation) from a virgin batch of MS1 feedstock over three consecutive AM builds.

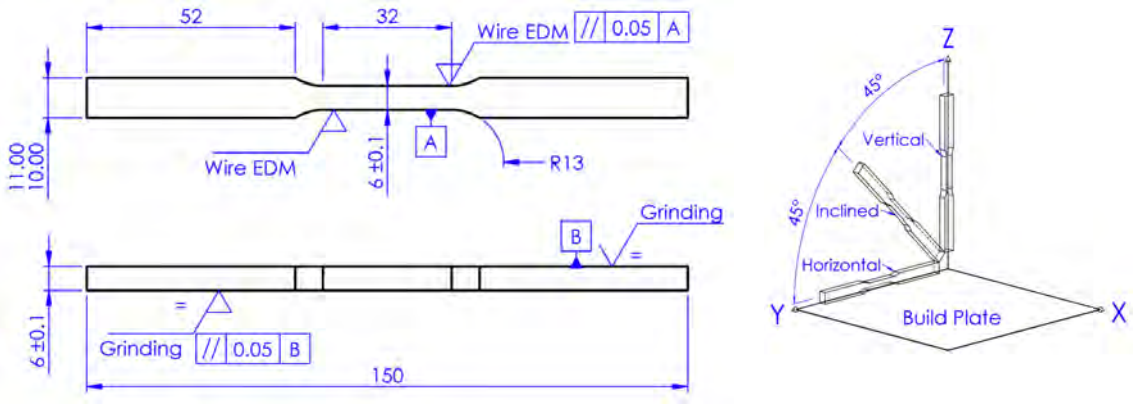

(a) (b)

Figure B.2: (a) Showing the finish-machined specimen geometry, and (b) the AM build volume coordinate system and test-specimen build orientations.

As shown in Figure B.3, the AM build leaves visible ridges upon parts' build surfaces and a stair-stepped effect on 45° sloping surfaces which are indicative of the layered fabrication process. High roughness at the surface can augment crack initiation thus leading to pre-mature failure. Furthermore, these ridges hinder the accurate evaluation of gage width and thickness dimensions. Ductility calculations are sensitive to the measurement of gage cross-sectional area, while the ASTM E8M standard

exhorts that particular attention be given to the uniformity and quality of surface-finish with regards high-strength specimens [100]. For these reasons, an additional 0.5mm of machinable material was added to each face prior to the AM-build. This surplus material, which was later machined by single-cycle precision computer numerically controlled (CNC) wire electrical discharge machining (EDM) profiling and surface-grinding operations, had the extra benefit of safeguarding against potential thermally induced distortion.

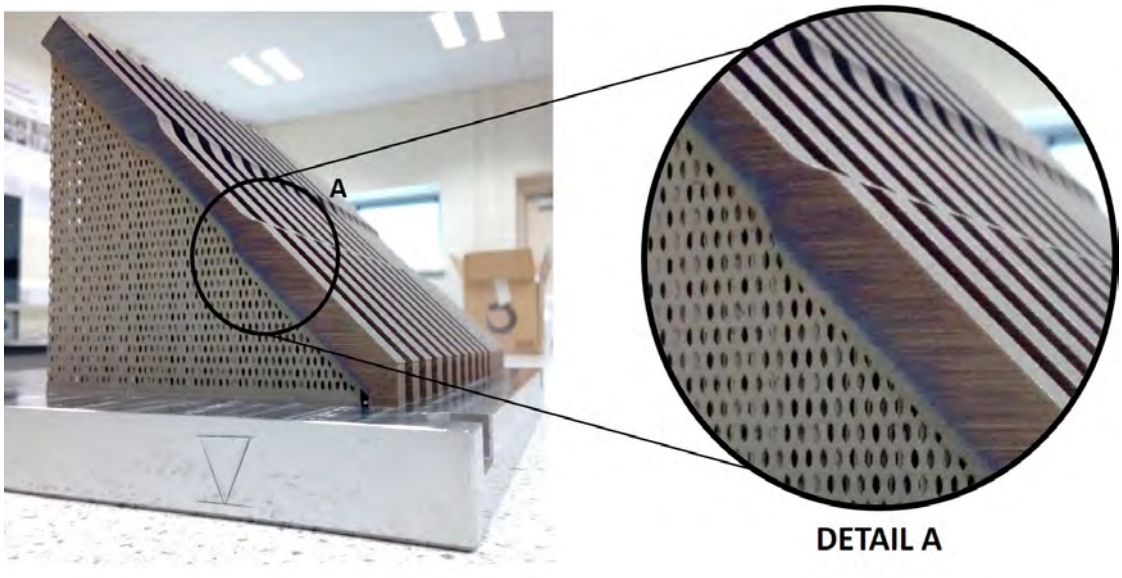

Figure B.3: DMLS fabricated samples of the 45° build orientation before detachment of the support scaffold from the parts/build-platform. Detail A highlights the presence of distinct surface ridges which are consequent to the layer-wise fabrication process.

The EOS M280 machine's hardware was driven by the factory default, undisclosed, and pre-optimized set of parameters *'MS1 Performance 2.0'* which has been developed by the manufacturer for this specific material and machine combination [99]. EOS claims that their set of parameters (*MS1 Performance 2.0*) ensures reliable mechanical properties. This offers a defined part property profile bolstering industry-level repeatability and quality [101]. A vertical support-scaffold connected the under-side of each specimen to the manufacturer's recommended building platform (Steel 1.2083 36mm thick DirectBase TS36P) [99]. This structure played two important roles during the elevated temperature production cycle - (a) it functioned as a passive heat-sink during manufacturing; and (b) it reinforced the 45° inclined

specimens against cross-platform re-coater forces and earthward gravitational forces. As verified by the post-build inspection, the process had achieved sound metallurgical bonding between layers, with a uniform and characteristic ridged surface. The parts were dimensionally accurate, however it is worth noting that a longitudinal shrinkage distortion (bowing) in the AM build direction (Z), to the extent of $\leq$ 0.1mm, was observed in several horizontal (0°) specimens after their removal from the build-plate. This shrinkage, which was rectified in the downstream machining operation, is understood to have been brought about by a build-up of thermal stresses developed between the raw-material and base-plate metal during the heating and cooling cycles over the opening number of layers.

The heat treatment (aging) was performed in a pre-heated Elite Thermal Systems 120 litre 6kW heavy duty-fan oven (air atmosphere) controlled by dual Eurotherm 3216 PID temperature controllers and cooled slowly in still air at ambient temperature ($23°C$). The experimental heat-treatment plan is shown in Table B.2, where T denotes tensile tests and H the Vickers hardness measurements performed for a set of 0°, 45°, 90° specimens.

Table B.2: Showing the experimental heat-treatments applied to full-sets of test-specimens (i.e. 0°, 45°, 90°), where the characters *'T'* and *'H'* symbolize a tensile, and/or Vickers Hardness test-campaign.

Temperature [$°C$]	**Aging time [hours,h]**										
	1h	**2h**	**3h**	**4h**	**5h**	**6h**	**8h**	**10h**	**12h**	**15h**	**16h**
460°C	-	-	-	-	H	T,H	T,H	H	T,H	-	H
490°C	-	-	H	T,H	H	T,H	T,H	-	H	-	-
525°C	-	-	H	T,H	H	T,H	T,H	H	-	H	-
540°C	-	H	-	T,H	H	T,H	T,H	H	-	-	-
600°C	T,H	T,H	H	T,H	H	T,H	H	-	-	-	-

The treatment temperature dictates the kinetics of phase separation in the alloy's matrix, and ultimately determines the population and size of precipitates which form, thus, aging temperature has the most significant effect on precipitate size and dispersion in maraging steels [4]. The EOS recommended heat-treatment temperature of $490°C$ allows a populous dispersion of hindering precipitates to form over the stated 6h aging period. It is the interaction between dislocations and precipi-

tates which determines the material's strength and ductility. Prolonged holding at temperatures below austenite start ($A_s \approx 560°C$) not only reduces the effectiveness of dislocation hindrance but will eventually lead to a decomposition of martensite by diffusion-controlled reactions to a stable blend of austenite and ferrite. Aging at temperatures approaching A_s reduces the population of developing precipitate particles and heightens the propensity for austenite reversion where its formation can even precede precipitation. Higher aging temperatures are employed when good toughness/ductility is sought, and to that end - the EOS M280 parameter sheet [97] outlines an aging treatment of 6 hours at $525°C$(-$600°C$). The experimental heat-treatments (Table B.2) were therefore selected to confirm EOS recommendations; to formulate a comprehensive evaluation of static mechanical properties; and to allow for wide-scale investigation of the anisotropy variation.

Characterization

A Taylor Hobson *Hommel Tester T500* surface profiler was used to measure the roughness variation due to surface orientation within the build volume. For each build orientation, the profiler's stylus was traced along specimens' loading axis using an assessment length of 4.8mm. Two roughness parameters were utilised:

- *Rz* representing the mean roughness depth by calculating the average value of the five highest peaks and five deepest valleys over the assessment length;
- *Ra* corresponding to the arithmetical mean surface roughness value of all profile deviations over the assessment length.

Archimedes' Principle density measurements, in compliance with ASTM B962-17 [102], were performed using a *Sartorius Quintix* laboratory balance (model 65-1S) equipped with accessory YDK03 density determination kit.

Uniaxial tensile tests were conducted at ambient temperature in a calibrated *Zwick/Roell (Dartec) M1000/RK* servo-hydraulic closed-loop testing machine equipped with 100kN capacity load cell and fitted with ±100kN fatigue rated hydraulic wedge

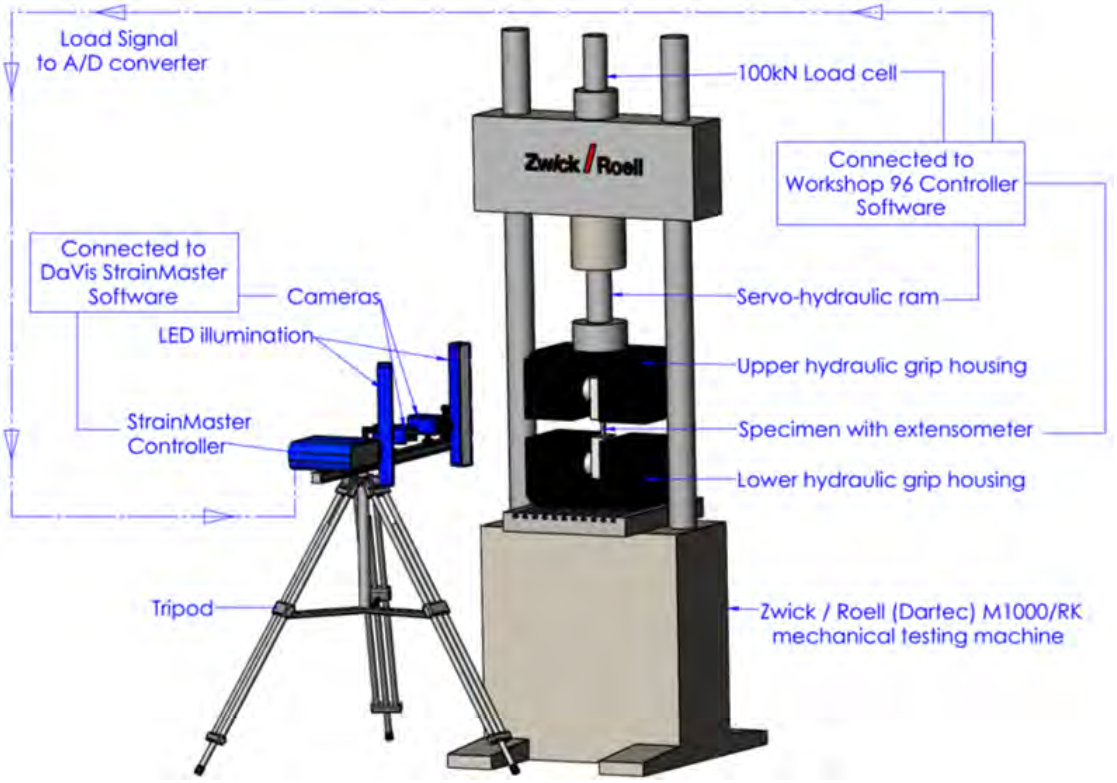

Figure B.4: Configuration of tensile test set-up including the 3D Digital Image Correlation (DIC) apparatus which allowed concurrent determination of test-specimen width and axial strains (ϵ_w and ϵ_l).

grips. The test routine followed strict adherence to the guidelines present in ASTM E8M [100]. The test was initially controlled (via 9600 series controller) to the elastic stressing rate of 10.34 MPa/s, using strain control from the extension feedback channel (Epsilon model 3542-025M-050-ST). Upon detection of yield, the test-rate maintained a constant plastic strain rate of $6.25 \times 10^{-4}/s$ controlled via the stroke feedback channel. At the end of the yield (detected from either reaching a 5% increase in stress, or an absolute strain limit of 2%), the test-velocity was commanded by a third rate, the tensile strength (R_m) rate: 0.0068/s. This strain rate was maintained to peak force, and through to failure.

Non-contact full-field strain and deformation was measured and analysed using *La Vision's* portable 3D Digital Image Correlation (DIC) apparatus. The apparatus comprised of (i) two 12-bit Imager E-lite CCD-chipped cameras fitted with 35mm lenses, (ii) two gated white light sources each containing twelve linear-configured LEDs, (iii) a *StrainMaster* Controller and data-acquisition unit with integrated

analogue-to-digital converter (A/D), and (iv) a dedicated PC complete with *Strain Master*® processing software. The experimental arrangement is shown in Figure B.4. Each camera was focussed onto the measurement plane providing an overlap region upon the specimen gage surface. The enclosed angle between cameras and the working distance between each camera and the test-specimen was ≈20° and ≈350mm respectively. Using the stereoscopic camera system's in-situ position, a global 3D-coordinate system was derived by means of a precursory calibration step involving a 3D two-level calibration target/plate. This included the generation of a fit mapping function with the calibration plate from which the average deviation of the dewarped calibration target positions to the ideal positions was lower than 0.3 pixel. This corresponds to an excellent fit, and an appropriate basis for the proceeding full-field 3D strain-measurement evaluations [107]. A high-contrast acrylic paint dark 'speckle' pattern (dark black speckles on a bright white background) was applied to the area of interest (i.e. the specimens' gage surface). Special attention was given to achieving a relatively fine pattern scale (for higher spatial resolution) with a non-repeating isotropic distribution. In this study, each subset (or "window") had an area of 37 pixels^2, which translated to approx. 1.75mm^2. The goal of the speckle is to provide each subset with a unique signature pixel arrangement from which the displacement pattern can be tracked in 3D space with micron accuracy by the StrainMaster software's pattern matching algorithm [106]. A sequence of images was captured during each tensile test (i.e. from zero applied load to fracture) at a periodic rate of 5Hz. A displacement vector corresponding to each subset was calculated by the StrainMaster least squares matching algorithm from a reference (un-deformed) image. The basic result of the DIC analysis was a full-field 3D displacement measurement evaluation containing thousands of measurement points. In accordance with ASTM test methods E132-04 and E517-18 [108, 109], Poisson (ν) and plastic strain ratios (R-values) have been evaluated using DIC data. In turn, the individual test-specimen R-values (R_0, R_{45}, and R_{90}), are unified by the parameter ΔR which is used to quantify planar anisotropy (i.e. in the AM Y-Z plane) by Eq.

B.1.

$$\Delta R = \frac{1}{2}(R_0 - 2R_{45} + R_{90}) \tag{B.1}$$

Metallographic samples were sectioned and mounted with Buehler Ltd. *PhenoCure* compression mounting compound, and standard finishing steps applied - including polishing with oil based monocrystalline diamond suspension ($6\mu m$ and 1 μm), *MetaDi* from Buehler Ltd.. Modified Fry's reagent was used to reveal the microstructure which was observed via an *Olympus BX60* Optical light microscope, and *Hitachi SU 70* Scanning Electron Microscope equipped with an *Oxford Instruments EDX attachment* for analysis of the comprising chemical elements.

The progress of the aging heat-treatment was evaluated using a calibrated *Zwick ZHV* Vickers macro-hardness tester and verified with a standard test block to the requirements of ASTM E92-92 [104]. Samples were sectioned, mounted, and polished, then subjected to a 30kg test force which was applied parallel to the AM material's tensile loading axis (i.e. perpendicular to the sectioned plane). At least 20 hardness measurements were performed on each test specimen, and the results and test statistics were computed using the R statistical software package [105].

The material's crystal structures were qualitatively analysed (for selective heat-treatments) via a *PANalytical Empyrean Pro* multipurpose X-ray diffractometer (XRD) using Cu Kα radiation. Crystallographic phase identification was achieved using HighScore Plus software.

Results and discussion

Surface roughness and density analysis

The as-built and machined surface roughness, along with density (ρ) measurements, are presented in Table B.3. The EOS quoted density of 8.0-8.1 g/cm^3, and roughness parameters for as-built horizontal up-facing or vertical (90°) surfaces produced with $40\mu m$ layer-thickness ($Rz = 28\mu m$ and $Ra = 5\mu m$) are in general agreement with

the presented results. The measurements imply that part density is not influenced by AM build orientation. Regarding chemical composition - there was close agreement between SEM-EDX and the published values [12] for MS1 as shown in Table B.1.

Table B.3: Axial surface roughness and density measurements (ASTM B962) for the as-built Horizontal (0°), Inclined (45°), and Vertical (90°) MS1 specimens.

	Build Orientation			
	0°	**45°**	**90°**	**Machined**
Rz (μm)	29.21	16.17	21.69	0.47
Ra (μm)	6.63	3.04	4.2	0.09
ρ (g/cm^3)	8.051	8.050	8.049	NA

As-built microstructure

A schematic representation of the laser scan strategy pertaining to the manufacturer's recommended set of parameters (*MS1 Performance 2.0*) is shown in Figure B.5. This set of parameters prescribed uni-direction line-scans with a laser hatch-spacing of $110\mu m$. The hatch-spacing and line-scan direction remained constant within each AM layer where each line-scan was segmented into stripe divisions of approximately 0.3mm - 0.6mm, presumably to prevent excessive localized heat build-up during fabrication. The scan-direction was rotated by 67° for each consecutive $40\mu m$-thick layer in an effort to homogenize the microstructure. The outcome is a practically fully dense part, with strong inter-layer and intra-layer metallic bonding. No significant process defects in the form of porosity or un-melted powder particles were observed in the microstructures. It is understood that the absence of defects is largely due to the powder characteristics, since an abundance of small spherical granules in the virgin feedstock augmented flow-ability and allowed maximum space occupancy during re-coating upon previously distributed layers.

Figure B.6 presents optical macrographs, and as-built SEM micrographs for each build-orientation. The AM characteristic laser melt tracks are apparent at low magnification in Figures B.6a, B.6b, and B.6c. The typical as-built horizontal maraging steel 300 macrostructure (Figure B.6a) has a complect appearance, with bundled

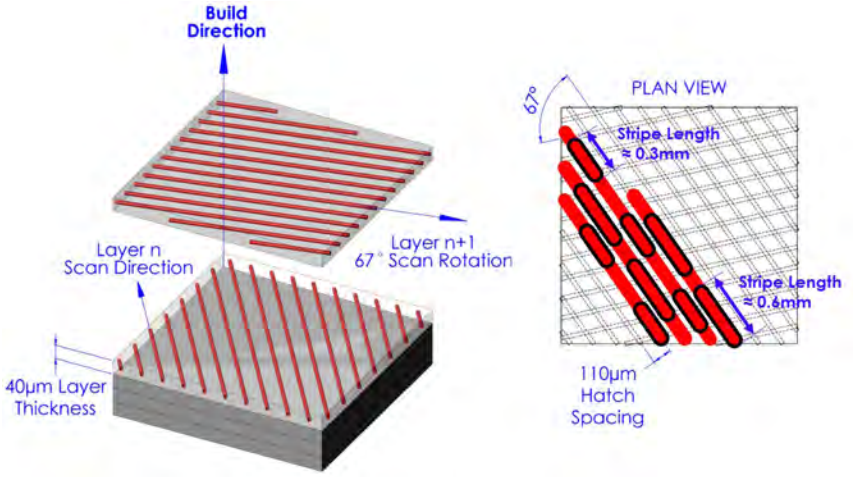

Figure B.5: Schematic representation of the DMLS laser scan strategy which has been inferred from microstructural observations. Each layer's uni-directional line-scan was divided into short stripes of length 0.3-0.6mm to prevent excessive localized heating.

interconnections of fan-shaped solidification cells between molten lines. The moderately sized melt-pool widths (45 - 70μm), and depths (35 - 55μm) are reflective of the applied laser energy input ($< 200W$). The observed melt-pool width is indicative of a laser focus diameter of $\approx 60\mu m$, while the measured melt-pool depth is typical for this powder layer-thickness ($40\mu m$). Larger laser focus-diameters ($100\mu m$) have been used with higher capacity AM platforms (laser power: 285W) administering equivalent layer-thickness [37]. By contrast to the horizontal cross-section, the 67° rotation of laser scan angle (between the sectioned and preceding layers) is clear on the vertical cross-section (Figure B.6c).

As observed in the high-magnification SEM images (Figures B.6d, B.6e, and B.6f), the AM laser scanning algorithm gives rise to various cellular morphologies including fine, coarse, and dendrite cell formations (highlighted on the images by dotted lines). The evolution mechanisms of these growth formations relate to the melt-region thermal flux direction which changes for successive layers and is theoretically explained in a recent study by Tan et al [37]. Assisted by rapid cooling rates (circa 10^3 to 10^8 $K.s^{-1}$), these very fine cellular formations orientate themselves concurrent with the direction of heat flow/removal [25, 28, 29, 31, 42, 86]. Interestingly, other research [29, 67] has failed to identify any dominant crystallographic or fibre texture with a preferred grain growth orientation from the AM processed alloy. This suggests that

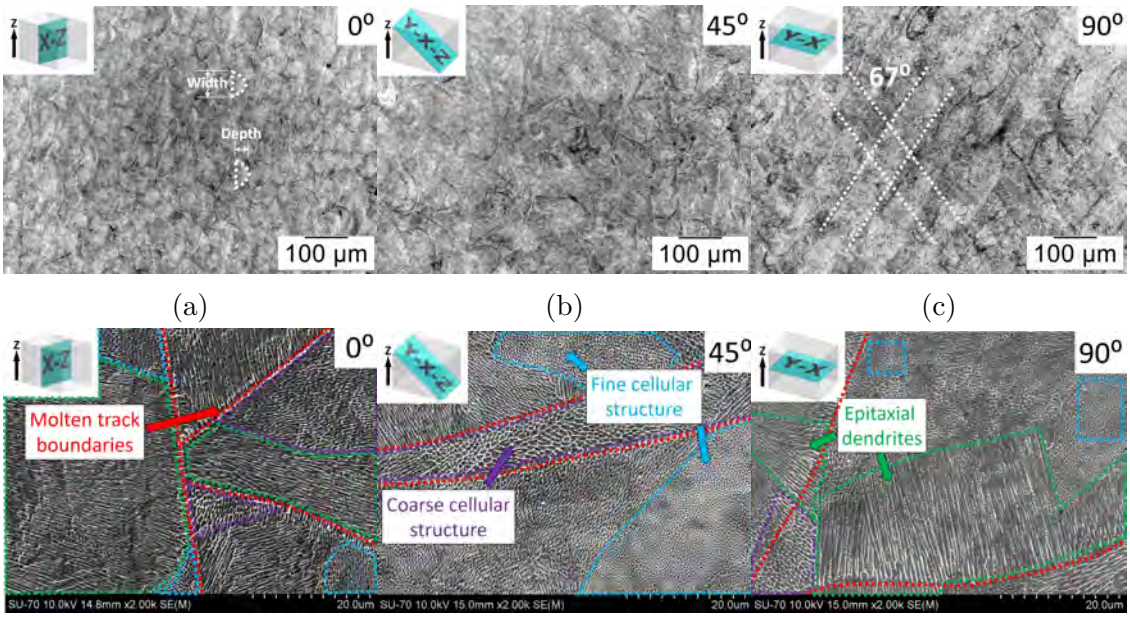

Figure B.6: Representative low magnification (optical) and high magnification as-built (SEM) cross-section images of the MS1 macrostructure/microstructure for three-build orientations: (a) and (d) horizontal (0°); (b) and (e) inclined (45°); and (c) and (f) vertical (90°). The optical images reveal melt-pool solidification patterns, whilst SEM reveals a mesostructure of circular and dendrite cells exhibiting retained austenite at cellular boundaries.

maraging steel 300 may be less susceptible to texture-generated anisotropy than other AM fabricated materials (see [58, 60, 62, 119]) which exhibit strong crystallographic preferred orientation. The SEM observed cellular morphology is believed to be a major contributor to the strength difference between AM as-built versus the solution-annealed conventionally produced alloy, which in-contrast does not display retained austenite in its microstructure, and exhibits random parent grains, each containing coarse and disordered packets of parallel lath-martensite [3, 8, 18, 86, 87]. Retained austenite is easily distinguishable in the high magnification images (Figures B.6d, B.6e, and B.6f) as the bright-colour phase which aggregates at cell boundaries. It occurs when the material cools rapidly from austenite finish (A_f) to ambient temperature, essentially freezing in place solute-rich austenite leaving it untransformed, whereas solute depleted austenite transforms into martensite. Accordingly, the importance of appropriate processing variables is evident since these will govern the volume of retained austenite in microstructure, and ultimately the part performance. To-date, however, no studies have quantified the effect of as-built (re-

tained) austenite on the post-heat-treated mechanical properties of AM-fabricated maraging steel 300.

Aged microstructure

Micrographs of the aged alloy, and their corresponding XRD spectra are presented in Figures B.7, and B.8, to demonstrate the effect of aging temperature on the reversion of metastable bcc martensite phase (Fe-α) to fcc austenite (Fe-γ). The reversion occurs during extended isothermal aging at temperatures which support the dissolution of first-stage metastable Ni_3Mo and Ni_3Ti precipitates ($T > 450$°C). These phases are later replaced with Fe_2Mo and/or Fe_7Mo_6 during a second stage development [28, 42][4]. As these new phases nucleate and grow they deplete the matrix of iron, further enhancing the Ni concentration, thus augmenting austenite reversion [5][4]. At higher temperatures these nucleation sites quickly saturate by diffusion of solute elements from the surrounding lattice. This effect combined with early onset of precipitate coarsening (overaging), causes a reduction in the alloys strength capabilities, i.e. a softening behaviour. Lower temperatures control/extend precipitate nucleation and growth, suppress austenite reversion, and allow a populous dispersion of small precipitates [4]. However, it takes considerably longer aging times for these precipitates to reach a stage where dislocation bowing is optimized, corresponding to a given temperature's peak-strength. The milder aging cycle of 6h at 460°C presents a microstructure (Figure B.7a) comparable in appearance to that of the as-built metal (Figures B.6d, B.6e and B.6f). Moreover, there is no noticeable phase change observed in the XRD spectra of as-built and 6h at 460°C treatments. As observed in Figure B.7, the austenite phase develops markedly at temperatures upwards of 490°C, where the bright cellular boundaries loose definition, and the volume fraction of the austenite phase readily increases. This is also reflected in the X-ray diffraction data (Figure B.8) where the intensities of Fe-α peaks reduce, and Fe-γ peaks increase with greater aging temperatures.

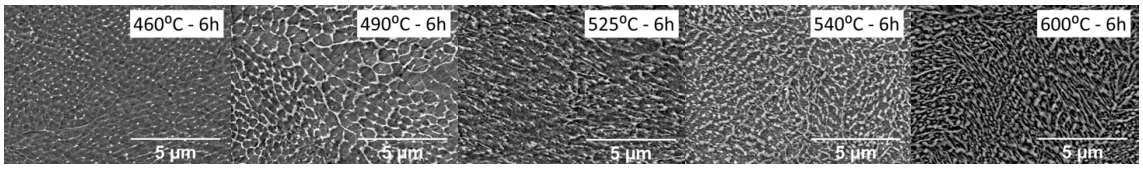

(a) (b) (c) (d) (e)

Figure B.7: SEM micrographs of AM maraging steel 300 aged for 6 hours at various temperatures (460, 490, 525, 540, 600°C) showing a reversion of austenite at solute rich cell boundaries with increased temperature.

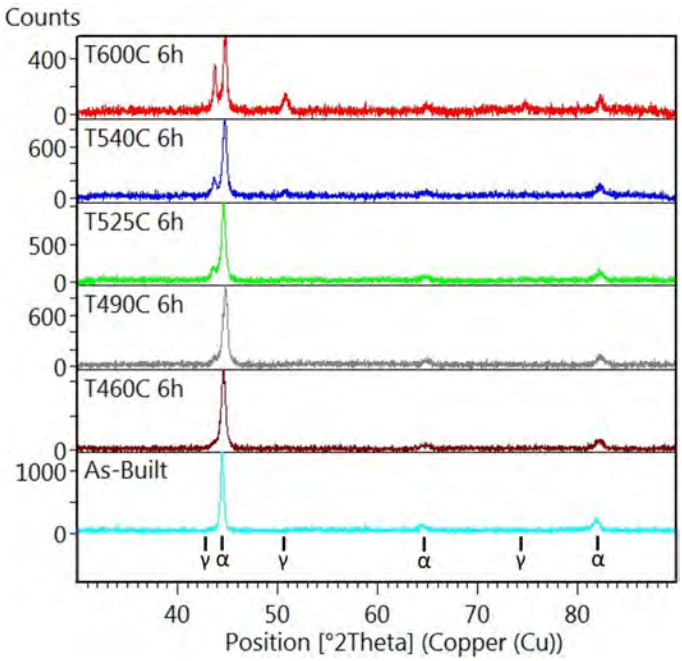

Figure B.8: XRD spectra for DMLS MS1 as a function of aging temperature. The Fe-α and Fe-γ diffraction positions are highlighted on the plot.

Mechanical Properties

Vickers hardness aging curves, and a selection of uni-axial Stress (σ) versus Strain (ϵ) curves are presented in Figures B.9, and B.10 respectively. Their associated mechanical property values are listed in Table B.4. The data convey the extent of mechanical property variation across the as-built build-orientations, and the examined heat-treatments. Despite the seeming closeness among the as-built strength and hardness values, an unusual ductility behaviour occurred in the 45° inclined orientation's stress versus strain curve (Figure B.10). In particular, a faster reduction in strength is observed, leading to failure at $\approx 50\%$ less elongation when compared to the other build-orientations. Furthermore, the as-built elastic properties of Elas-

ticity Modulus (E) and Poisson ratio (ν) display an inverse relationship with respect to build-orientation. This may be attributed to the alloy's fabrication route.

When analysing the effect of heat-treatment on mechanical anisotropy, Table B.4 data indicate that hardness measurements alone are the least effective method to reveal and quantify mechanical anisotropy and helps to explain why similar observations have not been presented in the research literature to-date. A relationship between *hardness* (H) and yield strength ($R_{p0.2}$) was devised from the available data, based on similar empirical relationships used for other metals. In particular, the typical linear rule-of-thumb for a broad range of metallic alloys given by Eq. B.2 [113] has been used.

$$H \approx 3 \times R_{p0.2} \tag{B.2}$$

Eq. B.2 holds true except in the cases of the as-built and severely overaged material (e.g. samples aged at $600°C$). Moreover, the hardness (H), described as the indenter force divided by the projected area of the indent (in MPa) is given by Eq.3.

$$H = HV_{30} \times 9.81 m/s^2 \tag{B.3}$$

Where HV_{30} is the Vickers hardness value. The bar-chart (Figure B.11) reinforces prior anisotropy observations for the as-built and aged alloy across the range of experimental treatments and suggests that a certain anisotropy remains following aging.

As shown for the hardness measurements in Figure B.9, even for the low aging temperature (460°C) the greatest percentage of the treatment's peak hardness is obtained within the early stages of aging (during underaging). The rate of early-stage hardening is due the populous development of small and coherent first-stage precipitates which shear the passing dislocations [4]. This lower temperature somewhat regulates early-precipitation diffusion kinetics allowing particles to grow by a greater extent before overaging dominates. For this reason, the greater population of particles at lower treatment temperatures provides an enhanced strength-

Table B.4: Mechanical properties data retrieved from tensile and Vickers hardness testing of MS1 produced by DMLS (Elasticity modulus (E); Poisson ratio (ν); Yield strength ($R_{p0.2}$); Tensile strength (R_m); Elongation to fracture (At); Reduction in area (Z); and Vickers hardness (HV)). EOS reference data [12] are shown with italics fonts.

Heat-Treatment	Orientation	E [Gpa]	ν	$R_{p0.2}$ [MPa]	R_m [MPa]	At [%]	Z [%]	HV_{30kgf} [kg/mm^2]
EOS As-Built[12]	*0°*	*160*±25	-	*1050*±100	*1100*±100	*10*±4	-	*(310-360)*
	90°	*150*±20	-	*1000*±100	*1100*±100	*10*±4	-	*(310-360)*
EOS Aged[12] 6h @ 490° C	*0°*		-				-	
	90°	*180*±20	-	*1990*±100	*2050*±100	*4*±2	-	*(>513)*
As-Built	**0°**	161	0.24	1069	1174	15.7	56	382
	45°	140	0.29	991	1144	6.8	56	327
	90°	122	0.35	892	1057	13.8	62	375
6h @ 460°C	**0°**	182	0.31	1908	1971	6.5	22	594
	45°	183	0.30	1850	1939	6.2	18	593
	90°	170	0.33	1803	1907	7.0	19	591
8h @ 460°C	**0°**	178	0.33	1951	2006	7.4	24	602
	45°	178	0.29	1907	1987	7.4	20	590
	90°	171	0.30	1849	1939	6.9	23	603
12h @ 460°C	**0°**	177	0.34	1979	2032	6.6	22	610
	45°	180	0.31	1941	2022	6.0	21	607
	90°	171	0.32	1888	1965	5.6	19	610
4h @ 490°C	**0°**	182	0.33	1961	2004	8.6	33	603
	45°	185	0.31	1895	1963	8.0	28	595
	90°	180	0.32	1875	1928	5.9	24	599
6h @ 490°C	**0°**	178	0.40	1901	1958	5.9	19	602
	45°	183	0.28	1925	1984	4.4	10	603
	90°	178	0.28	1893	1958	6.1	22	599
8h @ 490°C	**0°**	183	0.34	1969	2020	8.3	32	608
	45°	184	0.29	1930	1993	7.8	29	606
	90°	180	0.32	1912	1978	4.2	21	615
4h @ 525°C	**0°**	189	0.33	1811	1882	5.82	35	570
	45°	185	0.29	1811	1878	5.38	30	568
	90°	180	0.3	1797	1885	7.97	23	578
6h @ 525°C	**0°**	181	0.34	1768	1844	10.4	32	560
	45°	175	0.32	1747	1818	6.9	29	560
	90°	176	0.31	1741	1816	8.5	31	554
8h @ 525°C	**0°**	179	0.34	1729	1811	10.5	36	552
	45°	181	0.31	1714	1802	9.9	33	558
	90°	181	0.32	1723	1816	10.1	30	557
4h @ 540°C	**0°**	181	0.34	1700	1769	10.4	37	543
	45°	183	0.32	1697	1778	10.2	38	550
	90°	169	0.30	1656	1744	9.3	33	554
6h @ 540°C	**0°**	182	0.26	1661	1736	12.4	38	536
	45°	177	0.29	1666	1746	6.7	19	542
	90°	182	0.31	1640	1724	10.5	31	536
8h @ 540°C	**0°**	182	0.31	1625	1701	11.2	41	525
	45°	177	0.29	1620	1705	11.5	37	534
	90°	174	0.31	1579	1666	10.8	33	531
2h @ 600°C	**0°**	173	0.32	1326	1440	17.1	49	458
	45°	174	0.29	1312	1425	16.5	53	457
	90°	166	0.29	1290	1405	15.5	51	457
4h @ 600°C	**0°**	169	0.31	1267	1387	17.2	49	447
	45°	167	0.27	1263	1382	16.7	49	447
	90°	164	0.30	1253	1368	16.0	49	442
6h @ 600°C	**0°**	166	0.33	1214	1338	17.6	50	430
	45°	173	0.26	1211	1335	17.7	50	432
	90°	157	0.33	1172	1303	14.5	54	432

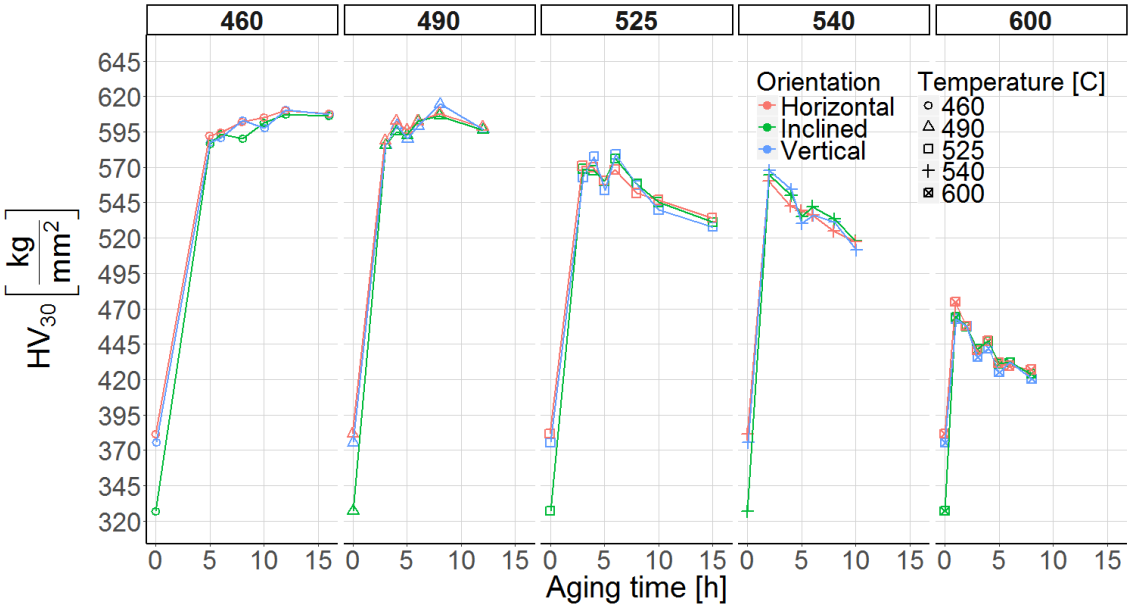

Figure B.9: Precipitation strengthening curves demonstrating the effect of heat-treatment time and temperature parameters on the attainable hardness and anisotropy of AM MS1.

ening effect, however, as previously mentioned, the time taken to achieve peak strength/hardness increases alongside. Despite the narrow temperature window, and harmonious strengthening-relationship between 460°C and 490°C, it takes 4h longer for the former to reach its peak-hardness condition.

As indicated in Table B.4, the obtained as-built and aged (6h at 490°C) mechanical properties agree with EOS published figures with exceptions for the as-built 90° elasticity modulus and yield-strength experimental values which under-perform slightly. As-built test-specimens displayed the largest hardness variation. The mean and standard deviation (SD) with respect to the build orientations was 362HV and 25HV in that order. This relatively large variation was reflected across the full range of as-built mechanical properties, for example: the mean and SD yield strength ($R_{p0.2}$), and total elongation (At), were 984MPa (with SD = 89MPa) and 12% (with $SD = 4.7\%$) respectfully. Higher recorded hardness values were observed jointly in specimens aged at 460°C for 12h; and 490°C for 8h which measured 609HV (with SD = 4HV), and 609HV (with SD = 5HV) respectively. Highest yield strength was 1936MPa (with SD = 46MPa) and tensile strength was 2006MPa (with SD = 36MPa) for the specimens aged at 460°C for 12h, but there was little mechan-

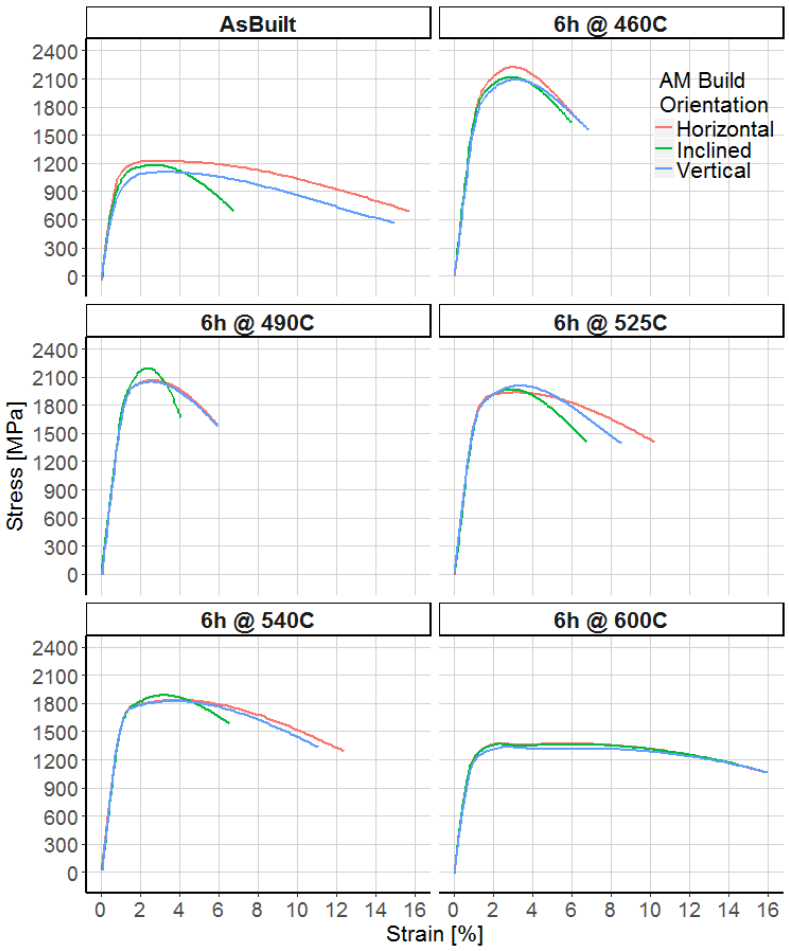

Figure B.10: Excerpt of σ-ϵ curves obtained from the as-built and aged (at 6h) test-specimens.

ical property difference between the 12h at 460°C and 8h at 490°C heat-treatments. These optimal strength values were accompanied by a sharp reduction in ductility, evaluated at 5-6% on average.

The aging and stress (σ) - strain (ϵ) curves show clear evidence of overaging when temperatures exceed 490°C, most noticeably at 600°C where the alloy is heated into the austenite phase transformation zone. This observed loss of hardness/strength is based on Orowan's mechanism of dispersion hardening, where passing dislocations loop around larger and more dispersed stage-two Fe_2Mo and/or Fe_7Mo_6 precipitates [63, 112]. The effectiveness of dislocation hindrance in the overaged specimens is much reduced due to the combined loss of precipitate-lattice coherency, and the increasing sparsity of these blocking particles. Overaged specimens also display increased strain-hardening, corresponding to the wider dispersion of particles whereby the build-up of subsequent gliding dislocation loops heighten the degree of back-

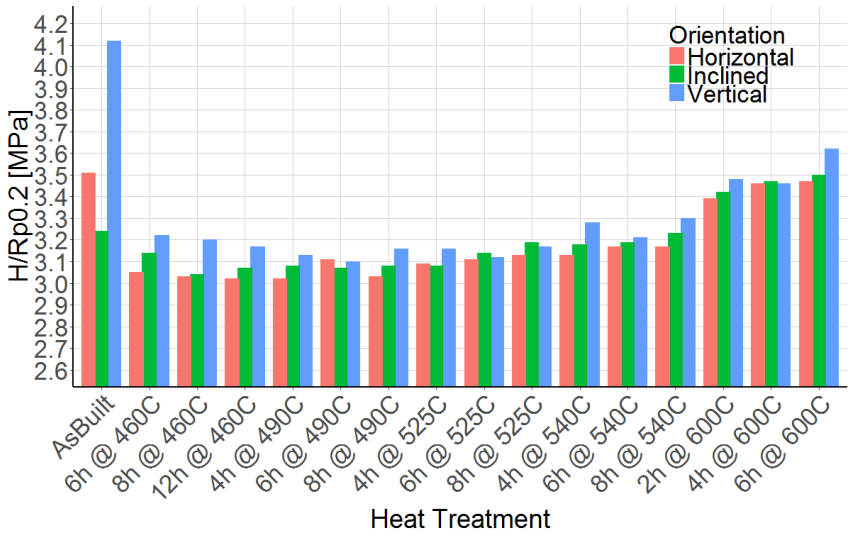

Figure B.11: Ratio of Hardness (H) to Yield Strength for the as-built and heat-treated MS1 examined.

stress in the lattice. These overaged AM MS1 properties, not previously reported, may be useful to AM practitioners when good toughness is sought, as indicated by the area under the σ versus ϵ curves.

Further evaluation of plastic anisotropy has been performed via the DIC obtained R-value measurements. The R-value is defined as the true width-to-thickness strain, given by Eq. B.4.

$$R\ value = \frac{\varepsilon_w}{\varepsilon_t} \tag{B.4}$$

The obtained results are shown in Figure B.12, which highlight (i) non-uniform transverse straining since $R_{isotropic} = 1$; and (ii) R-value variation between AM build orientation angles. As with the mechanical properties, a significant reduction in plastic strain anisotropy was observed following the application of aging heat-treatments. The precipitation of nanometric dislocation hindering precipitate particles is exclusively responsible hence. The test-specimens, regardless of their build orientation and heat treatment, consistently displayed a ratio of true width-to-thickness strains (R-values) below unity (< 1) within the alloy's elastic-plastic regime. While these harmonious trends indicate that the plastic-strain behaviour is more-or-less uniform in the Y-Z build plane, they signify greater thinning in specimens' thickness direction, and suggest that the 67° laser scan rotation be-

tween layers, and subsequent aging heat-treatment, are not sufficient to suppress anisotropic transverse strain behaviour. Depending on the engineering application, it may therefore be necessary to perform a solubilization treatment step prior to aging which could abolish any fabrication manifested microstructural patterning, achieve a derivative stress relaxation, ensure the dissolution of detrimental phases, and ultimately homogenise the microstructure. However, such circumstances incur additional processing cost, complexity and time, which subtracts from the overall AM maraging steel 300 appeal.

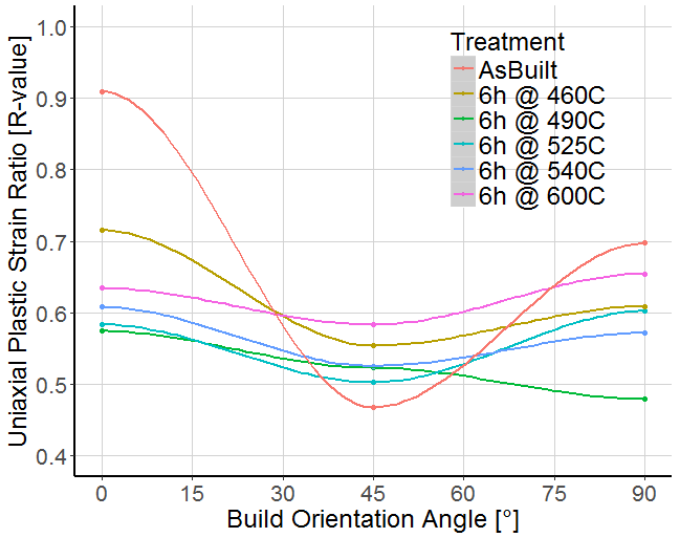

Figure B.12: Plot of R-values versus build orientation angle, evaluated at 1.5% axial strain. The trend patterns for this selection of representative heat-treatments are displayed using local polynomial regression fitting.

The experimental findings indicate that the AM induced anisotropy cannot be eliminated through application of the 6h at 490°C heat-treatment. Furthermore, this heat-treatment plan is not optimal for the alloy's strength, ductility, hardness, or anisotropy. To address this issue, mean mechanical property values (with respect to the build orientations) from the complete set of experimental results (as outlined in Table B.2) have been used to construct contour surface plots. In particular, bi-variate interpolation of x (aging time), y (aging temperature), and z (response variables: $R_{p0.2}$, R_m, At, HV, and ΔR-values (Eq. B.1) components has been applied to represent a smooth surface of z values at selected points distributed in the x-y plane using the R statistical software package [105, 115]. These plots (shown

in Figure B.13), may act as a guide for selection of tailored heat-treatments, when specific mechanical properties and anisotropy limits are required for an AM part.

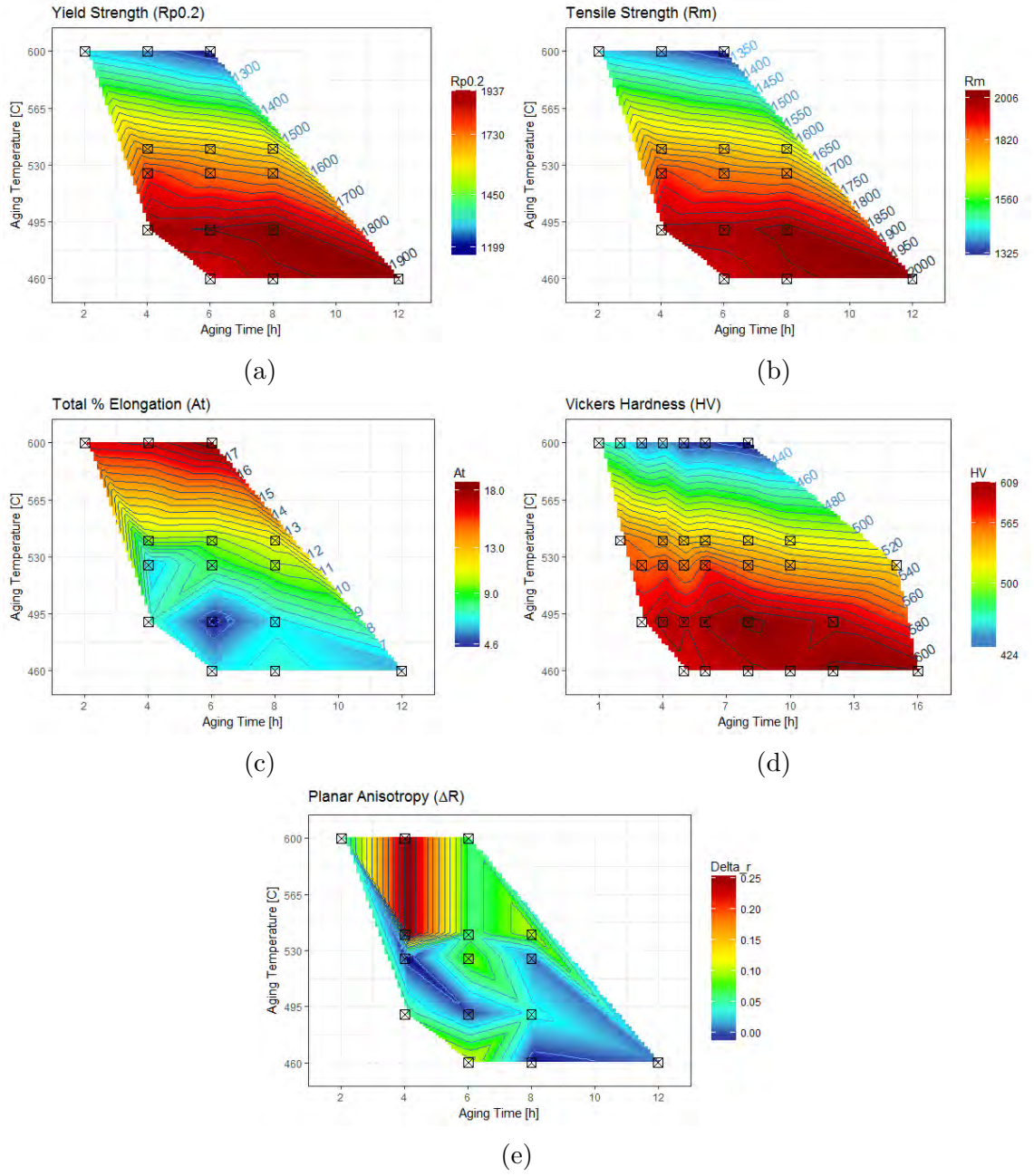

Figure B.13: Interpolated smooth surface contour plots of experimentally determined (marked) AM MS1 properties (a) Yield strength ($R_{p0.2}$); (b) Tensile strength (R_m); (c) Total % Elongation (At); (d) Vickers hardness (HV); and (e) Planar anisotropy (ΔR) evaluated at 1.5% axial strain.

Figure B.13 clearly communicates that the chosen aging parameters correspond to significantly different achievable mechanical properties in DMLS MS1. Remarkable strength and hardness can be installed by underaging the alloy between 460-525$°C$ (see Figures B.13a, B.13b, and B.13d), however, ductility (and toughness)

are markedly reduced in this condition (see Figure B.13c). When increased ductility is sought, the alloy can be aged at temperatures above $525°C$, though a loss of strength and hardness can be expected as overaging and austenite reversion rapidly take hold. The ΔR contour plot for R-values evaluated at 1.5% axial strain is shown in Figure B.13e. ΔR, calculated using Equation B.1, represents an overall measure of the variation of R-value in the Y-Z build plane (planar anisotropy) where for an isotropic material: $\Delta R = 0$. For AM materials, non-zero values of ΔR could be an indicator of preferred texture / alignment of the micro-structure due to the laser scanning pattern (especially in the distribution of second phases such as inclusions) / the presence of residual stresses [114]. The contour plot highlights that the range of ΔR variation is low across all treatments (<0.25 at 1.5% axial strain). Planar anisotropy is minimised in the underaged to peak-aged condition. The hypothesis is that the populous presence of small precipitates effectively conceals non-uniform transverse straining by blocking gliding dislocations in this stiff and brittle condition. Comparatively, a greater degree of planar anisotropy can be observed in the overaged and austenitized material, where a lattice with fewer blocking obstacles, and a higher volume fraction of ductile Fe-γ, sees ΔR deviate from zero.

Conclusions

As AM technology continues to mature, more is expected of the functional parts produced, with special attention towards achieving metallurgical soundness by tackling the factors which influence mechanical performance. This study has investigated the effect of three AM build-orientations (0°,45°, and 90°) on the as-built plastic anisotropy of maraging steel 300 (MS1) parts, fabricated on the commercially available EOS EOSINT M280 machine. This high-strength alloy's performance has been monitored through an array of strengthening heat-treatment plans to identify the combinations of time and temperature which can diminish anisotropy. In doing so, a broad collection of mechanical properties, material characteristics, and plastic anisotropy levels for additively manufactured standard test-specimens have been

evaluated and discussed in this novel experimental investigation. The important conclusions are summarized as follows:

1. Considerable anisotropy has been confirmed in as-built MS1;

2. Plastic anisotropy can be diminished significantly through aging heat-treatment, however, a degree of transverse strain anisotropy is likely to remain due to the AM material's fabrication history;

3. The 6h at 490°C heat treatment plan is not optimal in terms of strength, hardness, ductility and anisotropy properties for the DMLS MS1. A proposition of 8h at 490°C is offered where optimal design strength ($R_{p0.2}$ >1900 MPa) is sought, whereas the 8h at 525°C aging plan offers a good isotropic compromise between design strength ($R_{p0.2}$ >1700 MPa), and ductility ($A_t \approx 10\%$);

4. Heat-treatment parameters can be tailored to meet strength/ ductility/ anisotropy design requirements by using the obtained mechanical properties contour maps;

5. The as-built and overaged specimens showed higher levels of planar anisotropy compared to that of the underaged and peak-aged condition;

6. Hardness measurements alone are not effective towards quantifying anisotropy in DMLS maraging steel 300.